University of Strathclyde

Department of Naval Architecture, Ocean and Marine Engineering

DEVELOPMENT OF A BURST PRESSURE PREDICTION MODEL FOR FLAWLESS AND DENTED PIPELINES

Do-Han Oh

A thesis submitted in fulfilment of the requirements
for the degree of Doctor of Philosophy

Glasgow
2020

This thesis is the result of the author's original research. It has been composed by the author and has not been previously submitted for examination, which has led to the award of a degree.

To my family

ABSTRACT

Accurate prediction of the burst pressure of a pipeline is critical for pipeline design and safe operation. There are a number of analytical and empirical formulae derived from theoretical, numerical and experimental methods that can be used to predict the burst pressure of plain pipeline. However, there is not an equivalent method available to predict the burst pressure of dented pipeline and consequently the assessment of dents in pipelines is based on the depth or the shape of the dent.

Therefore, this thesis presents the development of practical burst pressure prediction models for the flawless pipelines, which is then extended to predict the burst pressure of dented pipeline.

Firstly, a study is carried out to develop a new methodology to predict the burst pressure for API 5L X-grade flawless pipelines using Finite Element Analysis (FEA). The FEA is performed using a bilinear material model with the tangent modulus calculated using the strain at Ultimate Tensile Strength (UTS). A new formula has been developed in this work to calculate the strain at UTS based on API 5L X-grade material coupon test data. A comprehensive nonlinear FEA based Parametric Study has then been conducted with this bilinear material model to derive an empirical formula for estimating the burst pressure of API 5L X grade flawless pipelines.

Secondly, an empirical formula for the assessment of the structural integrity of a pipeline with an unconstrained, hemispherical, plain dent has been developed, based on the formula derived for the unflawed pipeline. Parametric studies have been conducted using non-linear FEA of the burst pressure for API 5L X52, X65 and X80 grade pipelines with a dent. An empirical formula, that can predict the burst pressure of dented pipelines is proposed, based on the output dataset derived from the FEA based Parametric Study results.

Thirdly, a dent produced by a spheroidal indenter on API 5L X52 pipeline has been

studied to investigate the effect of the longitudinal and transverse dent lengths on the pipeline structural integrity using FEA. According to the FEA based Parametric Study results, it shows that the burst pressure prediction for the spheroidal dent is comparable with the burst pressure prediction for the hemispherical dent for a given dent depth and longitudinal dent length. Consequently, it is confirmed that the proposed burst pressure prediction formula for the hemispherical dent is applicable to examine the structural integrity of API 5L X52 grade pipelines with an unconstrained, spheroidal, plain dent.

Finally, the applicability of machine learning techniques such as Deep Neural Networks (DNN) for the prediction of burst pressure has been investigated for unflawed and dented API 5L X-grade pipelines. The burst pressure derived has been compared with the results of FEA based Parametric Study and the experimental test results and showed good agreement. Therefore, it is concluded that DNN can be another solution for predicting the burst pressure of API 5L X-grade flawless and dented pipelines.

ACKNOWLEDGEMENTS

I am very pleased to be awarded my PhD, and sincerely hope to thank everyone who helped make this possible.

First, I would like to sincerely appreciate Dr Julia Race, 1st supervisor, for giving me an opportunity to get on the PhD course. In addition, practical advice and valuable comment based on her academic knowledge and sufficient practical experience has been helpful to me during the whole PhD period. Furthermore, thanks to the full scholarship provided, my family could enjoy a stable life in the UK.

Also, I would like to thank Dr Selda Oterkus, 2nd supervisor, who has spent a lot of time counselling on career paths after being awarded PhD as well as given invaluable supervising for improvements in research quality.

As well, I am very grateful to Dr Enrong Chang, Dr Erkan Oterkus, Dr Tahsin Tezdogan, Dr Zhiming Yuan, Ms Susan Pawson and my friends in the laboratory for their great help in adapting to the PhD environment.

Next, I would like to appreciate Dr Yongwon Lee (Lloyd's Register, UK), Mr Hongseok Bae and Dr Byongug Jeong, who have shared a lot of time with me as a steering committee member of the Korean Scientists and Engineering Association in the UK and Europe Korea Marine and Ocean Engineers Association.

I would like to express my heartfelt thanks to Professor Jeomkee Paik, Professor Sungchul Shin, Professor Bongju Kim, Dr Juyoung Kang, Ms Jeongeun Lee and Mr Kiyong Kim (Pusan National University, South Korea), Professor Bonguk Koo (Changwon National University, South Korea), Professor Joonsoo Park (Kyungnam University, South Korea), Professor Namhyun Ahn (Koje University, South Korea), Professor Kwangjun Baik (Inha University, South Korea), Professor Hyunsoo Kim (Inha Technical College, South Korea) and Dr Dokyun Kim (Newcastle University, UK) for their constant encouragement and advice.

I would like to give my earnest thanks to Paul Philbert and Haesue Kang for sharing their bright energy and having fun with me and my family.

I would like to express special thanks to Ms Aecha Fullerton (Aeja Ko) and Mr John Fullerton for their wholehearted support to my family. Thanks to them, my family and I could stay happy and healthy in the UK.

I would like to take this opportunity to express my thanks to: Yonggu Oh and Anyeo Lee, my parents; Chayoung Choi, my mother in law; Kyungmin Oh, Jihyun Oh, Sohyun Oh, Byungho Bae, Jeongan Bae, Jinhwan Moon, in sisters' family; Changbaek Lee, Mikyung Lee, Jaejun Lee, Yoonsang Lee, Jeongmin Lee, Jaeseong Jeong and Yoonwoo Jeong, my in law's family.

Finally, I am grateful for the dedication and support of my beloved wife, Jieun Lee and my two children, Soobeen Oh and Gyujin Oh, during the PhD period, and I sincerely hope that this thesis is dedicated to them specially.

Do-Han Oh

CONTENTS

ABSTRACT ..... **I**

ACKNOWLEDGEMENTS ..... **III**

LIST OF FIGURES ..... **IX**

LIST OF TABLES ..... **XIV**

NOMENCLATURE ..... **XVIII**

CHAPTER 1 ..... **1**

1. INTRODUCTION **1**

1.1. Background 1

1.2. Aim and Objectives 4

1.2.1. Aim of Research 4

1.2.2. Objectives of Research 5

1.3. Outline of Thesis 5

CHAPTER 2 ..... **8**

2. LITERATURE REVIEW **8**

2.1. Definition and Context 8

2.2. The Effect of Dents on Pipeline Structural Integrity 9

2.3. Assessment Criteria for Dents 11

2.3.1. Strain-Based Calculation Method 11

2.3.2. Dent Depth-Based Calculation Method 14

2.4. Calculation of The Burst Pressure of Flawless Pipelines 16

2.5. Experimental Burst Pressure Studies on Plain Dents 18

2.6. The Existing Models for Burst Pressure of a Dent 20

2.7. Determination of Pipeline Failure Using FEA 22

2.7.1. Material Model for FEA 22

2.7.2. Stress-Based Approach and Strain-Based Approach 23

2.7.3. Finite Element Modelling 24

2.8. Determination of Pipeline Failure Using ANN 25

2.8.1. Application of DNN to Evaluate Structural Integrity of Pipelines 25

2.8.2. Activation Function 26

2.9. Summary 27

CHAPTER 3 29

3. METHODOLOGY 29

3.1. Finite Element Analysis 29
3.1.1. Definition of Burst Pressure Criteria 30
3.1.2. Definition of Material Model 33
3.1.3. Determining Burst Pressure Using FEA 38
3.1.4. Development of FEA Model for Flawless Pipelines. 39
3.1.5. Development of FEA Model for Pipelines with a Dent 42
3.2. Deep Neural Network 47
3.2.1. Development of Deep Neural Network 49
3.2.2. Deep Neural Network Architecture 50
3.2.3. Application to Burst Pressure Prediction for Flawless and Dented Pipelines 54
3.2.4. Implementation 60
3.3. Summary 61

CHAPTER 4 62

4. DEVELOPMENT OF A BURST PRESSURE PREDICTION MODEL FOR FLAWLESS PIPELINES 62

4.1. FEA Based Parametric Study 63
4.2. FEA Based Parametric Study Results 64
4.3. Derivation of Empirical Formula 69
4.4. Validation of FD Formula 70
4.5. Summary 76

CHAPTER 5 77

5. DEVELOPMENT OF A BURST PRESSURE PREDICTION MODEL FOR PIPELINES WITH A DENT 77

5.1. FEA based Parametric Study 78
5.1.1. Definition of Dent Depth and Dent Length 79
5.1.2. Pipeline Material Properties and Geometric Information 81
5.1.3. Variables for FEA Based Parametric Study 82
5.2. FEA Based Parametric Study (I) Results 83
5.2.1. Variation in von-Mises Stress with Loading Condition 83

5.2.2. Burst Pressure according to Dent Depth and Dent Length 84
5.2.3. Burst Location according to Dent Depth and Dent Length 85
5.3. Derivation of Empirical Formula 86
5.4. Validation of the PD Formula 91
5.4.1. Comparison with FEA based Parametric Study (I) Results 91
5.4.2. Comparison with FEA based Parametric Study (II) Results 92
5.4.3. Comparison with Experimental Results 94
5.5. Summary 95

CHAPTER 6 97

6. THE APPLICABILITY OF THE DEVELOPED FORMULA TO THE PIPELINES WITH SPHEROIDAL DENTS 97

6.1. FEA Based Parametric Study 97
6.1.1. Definition of Spheroidal Indenter 98
6.1.2. Definition of Dent Width 99
6.1.3. Pipeline Material Properties and Geometric Information 101
6.1.4. Variables for FEA Based Parametric Study 101
6.2. FEA based Parametric Study Results 102
6.2.1. Burst Pressure according to Dent Depth, Length and Width 102
6.3. Validation of Applicability of Developed Empirical Formula 106
6.3.1. Comparison with FEA Based Parametric Study Results 106
6.3.2. Comparison with Experimental Results 110
6.4. Summary 111

CHAPTER 7 112

7. DEVELOPMENT OF A DEEP NEURAL NETWORK MODEL FOR BURST PRESSURE PREDICTION 112

7.1. DNN Model for Flawless Pipelines 112
7.1.1. Comparison with FEA Based Parametric Study Results 113
7.1.2. Comparison with Experimental Results 114
7.2. DNN Model for Pipelines with a Hemispherical Dent 116
7.2.1. Comparison with FEA Based Parametric Study Results 117
7.2.2. Comparison with Experimental Results 119
7.3. Application of DNN Model to Pipelines with a Spheroidal Dent 120
7.3.1. Comparison with FEA Based Parametric Study Results 121

7.3.2. Comparison with Experimental Result 122
7.4. Summary 123

CHAPTER 8 125

8. SUMMARY AND CONCLUSIONS 125
8.1. Summary 125
8.1.1. Flawless Pipelines 125
8.1.2. Pipelines with a Hemispherical Dent 126
8.1.3. Pipelines with a Spheroidal Dent 127
8.1.4. DNN Model 128
8.1.5. Summary of PPMCC and MAPE 128
8.2. Conclusions 130
8.2.1. Suggestion for the Future Work 131

REFERENCE 133

APPENDIX A 144

APPENDIX B 153

APPENDIX C 167

LIST OF FIGURES

Figure 1.1 Overall procedure for the research on the burst pressure prediction subjected to the flawless pipelines and the pipelines with a dent. 4

Figure 2.1 Method for estimating strain in dents (ASME 2014). 12

Figure 2.2 Definition of dent depth (Cosham et al. 2004). 14

Figure 2.3 Indentation shape of Orynyak's model (Orynyak 2001). 21

Figure 3.1 Criteria for limit load estimation: (a) tangent intersection and strain based criteria, (b) elastic slope and deformation based criteria, (c) zero curvature criterion with non-zero tangent value at the inflection point, (d) zero curvature criterion with tangent value at the inflection point. 31

Figure 3.2 Definition of the burst pressure for the pipelines with a dent. 33

Figure 3.3 Typical Stress-Strain curve of carbon steel and bilinear material model for FEA. 34

Figure 3.4 Procedure for the development of an empirical formula to estimate the strain at Ultimate Tensile Strength of pipelines. 35

Figure 3.5 Material coupon test data plot and best-fit exponential curve using ε_{UTS_TEST} and the ratio of σ_{yield_TEST} to σ_{UTS_TEST}. 36

Figure 3.6 Pearson Product-Moment Correlation Coefficient between the strain calculated by the proposed formula and the strain from the material coupon test. 38

Figure 3.7 Determining busrt pressure of pipelines using Finite Element Analysis results. 39

Figure 3.8 Mesh size, loading and boundary condition of Finite Element Analysis model of flawless Pipeline: (a) loading condition, (b) mesh size, loading condition and boundary condition. 41

Figure 3.9 von-Mises equivalent stress and burst pressure according to the number of element. 42

Figure 3.10 Loading condition of Finite Element Analysis model for the pipelines with a dent. 43

Figure 3.11 Boundary condition of Finite Element Analysis model for the pipelines with a dent. 44

Figure 3.12 Convergence study results of the mesh size and model length for Finite Element Analysis: (a) number of elements through thickness, (b) length multiplier. 46

Figure 3.13 Comparison of the dent depth after removing indenter. 47

Figure 3.14 Relations between artificial intelligence, machine learning and neural networks. 48

Figure 3.15 Comparison with biological neural network and artificial neural network. 48

Figure 3.16 Diagram of the artificial neural networks. 49

Figure 3.17 ReLU activation function. 52

Figure 3.18 Selection of the number of hidden layers of the Deep Neural Network model to predict the burst pressure of flawless pipelines. 55

Figure 3.19 Selection of the epoch size for the Deep Neural Network model to predict the burst pressure of flawless pipelines. 56

Figure 3.20 Selection of the learning rate for the Deep Neural Network model to predict burst pressure for the flawless pipelines. 57

Figure 3.21 Selection of the number of hidden layers for the Deep Neural Network model to predict the burst pressure of pipelines with a dent. 58

Figure 3.22 Selection of the epoch size for the Deep Neural Network model to predict the burst pressure of pipelines with a dent. 58

Figure 3.23 Selection of the learning rate for the Deep Neural Network model to predict the burst pressure of pipelines with a dent. 59

Figure 3.24 Defined Deep Neural Network diagram 60

Figure 4.1 Procedure for the development of an empirical formula to predict the burst pressure of flawless pipelines. 62

Figure 4.2 Sample of von-Mises equivalent stress distribution from Finite Element Analysis results (2D Axisymmetric full expansion plot). 65

Figure 4.3 FEA based Parametric Study results summarized as the relationship between the burst pressure and the ratio between the diameter and the thickness of the pipeline for each material: Finite Element Analysis results for (a) X52 and (b) X56..... 66

Figure 4.3 (cont.) FEA based Parametric Study results summarized as the relationship between the burst pressure and the ratio between the diameter and the thickness of the pipeline for each material: Finite Element Analysis results for (c) X60 and (d) X65. 67

Figure 4.3 (cont.) FEA based Parametric Study results summarized as the relationship between the burst pressure and the ratio between the diameter and the thickness of the pipeline for each material: Finite Element Analysis results for (e) X70 and (f) X80. 68

Figure 4.4 Correlation between P_{Burst}/σ_{UTS} and D / t and R squared (R^2). 69

Figure 4.5 Average discrepancy and standard errors in association with the results of experiments and the prediction by analytical methods. 75

Figure 5.1 Procedure for the development of an empirical formula to predict the burst pressure of flawless pipelines. 78

Figure 5.2 Definition of the indenter radius (R_{ind}), initial dent depth (D_b) and initial dent length (L_b) before removal of the indenter. 80

Figure 5.3 Definition of the dent depth (D_a) and dent length (L_a) after removal of the indenter. 80

Figure 5.4 A schematic of von-Mises equivalent stress tendency at the burst section on the dented area with the loading conditions; where P1 to P5 are the nodes in the thickness direction within the dented area. 84

Figure 5.5 Effects of the dent depth and dent length on the burst pressure of pipelines with a dent. 85

Figure 5.6 Location of the burst occurred in accordance with the ratio of L_a to D and D to D_a. 85

Figure 5.7 Burst pressure of pipelines with a dent in accordance with the ratio of L_a to D. 86

Figure 5.8 Coefficients and exponent as a function of the ratio of D_a to D: (a) coefficient A_1, (b) coefficient A_2, (c) coefficient x_0, (d) exponent p. 89

Figure 5.9 Limitation of the PD formula by the relationship between the ratio of L_a to D_a and D_a to D. 90

Figure 5.10 Pearson Product-Moment Correlation Coefficient between the burst pressure calculated by the PD formula and the FEA based Parametric Study (I) results. 92

Figure 5.11 Pearson Product-Moment Correlation Coefficient between the burst pressure calculated by the PD formula and the FEA based Parametric Study (II) results. 93

Figure 5.12 Pearson Product-Moment Correlation Coefficient between the burst pressure calculated by the PD formula and the experimental results. 95

Figure 6.1 Indenter types used in Finite Element Aanlysis based parametric study: (a) hemispherical indenter, (b) spheroidal indenter. 98

Figure 6.2 Definition of the length (L_I) and width (W_I) of the spheroidal indenter: (a) L_I is greater than W_I, (b) L_I is less than W_I. 99

Figure 6.3 Definition of the dent width (W_a) after removal of the indenter: (a) the normalization of the LOC_i^D based on the LOC_i^O into the $LOC_i^{D'}$ based on the D, (b) definition of the dent width (W_a). 100

Figure 6.4 Burst pressure according to the dent depth, length and width: (a) at 50mm of L_I or W_I. 103

Figure 6.4 (cont.) Burst pressure according to the dent depth, length and width: (b) at 75mm of L_I or W_I and (c) at 100mm of L_I or W_I. 104

Figure 6.5 Burst pressure to the same dent length (L_I) and dent width (W_I). 105

Figure 6.6 Tendency of the burst pressure of pipelines with a spheroidal dent. 105

Figure 6.7 Comparison with the Finite Element Analysis and PD formula: for the ratio of initial dent depth to pipeline diameter, (a) 2.5%. 106

Figure 6.7 (cont.) Comparison with the Finite Element Analysis and PD formula: for the ratio of initial dent depth to pipeline diameter, (b) 5.0% and (c) 10.0%. 107

Figure 6.8 Scatter plot of the burst pressure by the PD formula and Finite Element Analysis: (a) L_a and W_a based approach. 108

Figure 6.8 (cont.) Scatter plot of the burst pressure by the PD formula and Finite Element Analysis: (b) W_a based approach with Pearson Product-Moment Correlation Coefficient. 109

Figure 6.8 (cont.) Scatter plot of the burst pressure by the PD formula and Finite Element Analysis: (c) L_a based approach with Pearson Product-Moment Correlation Coefficient. 110

Figure 7.1 Cost function (MAPE) per EPOCH for the flawless pipelines..... 113

Figure 7.2 Pearson Product-Moment Correlation Coefficient between the burst pressure computed by the Deep Neural Network model and the FEA based Parametric Study results for the flawless pipelines..... 114

Figure 7.3 Pearson Product-Moment Correlation Coefficient: (open square) between the burst pressure computed by the Deep Neural Network model and the experimental results, (closed square) between the burst pressure caclulated by the FD formula and the experimental results. 115

Figure 7.4 Cost function (MAPE) per EPOCH for the pipelines with a hemispherical dent. 117

Figure 7.5 Pearson Product-Moment Correlation Coefficient between the burst pressure computed by the Deep Neural Network model and the FEA based Parametric Study results for the pipeline with a hemispherical dent..... 118

Figure 7.6 Pearson Product-Moment Correlation Coefficient between the burst pressure computed by the Deep Neural Network model and the experimental results for the pipeline with a hemispherical dent. 120

Figure 7.7 Cost function in terms of the Mean Absolute Percentage Error for the pipelines with a spheroidal dent..... 121

Figure 7.8 Pearson Product-Moment Correlation Coefficient between the burst pressure computed by the Deep Neural Network model and the FEA based Parametric Study results for the pipeline with a spheroidal. 122

Figure 7.9 Pearson Product-Moment Correlation Coefficient between the burst pressure computed by the Deep Neural Network model and by the experiment for the pipeline with a spheroidal. 123

LIST OF TABLES

Table 2.1 Existing analytical solutions to estimate the burst pressure of a cylinder under pressure..... 17

Table 2.1 (Cont.) Existing analytical solutions to estimate the burst pressure of a cylinder under pressure. 18

Table 3.1 The guidance for the strength of the correlation by Evans (1996). 37

Table 3.2 Geometric information of API X70 for the set-up of FEA model..... 39

Table 3.3 Material properties of API X70 for the set-up of FEA model (API 2004). 40

Table 3.4 Boundary condition according to the loading condtion. 45

Table 3.5 Material properties and geometric information of Finite Element Analysis model from API 1156 (Kiefner et al. 1997). 46

Table 3.6 The guidance for the interpreting of MAPE results by Lewis (1982). 53

Table 3.7 Subject to trade-off studies for defining hyperparameters for flawless and dented pipelines. 55

Table 3.8 Mean Absolute Percentage Error according to the learning rate for the flawless pipelines. 57

Table 3.9 Mean Absolute Percentage Error according to the learning rate for pipelines with a dent..... 59

Table 3.10 Summary of the defined hyper-parameters for Deep Neural Network model. 60

Table 4.1 Material properties of the FEA model for parametric study (API 2004). 63

Table 4.2 Geometric information and bounding cases of the FEA model for parametric study (API 2004). 64

Table 4.3 Geometric information and material properties of 14 specimens of the experiment: Zhu and Leis (2012), Law and Bowie (2007), Liessem et al. (2004) and Zhang et al. (2014). 70

Table 4.3 (Cont.) Geometric information and material properties of 14 specimens of the experiment: Zhu and Leis (2012), Law and Bowie (2007), Liessem et al. (2004) and Zhang et al. (2014). *71*

Table 4.4 Average Discrepancy, Standard Error and Standard Error ranking for the normalized burst pressures through dividing the predictions by experimental results. ... *72*

Table 4.4 (Cont.) Average Discrepancy, Standard Error and Standard Error ranking for the normalized burst pressures through dividing the predictions by experimental results. *73*

Table 4.4 (Cont.) Average Discrepancy, Standard Error and Standard Error ranking for the normalized burst pressures through dividing the predictions by experimental results. *74*

Table 5.1 Material properties and geometric information of the Finite Element Analysis model for parametric study (I) (Kiefner et al. 1997) and (II) (API 2004). *81*

Table 5.2 Variables for the FEA based Parametric Study (I). *82*

Table 5.3 Variables for the FEA based Parametric Study (II). *82*

Table 5.4 Indenter radius (R_{ind}) according to the ratio of D_b to L_b and D_b to D. *83*

Table 5.5 Validation information from the experimental result of the hemispherical dent: X52 (1) and (2) (Kiefner and Alexander 1997), X52 (3) (Shuai et al. 2018). *94*

Table 6.1 Indenter types in accordance with the indenter length (L_I) and width (W_I). *97*

Table 6.2 Material properties and geometric information for Finite Element Analysis model of the pipeline with a spheroidal dent (API 2004). *101*

Table 6.3 Variables for the FEA based Parametric Study of the spheroidal dented pipelines. *102*

Table 6.4 Sample to explain the reasons for using the D_b/D ratio, the length (L_I) and the width (W_I) of the spheroidal indenter. *102*

Table 6.5 Validation information from the experimental result of the spheroidal dent (Bjørnøy et al., 2000). *111*

Table 7.1 Cost function in terms of Mean Absolute Percentage Error in accordance with the applied material of pipelines. *117*

Table 8.1 Summary of PPMCCs and MAPEs for all parametric studies. 129

Table A.1 Geometric information for the parametric analysis. 144

Table A.1 (cont.) Geometric information for the parametric analysis. 145

Table A.1 (cont.) Geometric information for the parametric analysis. 146

Table A.2 Burst pressure for the flawless pipelines by Finite Element Analysis (X52, X56, X60, X65, and X70). 147

Table A.2 (cont.) Burst pressure for the flawless pipelines by Finite Element Analysis (X52, X56, X60, X65, and X70). 148

Table A.2 (cont.) Burst pressure for the flawless pipelines by Finite Element Analysis (X52, X56, X60, X65, and X70). 149

Table A.3 Burst pressure of the flawless pipelines by Finite Element Analysis (X80). .. 150

Table A.3 (cont.) Burst pressure for the flawless pipelines by Finite Element Analysis (X80). 151

Table A.3 (cont.) Burst pressure for the flawless pipelines by Finite Element Analysis (X80). 152

Table B.1 La, La/D, Da, Da/D and Burst pressure for the FEA based Parametric Study (I). 153

Table B.1 (cont.) La, La/D, Da, Da/D and Burst pressure for the FEA based Parametric Study (I). 154

Table B.2 The 150 data generated by linear interpolation from the 50 FEA based Parametric Study (I) results. 155

Table B.2 (cont.) The 150 data generated by linear interpolation from the 50 FEA based Parametric Study (I) results. 156

Table B.2 (cont.) The 150 data generated by linear interpolation from the 50 FEA based Parametric Study (I) results. 157

Table B.2 (cont.) The 150 data generated by linear interpolation from the 50 FEA based Parametric Study (I) results. 158

Table B.2 (cont.) The 150 data generated by linear interpolation from the 50 FEA based Parametric Study (I) results. *159*

Table B.3 La, La/D, Da, Da/D and Burst pressure for the FEA based Parametric Study (II) for X52 material pipelines with a hemispherical dent. *160*

Table B.3 (cont.) La, La/D, Da, Da/D and Burst pressure for the FEA based Parametric Study (II) for X52 material pipelines with a hemispherical dent. *161*

Table B.4 La, La/D, Da, Da/D and Burst pressure for the FEA based Parametric Study (II) for X65 material pipelines with a hemispherical dent. *162*

Table B.5 La, La/D, Da, Da/D and Burst pressure for the FEA based Parametric Study (II) for X80 material pipelines with a hemispherical dent. *163*

Table B.6 Da, Da/D, La, La/D, Wa, Wa/D, and Burst pressure of the FEA based Parametric Study for X52 material pipelines with a spheroidal dent. *164*

Table B.6 (cont.) Da, Da/D, La, La/D, Wa, Wa/D, and Burst pressure of the FEA based Parametric Study for X52 material pipelines with a spheroidal dent. *165*

Table B.6 (cont.) Da, Da/D, La, La/D, Wa, Wa/D, and Burst pressure of the FEA based Parametric Study for X52 material pipelines with a spheroidal dent. *166*

NOMENCLATURE

Abbreviation and Acronym

AI	Artificial Intelligence
ANN	Artificial Neural Network
APDL	Ansys Parametric Design Language
API	American Petroleum Institute
ASME	American Society Mechanical Engineers
BEP	Bilinear Elasto-Plastic
DNN	Deep Neural Network
DNV	Det Norske Veritas
dSiLU	Derivative of Sigmoid-weighted Linear Unit
EGIG	European Gas Pipeline Incident Data Group
ELU	Exponential Linear Unit
EPRG	European Pipeline Research Group
EPP	Elastic-Perfectly Plastic
FEA	Finite Element Analysis
FEM	Finite Element Method
FNN	Feed-forward Neural Network
ILI	In-Line Inspection

LReLU	Leaky Rectified Linear Unit
MAPE	Mean Absolute Percentage Error
MNIST	Modified National Institute of Standard and Technology
PDAM	Pipeline Defect Assessment Manual
PHMSA	Pipeline and Hazardous Materials Safety Administration
PPMCC (r)	Pearsons Product-Moment Correlation Coefficient
PReLU	Parametric Rectified Linear Unit
PeLU	Parametric Exponential Linear Unit
ReLU	Rectified Linear Unit
RReLU	Randomized Rectified Linear Unit
SE	Standard Error
SeLU	Scaled Exponential Linear Unit
SReLU	S-shaped Rectified Linear Unit
SiLU	Sigmoid-weighted Linear Unit
SMYS	Specified Minimum Yield Strength
UTS	Ultimate Tensile Strength
UKOPA	United Kingdom Onshore Pipeline Operators' Association
FP formula	An empirical *formula* (4.3) to predict the burst pressure of Flawless Pipelines
PD formula	An empirical *formula* (5.6) to predict the burst pressure of Pipelines with a Dent

HSD	The length equal to the width of the indenter (same as the hemispherical indenter)
SLD	Spheroidal indenter towards length (the width less than the length of dent)
SWD	Spheroidal indenter towards width (the width greater than the length of dent)

Roman

b	Bias, which is a parameter in machine learning
C_w	Half width of dent
d, H	Dent depth
D	Outer diameter of pipeline
D_a	Dent depth measured after removal of the indenter
D_b	Initial dent depth measured before removal of the indenter
D_i	Dent depth based on the LOC_i^O
D_{in}	Inner diameter of pipeline
D_{ave}	Average of inner and outer diameter
e	Euler's number
E	Young's modulus
E_t	Tangent modulus
F	An action, force
F_{cb}	Smaller value between yield strength and ultimate tensile strength divided by 1.15
I	Degree of damage, I=1 means the ductile fracture of the material
k	Ratio of outer diameter to inner diameter, only for ASME (1962): k<1.5
K	Stiffness of material
L_a	Dent length measured after removal of the indenter

L_b	Initial dent length measured before removal of the indenter
L_I	Length of the spheroidal indenter
LOC_i^D	Shifted coordinate of LOC_i^O due to the indentation
$LOC_i^{D'}$	Transformed coordinate of LOC_i^D to normalize to the same shape used to define the dent length
LOC_i^O	Coordinate of the original pipeline
N	Total number of data
n^*	Number of observations
P_o	Burst pressure calculated by Orynyak's model
P_{Burst}, P_{max}	Burst pressure of pipelines
P_{Burst}^d	Burst pressure of pipelines with a dent
P_{Burst}^f	Burst pressure of flawless pipelines
$P_{exp.}$	Burst pressure from the experimental results
$P_{FP\ formula}$	Burst pressure calculated by the *FP formula*
$P_{probability}$	Probability value
R	Outer radius of pipeline
R_{ind}	Radius of the indenter
R_0	Initial pipeline surface radius that is equal to half of pipeline outer diameter
R_1	Radius of curvature after removal of indenter in a transverse plane

R_2	Radius of curvature after removal of indenter in a longitudinal plane
R^2	R squared, the coefficient of determination
t	Thickness of pipeline wall
t_v	*t*-value
u	a behaviour, displacement
Ux, Ux, Uz	Degrees of freedom that correspond to displacements about x-, y-, and z-axis
w	Weight, which is a parameter in machine learning
W_a	Dent width measured after removal of the spheroidal indenter
W_I	Width of the spheroidal indenter
x_{norm}	Normalized data of the feature
x_{min}	Maximum value of the feature
x_{max}	Minimum value of the feature
YT	Ratio of yield strength to ultimate tensile strength

Greek

α	Reduction factor of Orynyak's model
β	Nondimensional number of Orynyak's model
γ	Reduction factor
ε_{bc}	Bending strain in the hoop (circumferential) direction
ε_{bl}	Bending strain in the longitudinal direction
ε_{ml}	Longitudinal membrane strain
$\varepsilon_{fracture}$	Strain at fracture
ε_{i}	Longitudinal membrane strain
ε_{o}	Longitudinal membrane strain
ε_{UTS}	Strain at ultimate tensile strength
ε_{yield}	Strain at yield strength
σ_1	Maximum principal stess
σ_2	Median principal stress
σ_3	Minimum principal stress
$\sigma_{equi.}$	von-Mises equivalent stress
$\sigma_{flow.}$	Average of yield strength and ultimate tensile strength
σ_{UTS}	Ultimate tensile strength
σ_{yield}	Yield strength
ω	Ratio of yield strength to ultimate tensile strength

CHAPTER 1

1. INTRODUCTION

1.1. Background

Rapid industrialization and population growth have made the oil and gas industry one of the most closely associated industries in life with the survival of humankind, and the need to reliably supply oil and gas to even more remote areas has emerged. Accordingly, some means to transport oil and gas products, such as rail, truck, and pipelines have been developed. Amongst them, the pipeline is known as the most efficient, cost-effective and safest method (Green et al. 2015, About Pipelines 2012).

However, although pipelines have been recognized and widely used as an economical and safe way to transport oil and gas products, the need to maintain the pipeline in a safe state has arisen. Because the failures of the oil and gas pipelines are accompanied with not only serious consequences that effect on the environment, personnel and population but also serious economic losses caused by difficulties in gas, oil and petroleum products supply. The US Department of Transportation's Pipeline and Hazardous Materials Safety Administration (PHMSA) web site (PHMSA 2020) announces the significant incident consequences summary statistics from 2005 through 2020, and according to the report, the maximum fatalities and injuries per year reported 19 and 103 in 2010, respectively, and the maximum total costs including industry costs and public costs have marked over 18 billion dollars in 2018.

According to Baker (2004), the incidents of the pipeline for the crude oil from 1968 to 2003 and for the gas from 1970 to 2003 recorded 8721 and 24150, respectively.

Amongst them, dent-caused incidents occurred 14 cases from the pipeline for the crude oil and 3 cases from the pipeline for gas, resulted in 11644 barrels leakages with $12.6 million in damage and 17423 barrels leakages with $14.9 million in damage, respectively.

In addition, Chevron Pipe Line Company reported a breakdown for the Grand Bay 10-inch pipeline that is part of the Cypress pipeline system located in Plaquemines Parish, Louisiana, resulting in approximately 80 barrels of crude oil spills and $906,000 of property damage. Failure investigations have shown that the causes of this failure are the structural instability due to a dent already created at the location of the failure, and a lack of capacity to bear the plastic deformation occurring in the stress concentration area (PHMSA 2012).

Risk factors that cause the serious losses mentioned above include gouges, cracks, dents, dents containing gouges and/or cracks, and so on. In particular, the dent is one of the major mechanical damages of oil and gas pipelines caused by external interference, which can cause local stress increase and the burst of pipelines. According to the 10th Report of the European Gas Pipeline Incident Data Group, 28.37% of pipeline accidents between 2007 and 2016 was reported to have been caused by the mechanical damage such as dents and/or gouges due to the external interference (EGIG 2018).

According to the United Kingdom Onshore Pipeline Operators' Association (UKOPA) Pipeline Product Loss Incidents and Faults Report (Goodfellow et al. 2019), the product loss incidents by external interference indicated 21.3% of total failure during the period 1962 to 2017. In addition, they analysed the fault data about the part-wall defects such as corrosion defects, dents, gouges, weld defects, mill defects, cracks and others. According to the results, the dent has taken about 7.5% of total defects.

To solve and overcome these problems, people began to be interested in how to run the oil and gas business economically, and the need of the accurate and reliable model to evaluate the capacity of the pipeline with or without damage has arisen.

In view of economics, for a time, the USA and Canadian regulations allowed the 80% of the specified minimum yield strength (SMYS) for the circumferential stress in the operational condition, but the design allowance in current ASME 31.8 (2014) is the 72% of SMYS (McLamb et al. 2002). In addition, the allowance of the dent depth for the unconstrained, plain dent according to the codes and regulations like ASME B31.8 (2014), the American Petroleum Institute API 1156 (Kiefner et al. 1997), the European Pipeline Research Group EPRG (Roovers et al. 1999), and the Pipeline Defect Assessment Manual PDAM (Cosham et al. 2004) applies predominantly 6 or 7 % of pipeline diameter.

However, the mentioned above defect assessment methodologies currently in use focuses on the dent depth and are recognized as conservative methods. This means that these methodologies are not reasonable from an economic perspective.

In addition, the requirement for the research of appropriate methods to assess the structural integrity of the dented pipelines has arisen from the concern expressed amongst pipeline operators regarding the best practice for the safe and economic operation of dented pipelines (Race, 2008). Furthermore, there is no empirical formula for calculating the failure pressure of a dented pipeline (Cosham et al. 2000, 2005).

Therefore, it is necessary to develop the validated, pragmatic and usable models for the flawless pipelines and pipelines with a dent through the study on the assessment of structural integrity of oil and gas pipelines based on the parametric studies using Finite Element Analysis (FEA).

In addition, the dataset from the parametric studies using FEA will be used to develop the Artificial Neural Network (ANN) model to estimate the burst pressure of dented and undented pipelines. The developed ANN model can be used by the field engineers and operators to determine the structural integrity of dented and undented pipelines without FEA and to make a decision whether the defected pipelines are repaired or not.

The overall procedure for the research of the burst pressure of the flawless pipelines and pipelines with a dent is illustrated in Figure 1.1.

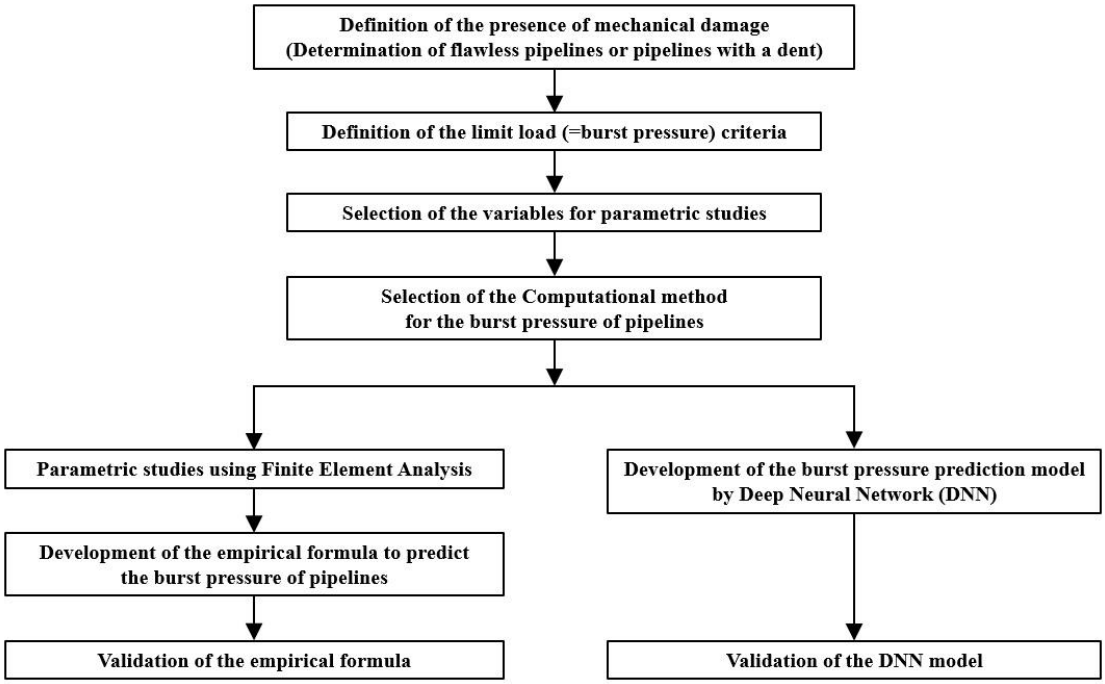

Figure 1.1 Overall procedure for the research on the burst pressure prediction subjected to the flawless pipelines and the pipelines with a dent.

1.2. Aim and Objectives

1.2.1. Aim of Research

As part of the safe and economical operation of pipelines, an accurate assessment of the structural integrity of pipelines with a dent is urgently required. Nevertheless, to date, there is no empirical formula to accurately and efficiently predict the burst pressure of a dented pipeline, so operators and field engineers rely on guidelines for dent depth or strain of dent. Therefore, this study aims to develop a method to predict the burst pressure of API 5L X grade pipelines with an unconstrained, hemispherical or spheroidal, plain dent using parameters readily available in the field without conducting FEA.

1.2.2. Objectives of Research

A dent on pipelines is a threat to reduce the stiffness of the flawless pipeline. That is, an empirical formula to predict the burst pressure of pipelines with a dent can be defined as the burst pressure of flawless pipelines multiplied by a reduction factor. Therefore, the aim of this research can be achieved and validated by conducting the followings:

(1) An empirical formula to predict the burst pressure of flawless pipelines is developed using the nonlinear FEA parametric study results, and a bilinear material model is employed to include strain hardening effects in the FEA model.

(2) An empirical formula to estimate the strain at UTS for determining a bilinear material model is developed using the material coupon test data.

(3) An empirical formula to calculate the reduction factor caused by a dent is developed using the nonlinear FEA results from the parametric study for pipelines with a hemispherical dent. Finally, an empirical formula to predict the burst pressure for dented pipelines is derived by multiplying the reduction factor with the formula for flawless pipelines.

(4) To investigate the effect of the dent shape on the formula according to the dent length and dent width, pipelines with a spheroidal dent are used. In addition, the formula for predicting the burst pressure of pipelines with a hemispherical dent is validated for its applicability to a pipeline with a spheroidal dent.

(5) The applicability of Deep Neural Network (DNN) to predict the burst pressure of flawless and dented pipelines is investigated.

1.3. Outline of Thesis

This thesis is structured as follows:

Chapter 1 describes the research background and motivation for the development of a model and the aims of the research.

Chapter 2 discusses the literature reviews about the definition of the burst pressure of pipelines, the prediction and evaluation method of the burst pressure of the pipelines with and without a dent, the application of ANN to evaluate the structural integrity of pipelines, and the activation functions of DNN.

Chapter 3 presents the methodologies about flawless pipelines, the pipelines with an unconstrained, plain dent, and the DNN as a new solution to predict the burst pressure of the pipelines with or without a dent.

Chapter 4 addresses a new formula that predicts the burst pressure of flawless pipelines termed the *FP formula*. The *FP formula* has been derived using the results of nonlinear FEA based Parametric Study. For the validation of the *FP formula*, the comparison has been carried out between the 14 experimental results and the results calculated by 22 formulae including the *FP formula*.

Chapter 5 suggests a new empirical formula to estimate the burst pressure of the pipelines with an unconstrained, hemispherical, plain dent termed the *PD formula*. The *PD formula* has been obtained based on the nonlinear FEA based Parametric Study results, and validated by comparison with the 80 cases of nonlinear FEA based Parametric Study results and the three experimental results.

Chapter 6 examines the effects of the dent length and the dent width on the pipeline structural integrity and investigated the applicability to pipelines with a spheroidal dent of the *PD formula*.

Chapter 7 proposes DNN models that can predict the burst pressure of flawless pipelines, pipelines with a hemispherical and spherical dent. The DNN model has been developed using the FEA based Parametric Study results. For the validation of DNN models, the burst pressure computed by the DNN model has been compared with the FEA based Parametric Study results and the experimental test results.

Chapter 8 wraps up the novelties, contributions, and limitations of this research, the suggestions for the future works, and conclusions.

CHAPTER 2

2. LITERATURE REVIEW

As oil and gas pipelines have become a main way of supplying energy to human life, their importance has increased and they have been recognized as the most valuable transportation method. Since Barlow presented a model for predicting pipeline burst pressure in 1836, many papers have been published relating to the burst pressure prediction of flawless pipelines, as well as pipelines with a dent.

Even there are many formulae for the prediction of the burst pressure of flawless pipelines, there is no formula to calculate the burst pressure of pipelines with a dent. Majority of codes and regulations regarding the pipelines with a dent have proposed recommendations on the evaluation of the structural integrity of the pipelines and they proposed the limit of the dent depth defined by the ratio of the dent depth to the diameter of the pipelines.

In addition, researches using the DNN based on ANN amongst machine learning methods, which is believed to be a solution in the future, including the present, have been conducted in various fields. And, few studies on the prediction of the burst pressure of pipelines with damages have been reported, and no papers have been published on the prediction of the burst pressure of pipelines with a dent.

2.1. Definition and Context

It is necessary to define the terms used in research related to dents, and the definitions of the terms related to dents are as follows:

Dent a change of the curvature into inward of the pipelines formed by external forces as a result of the plastic deformation.

Smooth dent	a dent that has a smooth change in the curvature of the pipeline wall.
Plain dent	a dent that has a smooth change in the curvature with no pipeline thickness reduction and mechanical damage like gouges, scrapes, and metal loss.
Kinked dent	a dent that deforms the pipe curvature abruptly. In here, "abruptly" is defined as the ratio of curvature radius in any direction to the pipe thickness is less than five.
Rebound	the elastic recovery of indentation after the removal of indenter.
Reround	the deformation of the dent toward the opposite direction by pressure acting on the inside of pipelines.
Constrained	the condition that does not allow the *Rebound* and *Reround* phenomenon because of the continuation of indenter.
Unconstrained	the condition that allows the *Rebound* and *Reround* phenomenon because of the removal of indenter.

Where the ratio to define the "abruptly" is based on the Pipeline Defect Assessment Manual PDAM (Cosham et al 2004).

The main theme of this research is focused on the behaviour of the *plain*, *smooth* and *unconstrained* pipeline. Consequently, the literature review in this chapter discusses the current research and guidance regarding the mentioned type of pipelines. As well, the literature review regarding flawless pipelines and ANN is presented.

2.2. The Effect of Dents on Pipeline Structural Integrity

Dents as one of the threats to reduce the structural integrity of pipelines are not severe, while dents accompanied by the other mechanical defects such as gouge and scratch result in immediate failure about 80% of the time (Rosenfeld 2001).

Even though the dent itself cannot be an immediate threat to the structural integrity of pipelines, but can be a factor to create a problem over a long period of time through developing the coating damage, corrosion, or punctures (Baker 2004).

Fields et al. (1994) figured out that if the contour of dents takes the changes abruptly, the dent is critical. In addition, they introduced the information that the highest stresses and strains in the dented area was occurred not in the apex of the dent depth but at the shoulder of the dent. Also, they said that dents could be a factor that makes pipelines more vulnerable to fatigue failure, and it can be serious than an immediate failure.

Cosham et al. (2000) investigated the effect of dents on pipeline integrity. According to this research, a plain dent can cause high localized stress and strain increase, but pipelines with a dent can keep a stable status due to the ductility of the pipeline material.

In addition, Cosham et al. (2004), through a study on the effect of a dent on the structural integrity of pipelines, figured out that the plain dent was a crucial factor inducing the reduction of the resistance for burst if the dent depth is seriously deep. They also summarized the burst pressure results of the experiment from Eiber et al. (1981), Kiefner et al. (1996, 1997), Hopkins et al. (1983, 1989, 1992), Bjørnøy et al. (2000), Belanos et al. (1958), Jones (1982), Wang et al. (1982) and found out that only 14 test specimens were bursting in the dented area amongst more than 75 burst pressure results of the experiment.

When examining the effect of dents on pipelines, it is necessary to evaluate the effects on the pipeline structural integrity not only by the depth and length of a dent but also the ratio of the dent length to dent width. To do this, researchers used the ellipsoidal, cylindrical or rectangular indenter.

Wu et al. (2016) studied the damage level with ellipsoidal dent using Oyane ductile fracture criterion (Oyane et al. 1980) that was derived based on the plasticity theory for porous materials and presented a new cumulative damage evaluation model expressed with the dent depth and the ratio of thickness to diameter of the pipeline. And, they found that the longer dent length had smaller cumulative damage than a shorter dent length under the condition of the same dent width. In the case of the width of a dent, the bigger width of dent had the increased cumulative damage,

according to the increasing of dent depth under the same dent length up to the specific dent depth. However, after the specific dent depth, the bigger width of dent had the decreased cumulative damage.

Bjørnøy et al. (2000) performed the pipeline burst tests with a cylindrical indenter, it was found that the deep dent (more than 20% of the pipeline outer diameter) could reduce the burst capacity of pipelines significantly.

Oshana (2013) assessed the location of the maximum structural deformation based on the results of experiments with rectangular indenter and found out that the maximum hoop strain occurred at the dent apex. On the other hand, the maximum longitudinal strain found somewhere else, not in the dented area. In addition, he figured out that the maximum strain was found in the hoop direction from the results of experiments with the rectangular indenter, while the maximum strain was observed in the longitudinal direction from the results of experiments with the hemispherical indenter.

Based on this review of the effects of dents, one can conclude that dents have less possibility to be a threat that can reduce the structural integrity of the pipeline immediately, but it can be a potential threat to cause the pipeline incidents.

2.3. Assessment Criteria for Dents

There are two ways to assess the acceptability of pipelines with dent defects; a dent depth-based calculation method and a strain-based calculation method. The dent depth-based calculation method is a conventional method that has been used for a long time and widely, whereas the strain-based calculation method is an alternative method introduced recently to assess the dent severity.

2.3.1. Strain-Based Calculation Method

The idea of the strain-based calculation method has been suggested that using the strain taking into account the shape of the dent is more suitable than the dent depth

to evaluate the dent effect. Based on this trend, the acceptance criteria and methods for calculating a strain were introduced in ASME B31.8 published in 2004 (ASME 2004) and equations to calculate strains have been updated in 2007 edition of ASME B31.8 (ASME 2007). The equations have become the current form.

ASME B31.8 (2014) proposed the strain limit with 6% and the equations to calculate the strain on the inside and outside pipeline surface. The proposed equations are composed of bending strain in the hoop direction (ε_{bc}), bending strain in longitudinal direction (ε_{bl}) and longitudinal membrane strain (ε_{ml}). Each equation requires dent length after deformation (L) and dent depth (d) as well as the values of the radius of curvature as illustrated in Figure 2.1.

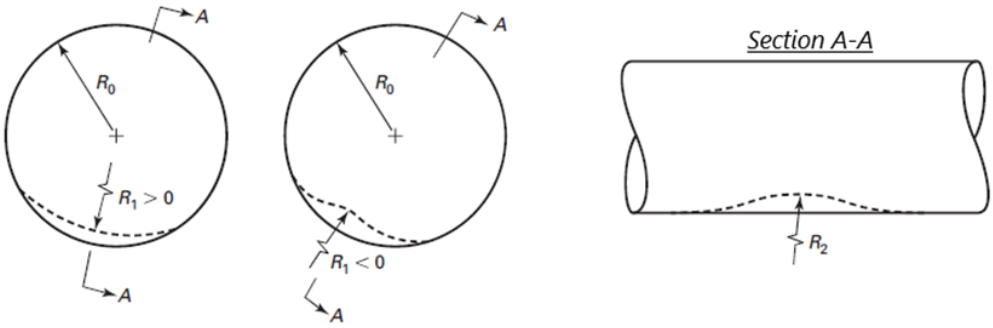

Figure 2.1 Method for estimating strain in dents (ASME 2014).

Where R_0, R_1, and R_2 are the initial pipeline surface radius that is equal to half of pipeline outer diameter, radius of curvature after removal of indenter in a transverse plane, and radius of curvature after removal of indenter in a longitudinal plane, respectively.

The equations, (2.1) and (2.2), to calculate the total strain on the inside (ε_i) and outside (ε_o) pipeline surface are expressed as follows:

$$\varepsilon_i = \sqrt{{\varepsilon_{bc}}^2 - \varepsilon_{bc}(\varepsilon_{bl} + \varepsilon_{ml}) + (\varepsilon_{bl} + \varepsilon_{ml})^2} \quad (2.1)$$

$$\varepsilon_o = \sqrt{{\varepsilon_{bc}}^2 + \varepsilon_{bc}(-\varepsilon_{bl} + \varepsilon_{ml}) + (-\varepsilon_{bl} + \varepsilon_{ml})^2} \quad (2.2)$$

Where $\varepsilon_{bc} = \frac{t}{2}\left(\frac{1}{R_0} - \frac{1}{R_1}\right)$, $\varepsilon_{bl} = -\frac{t}{2}\left(\frac{1}{R_2}\right)$, and $\varepsilon_{ml} = \frac{1}{2}\left(\frac{d}{L}\right)^2$

When the larger one of the two strain values (ε_i and ε_o) is less than the strain limit, it means that the dent is not necessary to be repaired.

To calculate the total strain using equation (2.1) and (2.2), the values of R_1, R_2 and L are required. To obtain these values accurately, it is necessary to eliminate background noise from the raw caliper data from the ILI measurement, as well as to be interpreted correctly (Race 2008). However, this has never been easier.

According to Dotson et al. (2014), the strain-based calculation method was evaluated in a more complex way for using in the field than the dent depth-based calculation method. Because the estimation of the radius of curvature can be easily affected by the undulations in In-Line Inspection (ILI) data during transforming data to be usable. In addition, the estimation of the radius of curvature can differ depending on whether the local curvature or global curvature is applied.

Noronha et al. (2010) presented a fourth-order B-spline interpolation method to estimate the deformed dent geometry and strain accurately. Based on the research results, the ILI data from 16 sensors is sufficient to get the precise dent geometry, while the ILI data from 64 sensors is required to obtain the accurate circumferential bending strain. That is, the strain-based calculation method requires more information to evaluate the structural integrity of the dented pipeline than dent depth-based calculation method.

In addition, Maziar et al. (2013) conducted the comparison with the total strain by ASME 31.8 code and the strain by FE simulation, and the results showed big errors between 25.5% through 26% for the inner surface and between 28.7% through 29.6% for the outer surface.

From the literature review results of the above strain-based calculation method, it has confirmed that the strain-based calculation method is not straightforward for the field engineers and operators to evaluate the structural integrity of the pipeline.

Because it is difficult to use the ILI data and field measurement data compared to the dent depth-based calculation method. In other words, it can be seen that the strain-based calculation method is not suitable for achieving the objective of this research to develop a practical and easy-to-use method.

2.3.2. Dent Depth-Based Calculation Method

Understanding how to measure and define a dent depth is the prerequisite of the research for the dent depth-based calculation method. According to Cosham et al. (2004), a pipeline dent is defined as inward plastic deformation of the pipeline having a circular cross-section. As shown in Figure 2.2, dent depth is defined the maximum distance from the original outer surface of the pipeline to the deformed outer surface of the pipeline in a permanent plastic deformation condition that takes into account the rebound and/or the reround effects depending on the boundary conditions at the installed location of the pipeline.

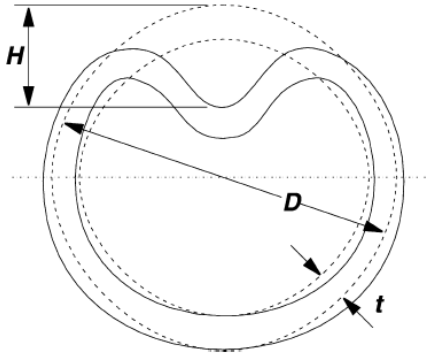

Figure 2.2 Definition of dent depth (Cosham et al. 2004).

In addition, various methods have been proposed to obtain the dent depth more accurately. Wu et al. (2015) studied to find out the optimal solution, which can calculate the dent depth using linear superposition of general solution for beam, beam on Winkler foundation, bivariate polynomial function, or modified cubic spline interpolation. The dent depth defined by the above-mentioned methods was compared with the displacement by FEA, and it was confirmed that the displacement calculated by the modified cubic spline interpolation was in good

accord with the FEA results.

Arumugam et al. (2010) discussed the application of the laser mapping tool to measure the profile of dent accurately. Basically, this method is developed to get the accurate strain for the stain-based calculation method based on the appendix R in ASME 31.8 (2014), it is applicable to get the dent depth information through this method.

Noronha et al. (2010) proposed an application of the fourth-order B-spline interpolation method to predict more precise dent contour. Dent profiles that were estimated by the proposed fourth-order B-spline method using ILI data by changing the number of sensors were compared with the FE results. According to the comparison results, the deformed geometry of dents derived by applying the proposed fourth-order B-spline interpolation method using the ILI data extracted from 16 sensors showed good agreement with the FE results.

To evaluate the structural integrity of the pipelines with dents, there are many safety-focused standards from the American Society of Mechanical Engineers ASME B31.8 (2014), the American Petroleum Institute API 1156 (Kiefner et al. 1997), the European Pipeline Research Group EPRG (Roovers et al. 1999), and the Pipeline Defect Assessment Manual PDAM (Cosham et al. 2004). Especially, according to the summary of each standard's acceptance criteria for the unconstrained, plain dent, the dent depth to pipeline diameter ratio for the allowable dent depth is up to 6% for ASME 31.8 and API 1156, 7% for EPRG and PDAM. To apply the mentioned criteria, the precise calculation of the displacement is required.

However, there is some research to evaluate the suitability of the dent depth criteria. Allouti et al. (2012) investigated the effect of dent depth on the burst pressure of an A37 steel grade pipeline with plain dent by conducting five experiments and FEA. They finalized that the dent depth criterion less than 10% of the pipeline diameter is conservative.

However, Dinovitzer et al. (2000) noted an occurrence of leakage incident from the pipeline with a dent depth less than 3% of pipeline diameter.

Kiefner et al. (1997) investigated the burst pressure of API X52 pipelines with an unconstrained and hemispherical dent by carrying out some experiments. The dent depth after elastic rebound was 7.9% and 10.7% of the pipeline diameter, which was exceeded the allowances of ASME 31.8, API 1156, EPRG and PDAM. However, they did not burst at the operating pressure, and even when the burst was caused by increasing the internal pressure, the burst occurred in somewhere else, not in the dented area. Finally, they concluded that smooth dent does not provide adverse effects on the structural integrity of pipelines.

According to the literature reviews, the assessment criteria for dents have focused on the limit of the acceptance of dent depth or strain, and there is no empirical formula to predict the burst pressure of pipelines with a plain dent. Consequently, it is required to precisely predict the burst pressure of pipelines with a dent to maintain a safe state even in the damaged condition.

2.4. Calculation of The Burst Pressure of Flawless Pipelines

The existing formulae to predict the burst pressure of flawless cylindrical vessels are listed in Table 2.1. The equations are categorized into three different types according to the failure criterion used. The first sets of equations use the Tresca criterion, which is defined as the occurrence of yielding when the maximum shear stress at any point reaches a maximum allowable shear stress. In this criterion, the maximum shear stress is calculated as half the difference between the maximum and minimum principal stresses. The Tresca based failure criteria include ASME (1962), Barlow OD, ID or Flow (1836), Bailey-Nadai (1930), Fletcher (2003), Turner (1910), Stewart et al. (1) (1994), DNV (2013) and Max. Shear Stress (Christopher et al. 2002).

The second group of equations are based on the von-Mises criterion which assumes that failure takes place when the maximum distortion energy reaches the failure

limit equal to the distortion energy required to cause yield in a tensile test. Amongst this group there are nine sets of equations, i.e. Bohm (1972), Faupel (1956), Marin and Rimrott (1958), Marin and Sharma (1958), Soderberg (1941), Svensson (1958) and Stewart et al. (2) (1994), and Nadai (1931, 1963).

The final group of equations applies the average shear stress criterion, which defines failure as the point when the average shear stress reaches the allowable average shear stress. The allowable average shear stress is calculated using the average of the maximum shear stress and the von-Mises equivalent shear stress, as proposed by Zhu and Leis (2005, 2006, 2007, 2010, 2012).

Zhu and Leis (2010, 2012) compared the burst pressures predicted by all of the equations in Table 2.1 with experimental burst pressure results for pipelines. The results showed that there are discrepancies between the burst pressure calculated by equations, this is because most of these formulae were developed from either simple theoretical methods or empirical fits to a limited set of experimental data for the specific material considered. In other words, it is not straightforward to get a single formula that was accurately able to predict the burst pressure over the range of the tests performed.

Table 2.1 Existing analytical solutions to estimate the burst pressure of a cylinder under pressure.

Tresca Criterion Category

ASME (1962)	$P_{max} = \sigma_{UTS}\left(\frac{k-1}{0.6k+0.4}\right)$	DNV (2013)	$P_{max} = \frac{2t}{D-t} f_{cb} \frac{2}{\sqrt{3}}$
Barlow OD (1836)	$P_{max} = \sigma_{UTS}\frac{2t}{D}$	Fletcher (2003)	$P_{max} = \frac{2t\sigma_{flow}}{D_{in}(1-\frac{\varepsilon_{UTS}}{2})}$
Barlow ID (1836)	$P_{max} = \sigma_{UTS}\frac{2t}{D_{in}}$	Max. Shear Stress (2002)	$P_{max} = 2\sigma_{UTS}\left(\frac{k-1}{k+1}\right)$
Barlow Flow (1836)	$P_{max} = \sigma_{flow}\frac{2t}{D_{in}}$	Turner (1910)	$P_{max} = \sigma_{UTS}\ln(k)$
Bailey-Nadai (1930)	$P_{max} = \frac{\sigma_{UTS}}{2n}\left(1-\frac{1}{k^{2n}}\right)$	Stewart et al. (1) (1994)	$P_{max} = \frac{t}{2^{(n-1)}}\frac{\sigma_{UTS}}{D_{ave}}$

Table 2.1 (*Cont.*) Existing analytical solutions to estimate the burst pressure of a cylinder under pressure.

von-Mises Criterion Category			
Bohm (1972)	$P_{max} = \sigma_{UTS}\left(\frac{0.25}{0.227+n}\right)\left(\frac{e}{n}\right)^{n}\frac{2t}{D_i}\left(1-\frac{t}{D_{in}}\right)$		
Faupel (1956)	$P_{max} = \frac{2}{\sqrt{3}}\sigma_{yield}\left(2-\frac{\sigma_{yield}}{\sigma_{UTS}}\right)\ln(k)$	Nadai (1963)	$P_{max} = \frac{\sigma_{UTS}}{\sqrt{3}n}\left(1-\frac{1}{k^{2n}}\right)$
Marin and Rimrott (1958)	$P_{max} = \frac{2}{\sqrt{3}}\frac{\sigma_{UTS}}{(1+\varepsilon_{UTS})}\ln(k)$	Soderberg (1941)	$P_{max} = \frac{4}{\sqrt{3}}\sigma_{UTS}\left(\frac{k-1}{k+1}\right)$
Marin and Sharma (1958)	$P_{max} = \frac{4t}{(\sqrt{3})^{(n+1)}}\frac{\sigma_{UTS}}{D_{in}}$	Svensson (1958)	$P_{max} = \sigma_{UTS}\left(\frac{0.25}{0.227+n}\right)\left(\frac{e}{n}\right)^{n}\ln(k)$
Nadai (1931)	$P_{max} = \frac{2}{\sqrt{3}}\sigma_{UTS}\ln(k)$	Stewart et al. (2) (1994)	$P_{max} = \frac{4t}{(\sqrt{3})^{(n+1)}}\frac{\sigma_{UTS}}{D_{ave}}$
Average Shear Stress Yield Criterion Category			
Zhu and Leis (2006)	$P_{max} = \left(\frac{2+\sqrt{3}}{4\sqrt{3}}\right)^{n+1}\frac{4t\sigma_{UTS}}{D_{ave}}$	Zhu and Leis (2007)	$P_{max} = \left(\frac{2+\sqrt{3}}{4\sqrt{3}}\right)^{q}\frac{4t\sigma_{UTS}}{D_{ave}}$

Where

P_{max} : Burst Pressure	t: pipe wall thickness	ε_{UTS}: strain at UTS
D_{in}, D, D_{ave}: Pipe inner, outer and average diameter, respectively	σ_{yield} , σ_{UTS}: yield and ultimate tensile strength of pipe material, respectively	$q = 1 + 0.239\left(\frac{1}{YT}-1\right)^{0.596}$
$n = ln(1+\varepsilon_{UTS})$	$f_{cb} = \text{Min.}\left[\sigma_y; \frac{\sigma_{UTS}}{1.15}\right]$	$\text{YT} = \frac{\sigma_{yield}}{\sigma_{UTS}}$
$k = \frac{D}{D_i}$, only for ASME: k < 1.5	$\sigma_{flow} = \frac{\sigma_{yield}+\sigma_{UTS}}{2}$	e = Euler's number

2.5. Experimental Burst Pressure Studies on Plain Dents

Some researchers have conducted experiments to demonstrate the effects of dent that is produced on the pipeline. There are various conditions depending on the environment where a pipeline is installed and an indenter shape. The environmental conditions are classified into the constrained or unconstrained dent, and the applied

indenter has a shape of a dome, a bar and a pyramid. Under the mentioned above conditions, Kiefner et al. (1997) have conducted experiments such as unconstrained smooth dent produced by dome shaped indenter and bar shaped indenter, constrained smooth dent dome shaped dent, and pyramid shaped dent. Amongst the experiments, 20 tests were performed under the unconstrained smooth dome dent condition. In particular, four of the 20 experiments were burst tests, two of four were under the condition where the dent produced on the weld seam, and the other two tests were under the condition where the dent was generated on the pipeline surface, not the weld. The latter is perfectly consistent with this study condition. The geometric information of the pipeline employed to the last two experiments is 323.85*mm* in diameter and 4.7752*mm* in thickness, and X52 material is used. The applied initial dent depths are 18% and 12% of the diameter. And, the dent depths after removal of indenter are 7.9% and 10.7% of the pipeline diameter exceeding the dent depth criteria of ASME B31.8 (2014), EPRG (Roovers et al. 1999) and PDAM (Cosham et al. 2004). The detail information mentioned above is listed in Table 5.5. According to the test results, the burst occurred in somewhere else and the burst pressure was 15.81 MPa and 15.95 MPa.

Allouti et al. (2012) carried out five experiments on the A37 steel grade pipeline to investigate the effect of dent depth on the burst pressure of a pipeline with a plain, unconstrained, dome-shaped dent. However, two of five experiments are not reviewed because there is no dent width information. Based on the applied geometric information of pipeline, the outer diameter is 88.9*mm* and the thickness is 3.2*mm.* The dent widths were 50*mm*, 44*mm* and 40*mm.* The dent depths were measured approximately with 14*mm* (16% of outer diameter), 11.8*mm* (13% of outer diameter) and 8.9*mm* (10% of outer diameter) exceeding the dent depth criteria of ASME B31.8 (2014), API 1156 (Kiefner et al. 1997), EPRG (Roovers et al. 1999) and PDAM (Cosham et al. 2004). And, the results of burst pressure were 31.0 MPa, 31.6 MPa, and 30.8 MPa, which is similar to the burst pressure of a flawless pipeline of 31.03 MPa.

In addition, Shuai et al. (2018) carried out an experiment to examine the strain

behaviour due to the increase in the internal pressure of a pipeline with a plain, unconstrained, dome-shaped dent. The X52 grade pipeline specimen has a diameter with 720*mm* and thickness with 8.1*mm*. The dent depth after removal of indenter is 6.76% of the pipeline diameter (48.68*mm*) exceeding the dent depth criteria of ASME B31.8 (2014) and API 1156 (Kiefner et al. 1997). The detail information is listed in Table 5.5. According to the test results, the burst occurred in somewhere else, not dented area. And, the burst pressure was 10.72 MPa, which is close to the burst pressure of a flawless pipeline of 10.53 MPa.

Bjørnøy et al. (2000) conducted in total 14 full scale tests on pipelines with a dent, a dent with notch, and a dent with notch ground. Amongst the experiments, five tests were performed for the X52 grade pipelines that have 273*mm* outer diameter and 9.3*mm* thickness under the unconstrained, smooth, cylindrical dent condition. The dent depths after removal of indenter are 26%, 28%, 20%, 12% and 20% of the pipeline diameter exceeding the dent depth criteria of ASME B31.8 (2014), EPRG (Roovers et al. 1999) and PDAM (Cosham et al. 2004). Just one case in these five tests is suitable for this research and the detail information is listed in Table 6.5. According to the test result, the burst occurred away from the dent and the burst pressure was 42 MPa.

2.6. The Existing Models for Burst Pressure of a Dent

To date, there is no empirical formula to accurately and efficiently predict the burst pressure of pipelines with a dent. However, there are guidelines for dent depth and strain, and a model that can estimate the reduction factor of pipeline capacity and the degree of damage due to a dent has been proposed.

Orynyak et al. (1999, 2004) proposed a theoretical evaluation model based on the plastic hinge mechanism for a pipeline with a dent. The proposed model was developed based on the assumption that the dent is an infinite symmetric dent to the longitudinal direction as shown in Figure 2.3, which consequently estimates the capacity of the pipeline conservatively. According to Allouti et al. (2012), there are

83.3%, 87%, and 87.4% errors between the burst pressure calculated by the Orynyak model and the experimental results.

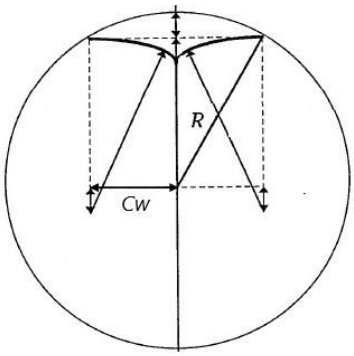

Figure 2.3 Indentation shape of Orynyak's model (Orynyak 2001).

In the Figure 2.3, *R* is the outer pipeline radius and C_w is the half width of dent.

The proposed reduction factor (α) is expressed as a function of the nondimensional number β as follows (2.3):

$$\alpha = \sqrt{\beta^4 + 1} - \beta^2 \tag{2.3}$$

Where

$$\beta = \frac{C_w}{\sqrt{Rt}}$$

Therefore, the equation (2.3) can be rewritten as follows (2.4):

$$P_O = \alpha \times \frac{\sigma_{UTS} \times t}{R} \tag{2.4}$$

Wu et al. (2016) studied the damage level with ellipsoidal dent using the Oyane ductile fracture criterion (Oyane et al. 1980) based on the plasticity theory of porous materials. The degree of damage is defined in terms of the integral value *I*, and the value of *I* equal to one means the ductile fracture of the material (Allouti et al. 2012). A new cumulative damage assessment model derived from the nonlinear regression analysis using FEA results has been proposed, it is stated to be very limited. The proposed models are expressed as follows (2.5~2.7) depending on the

conditions:

(a) Using dent depth (d) and internal pressure of pipeline (P)

$$I = -0.0345 + 0.0145P + 0.0043d^{0.5}\ln(d) \quad (2.5)$$

(b) Using dent depth (d) and the ratio of minor axix (a) to major axis (b) of ellipsoidal indenter

$$I = 0.0222\left(\frac{a}{b}\right)^{-0.1} d^{0.53} \ for\ \frac{a}{b} = 0.3 \text{ or } 0.45\ (b = 200mm) \quad (2.6.a)$$

$$I = -0.048 + 0.02\left(\frac{a}{b}\right) + 0.035d^{0.44} \ for\ \frac{a}{b} = 0.3 \text{ or } 0.4\ (b = 300mm) \quad (2.6.b)$$

(c) Using dent depth (d) and the ratio of thickness (t) to outer diameter (D) of the pipeline

$$I = 79072\left(\frac{t}{D}\right)^{4.47} + 0.017d^{0.56} \quad (2.7)$$

2.7. Determination of Pipeline Failure Using FEA

The burst pressure of a pipeline refers to the internal pressure that causes a pipe to burst or fracture. Accurate prediction of the burst pressure is critical for pipeline design and safe operation. It is usually achieved by using analytical and empirical formulae derived from theoretical, numerical and experimental methods. Therefore, in order to be able to define or develop an accurate formula for burst pressure over a range of pipeline geometries and materials, a large and representative set of experimental data is required. However, pipeline burst experiments can be expensive and time consuming to conduct. Hence, researchers use numerical methods to determine the burst pressure of pipelines; the most commonly used of which is nonlinear Finite Element Analysis (FEA).

2.7.1. Material Model for FEA

In order to perform nonlinear FEA, a material model should be defined, and the widely used is a multi-linear material model using a stress-strain curve derived from a material coupon test. However, this method has the disadvantage in terms of the time and cost effectiveness. Therefore, the next preferable method is using a Bilinear Elasto-Plastic (BEP) material model, but a BEP material model also cannot be defined if there is no strain value at the Ultimate Tensile Strength (UTS). Thus, some researchers use a failure-strain value or even an Elastic-Perfectly Plastic (EPP) material model with a tangent modulus of zero if it is not available, which is rougher than using a BEP material model (MacDonald 2007).

Ramberg et al. (1943) presented a simple equation as known as Ramberg-Osgood equation to describe the stress-strain curve. However, to obtain the strain at UTS using Ramberg-Osgood material model, it is necessary to determine the constants depending on the applied material. That means even using Ramberg-Osgood equation, it is impossible to get the strain at UTS without sufficient material data. Therefore, in order to reasonably define the tangent modulus for a BEP material model, it is needed to develop a method, which can calculate the strain at the UTS based on the material coupon test data.

2.7.2. Stress-Based Approach and Strain-Based Approach

One of the significant factors to evaluate the FEA results carried out to assess the structural integrity of the dented pipeline is to select whether a stress-based approach or strain-based approach.

Lower (2014) discussed that the stress-based approach is a conventional evaluation method and mainly focusing on the allowable strength, which is the SMYS or strength multiplied by a factor less than one. This method follows Hooke's law and the design margin using this method is defined as the difference between the allowance and SMYS. This method does not take into account the strain hardening effect, resulting in conservative and costly inefficient designs. On the other hand, the strain-based approach considers the strain hardening effect and evaluates strain

demand and strain capacity of the material. The strain corresponding the design load must be smaller than the allowable strain, and the difference between the allowable strain and the ultimate strain corresponding to the ultimate stress obtained from the material test results is the design margin. This approach has the advantage of making full use of the material capacity, which makes it economical to design.

2.7.3. Finite Element Modelling

Most researchers have used a similar method for performing the pipeline structural strength finite element analysis. Before the finite element analysis technique developed like today, usually, a shell element was mainly used, and nowadays, it is very general to use a solid element due to the development of related technologies.

For the simulation of the dented pipeline using FEA, Allouti et al. (2012) and Liu et al. (2017) conducted a nonlinear FEA and employed a quarter of pipeline model using C3D8R solid element with the material model composed of true stress-strain data.

Shuai et al. (2018) have performed a nonlinear FEA to estimate the burst pressure of dented pipeline. A solid element was used to model a quarter of the pipeline, and contact elements were applied to the area where the indenter and the pipeline surface are contacted. TARG170 and CONTA174 elements were used for the contact area of indenter and the contact area of the pipeline surface, respectively. For this analysis, true stress-strain curve obtained by Ramberg-Osgood model was employed as a material model.

Wu et al. (2015) carried out the FEA to estimate the displacement of the dented pipeline using the shell 181 element based on the thin shell structure. Using the shell element can reduce the computation time but it is impossible to evaluate the stress distribution collinear with thickness direction. Wu et al. (2012) have carried out a simulation of a dented pipeline using shell 63 element for a half model of pipeline.

Deolia et al. (2016) carried out to predict the burst pressure of flawless pipelines using the shell element (Tria3) and material model derived by Ramberg-Osgood equation.

Kulkarni et al. (2015) determined the burst pressure of Liquid Petroleum Gas cylinder through FEA. Carrying out this nonlinear analysis, 2D solid element (Plane 42) was employed and applied the axisymmetric model of the vessel.

2.8. Determination of Pipeline Failure Using ANN

Deep Neural Network is defined as the neural networks that have two or more hidden layers (Nielsen 2015). In addition, DNN is on the basis of ANN algorithm and is a method amongst various machine learning methods.

2.8.1. Application of DNN to Evaluate Structural Integrity of Pipelines

Limited research has been conducted on the burst pressure of pipelines with defects using ANN, and (to date) there are no studies on the burst pressure prediction of pipelines with a dent using ANN. Xu et al. (2017) applied an ANN to predict the burst pressure of corroded API X80 subsea pipelines. In this research, they used the feed-forward neural network (FNN) with a back-propagation algorithm combined with the gradient descent rule. The ratio of *training*, *validation*, and *test dataset* were set at 70%, 15%, and 15%, respectively. They concluded that the ANN predicted the burst pressure of corroded pipelines more accurately than two of the codified corrosion assessment methodologies (ASME 2012, DNV 2008).

Liu et al. (2019) also investigated the application of ANN for the prediction of the failure pressure of API X80 pipes with corrosion defects. They applied multilayer FNN with a back-propagation algorithm and the ratio of *training*, *validation*, and *test dataset* to a total dataset of the ANN model were 76%, 12%, and 12%, respectively. They also concluded that the ANN model predicted more accurate results than ASME B31G (2012), API 579 (2016) and DNV-RP-F101 (2008).

2.8.2. Activation Function

In addition, it needs to review the activation functions in the neural networks. One of the most important factors in neural network to obtain the best results is the selection of a suitable activation function based on the understanding of the pros and cons (Pedamonti 2018).

The purpose of the use of activation functions is to calculate the weight and bias to minimize the errors in the output and decides the activation of the neuron based on the calculated weight and bias. The use of activation function can impart nonlinearity to the output of neurons. There are many papers and articles regarding the advantages, disadvantages, and comparison of the activation function.

Nwankpa et al. (2018) investigated 21 activation functions applicable in deep learning and summarized the advantages, disadvantages, and the trend of actually using the activation function compared to the latest research. And, they classified the activation functions in the form of representative function like rectified linear unit (ReLU) (Nair et al. 2010), Sigmoid, and exponential linear unit (ELU) (Clevert et al. 2015) with variants. The ReLU category includes Leaky ReLU (LReLU) (Maas et al. 2013), Parametric Rectified Linear Units (PReLU) (He et al. 2015), Randomized Leaky ReLU (RReLU) (Xu et al. 2015) and S-shaped ReLU (SReLU) (Jin et al. 2015). The Sigmoid category is consisted of Sigmoid-Weighted Linear Units (SiLU) (Elfwing et al. 2017) and Derivative of Sigmoid-Weighted Linear Units (dSiLU) (Elfwing et al. 2017). The ELU category has the Parametric Exponential Linear Unit (PeLU) (Trottier et al. 2017) and scaled exponential linear unit (SeLU) (Klambauer et al. 2017).

In addition, Pedamonti (2018) presented the non-linear activation function for DNN on the modified national institute of standard and technology (MNIST). In here, the Sigmoid, ReLU and the variants of ReLU such as LReLU, ELU, and SeLU were compared. As mentioned above, there are many activation functions and amongst them, ReLU is one of the best activation functions to carry out the DNN.

Cent et al. (2018) concluded that ReLU is the best activation function after reviewing 10 activation functions. Pedamonti (2018) mentioned that ReLU is a better neuron replacing Sigmoid function.

2.9. Summary

In this chapter, many papers reviewed regarding the definition of the burst pressure, burst pressure prediction and evaluation method for flawless pipelines and pipelines with a dent, and application of the deep neural network.

Based on this review of the effects of dents, dents are not the main factor immediately threatening the structural integrity of the pipeline, and experimental results support it. However, pipeline dents can be a potential threat to cause pipeline incidents, so it is necessary to evaluate the dented pipeline precisely to prevent incidents caused by dents.

There are two ways to evaluate the structural integrity of pipelines. One is the dent depth-based calculation method, the other is strain-based calculation method. The strain-based calculation method is more complex to use than dent depth-based calculation method and is not suitable for achieving the objective of developing a practical and easy-to-use method. On the other hand, in the case of dent depth-based calculation method, this method is more straightforward than the strain-based calculation method, but the assessment criteria for dents have focused on the limit of the acceptance of dent depth or strain, and there is no empirical formula to accurately and efficiently predict the burst pressure of pipelines with a plain dent.

For the prediction of burst pressure of the flawless pipeline, 21 equations are reviewed and the review results showed that there is no single formula that was accurately able to predict the burst pressure over the range of the experiments performed.

Although there is no empirical formula to accurately and efficiently predict the burst pressure of pipelines with a dent, there are dent depth criteria from the

standards and regulations. In addition, models have been proposed to estimate the reduction factor of pipeline capacity and the degree of damage. However, mentioned above methods do not work well for the estimation of the dented pipeline.

There have been limited studies on the burst pressure of pipelines with defects using ANN, but no studies have been published on the burst pressure prediction of pipelines with a dent using ANN. And, after reviewing the various activation functions, it is concluded that ReLU is one of the best activation functions to carry out the DNN.

Consequently, it is necessary to develop the validated, pragmatic and usable burst pressure prediction models for the flawless pipelines and pipelines with a dent, and it is also worth developing an ANN model.

CHAPTER 3

3. METHODOLOGY

In this chapter, the methodologies that have been used to determine the burst pressure of both flawless pipelines and pipelines with an unconstrained, plain dent are presented. The first section (Section 3.1) describes the Finite Element Methodology and the second section (Section 3.2) describes the Deep Neural Network approach.

3.1. Finite Element Analysis

There are various numerical methods such as Finite Element Method (FEM), Boundary Element Method (BEM), Finite Difference Method (FDM), Finite Volume Method (FVM), etc., among which FEM can easily handle complex geometry, complex restrains, complex loading and a variety of engineering problems such as solid mechanics, dynamics, Fluids (De Weck et al. 2004). Therefore, FEM, which is one of the reasonable and useful methods, is used widely to solve the problem by idealizing and simplifying the problem of reality into an engineering problem.

The Finite Element Analysis (FEA) refers to a computer simulation process used in engineering analysis, and solves a problem using the FEM that is a numerical method to solve a structure or continuum problem through discretization. In structural analysis, a deformation and stress are calculated for a force, and the following equation (3.1) is used:

$$[K]\{u\} = \{F\} \tag{3.1}$$

Where *K* is a property (stiffness), *u* is a behaviour (displacement), and *F* is an action (force).

In this research, the commercial software ANSYS Mechanical APDL versions 17.1 is employed to carry out the pre-processing, solving and post-processing of nonlinear FEA for the flawless pipelines and pipelines with a dent.

3.1.1. Definition of Burst Pressure Criteria

In the numerical method perspective, how to determine the limit load is important. For a long time, a number of researches have been conducted on the limit load criteria, and the papers have been published. The differences between the reviewed limit load criteria are illustrated on schematic loading plots presented in Figure 3.1 (a-d).

Figure 3.1 (a) presents the strain-based criterion. In the 1% plastic strain criterion proposed by Townley et al. (1971), the limit load is defined as the load that induces a plastic strain of 1% in the material. Save (1972) suggested the tangent intersection criterion i.e. the limit is represented by the load at the intersection between tangents of the elastic and plastic parts of the loading-deformation curve. The limit load in the thrice δ criterion (Schroeder 1985) is defined as the load where its deformation reaches three times the tangent intersection load proposed by Save (1972).

Several criteria are included in ASME codes (1971, 1974, 1986) and they are the 0.2% offset strain, twice elastic deformation and twice elastic slope criterion, respectively. The limit load for the 0.2% offset strain criterion is given by the load corresponding to the intersection of the line parallel to the elastic slope at the plastic strain of 0.2% and the stress-strain curve as shown in Figure 3.1 (a). The twice elastic deformation criterion defines the limit load as the load at the point where the magnitude of the deformation is twice the elastic deformation at yield whilst the load at the intersection point between the twice elastic slope line and the load-deformation curve is defined as the limit load in the twice elastic slope criterion as shown in Figure 3.1 (b). The triple elastic slope criterion defined by Demir and Drucker (1963) is similar to the twice elastic slope criterion but with the limit load defined at three times of the elastic slope at yield. Based on a similar concept,

Kirkwood (1986, 1989) proposed a five times elastic slope criterion whilst a fifteen times elastic slope criterion was defined by Lynch and Moffat (2000) as shown in Figure 3.1 (b).

It can be seen in Figure 3.1 (c) and (d) that there are two methods proposed as part of the zero curvature criterion (Zhang et al. 1989). If the tangent value at the inflection point is not zero as shown in Figure 3.1 (c), the limit load is determined according to the tangent intersection criterion. When the tangent value at the inflection point is zero as shown in Figure 3.1 (d), the limit load is the load corresponding to the inflection point on the load-deformation curve.

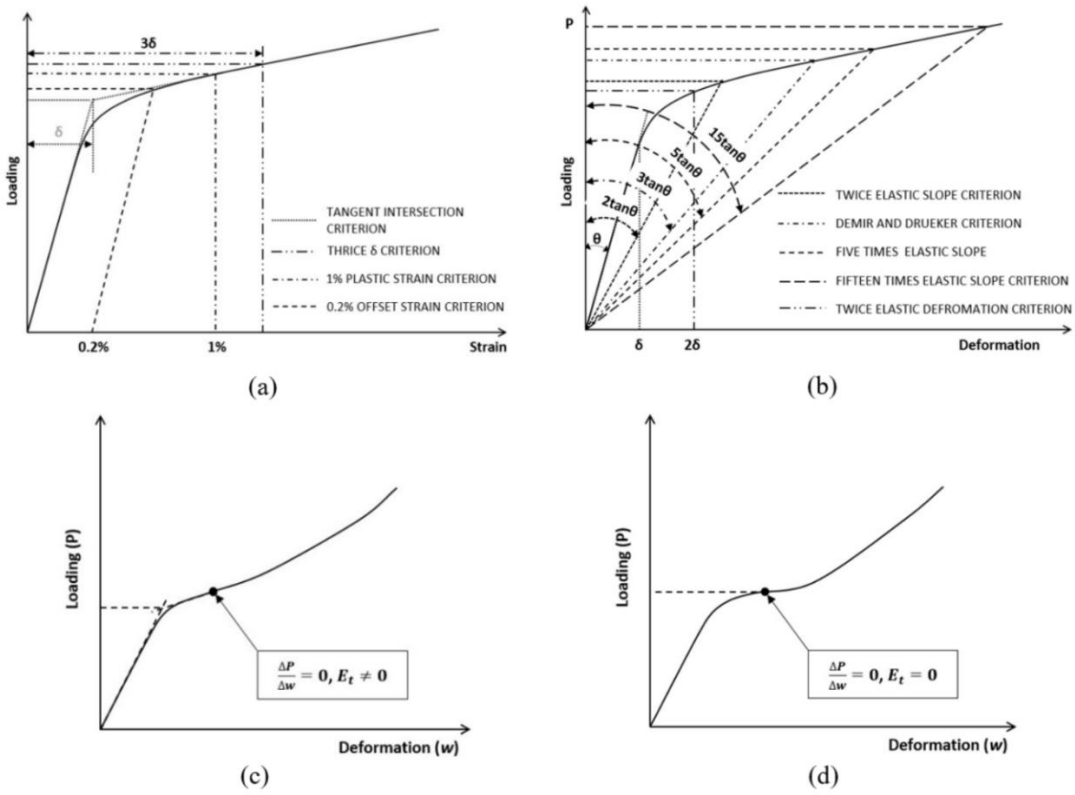

Figure 3.1 Criteria for limit load estimation: (a) tangent intersection and strain based criteria, (b) elastic slope and deformation based criteria, (c) zero curvature criterion with non-zero tangent value at the inflection point, (d) zero curvature criterion with tangent value at the inflection point.

Chen et al. (2016) assessed the aforementioned limit load criteria by performing nonlinear FEA on a pressure vessel using an elastic perfectly plastic material model.

The predictions using the different failure criteria outlined above were compared with the burst pressure results of the experiment. It was found that, in the majority of cases, the burst pressure was overestimated by the limit load predictions. In addition, it is observed from the current work that some complicated post-processing work, such as locating an intersection point, is required for most of these criteria in order to find the limit load.

Therefore, it can be concluded that, in order to be able to develop an empirical formula for predicting burst pressures of pipelines using numerical techniques, such as FEA, an objective method for determining the limit load is required.

In this research the limit load or burst pressure is defined differently depending on the presence or absence of defects in the pipeline. This is to take a more conservative approach for the flawless pipeline to take into account the design margin for burst pressure, and in the case of a dented pipeline, a more precise approach to take into account the limit state of the structure.

Thus, the limit load or burst pressure of flawless pipelines is defined as the pressure that corresponds to be a point when the maximum von-Mises equivalent stress of just one node of the numerical model reaches the ultimate tensile strength (UTS). The reason for selecting just one node and using the UTS of the material to define the burst pressure is to reflect the conservative approach, and the practical approach considering strain-hardening effects.

On the other hand, the burst pressure of dented pipelines is defined as the load when the von-Mises equivalent stress at all nodes arranged collinearly along the thickness direction of the numerical model reaches the UTS of the applied material (see the white dotted line in Figure 3.2), where the grey colour means that the stress level is more than the ultimate tensile strength of the material applied.

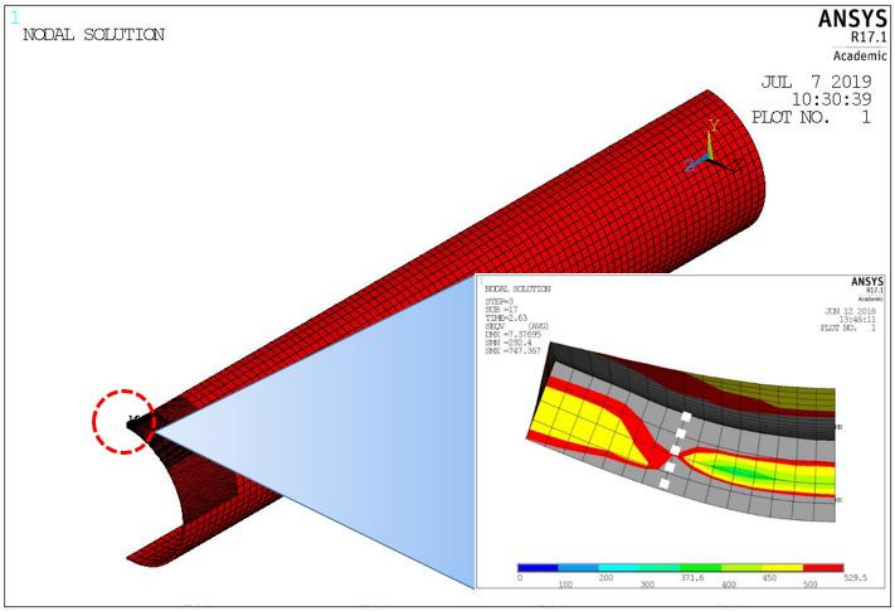

Figure 3.2 Definition of the burst pressure for the pipelines with a dent.

3.1.2. Definition of Material Model

As discussed in Section 2.7.1, the selection of an appropriate material model, i.e. stress-strain curve is critical if reliable and accurate nonlinear FEA results are to be obtained. Ideally, an actual stress-strain curve derived from a tensile test of the material being represented by the model should be used. However, this information may not be available at the early design stage and it may be expensive and time consuming to perform a material coupon test from the actual component. In practice, the bilinear material model or elastic-perfectly plastic material model are generally assumed in nonlinear FEA. In both models, two linear lines represent the elastic region and the plastic region. The slopes of the lines are known as the Young's modulus (E) and tangent modulus (E_t), respectively, as shown in Figure 3.3. The issue with the elastic perfectly plastic material model is that the strain hardening effect is not considered and thus it usually produces a fairly conservative result. A bilinear material model, as shown in Figure 3.3, which considers strain hardening is therefore proposed in this study.

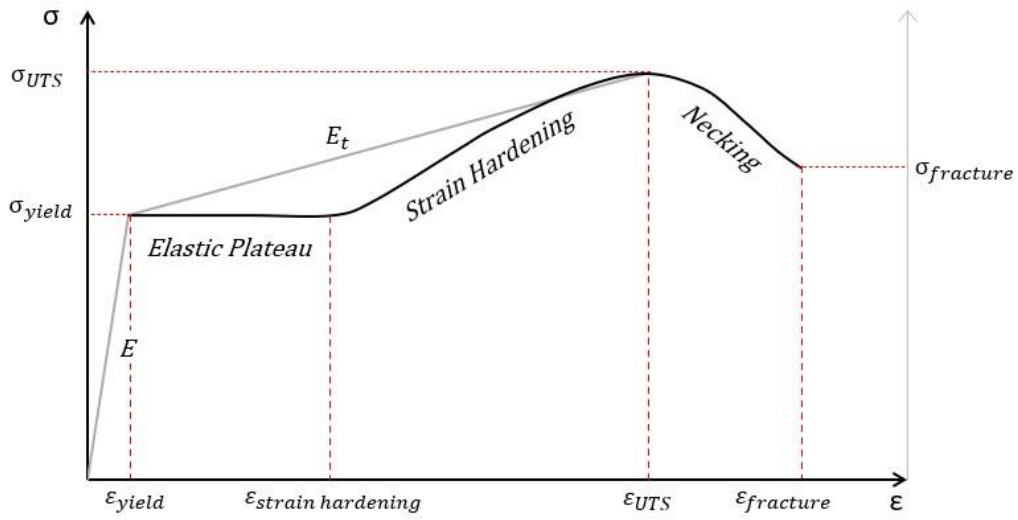

Figure 3.3 Typical Stress-Strain curve of carbon steel and bilinear material model for FEA.

For the plastic region, E_t is defined by the following formula (3.2):

$$E_t = \frac{\sigma_{UTS} - \sigma_{yield}}{\varepsilon_{UTS} - \varepsilon_{yield}} \tag{3.2}$$

where ε_{yield} and ε_{UTS} are the strain at yield strength (σ_{yield}) and UTS (σ_{UTS}). The values for σ_{UTS}, σ_{yield} and ε_{yield} can be readily obtained for different pipeline materials. However, the ε_{UTS} is usually not readily available and can only be obtained from an experimental stress-strain curve data. For this reason, MacDonald (2007) mentioned the use of $\varepsilon_{fracture}$ instead of ε_{UTS} to calculate the E_t using the formula presented in formula (3.3):

$$E_t = \frac{\sigma_{UTS} - \sigma_{yield}}{\varepsilon_{fracture} - \varepsilon_{yield}} \tag{3.3}$$

where $\varepsilon_{fracture}$ is the strain at fracture. However, it can be seen from Figure 3.3 that $\varepsilon_{fracture}$ is usually larger than ε_{UTS} for pipeline materials. Thus, the tangent modulus E_t is underestimated if formula (3.3) is used.

In this research, a procedure for deriving an empirical formula to estimate the strain at UTS has been developed and is described in Figure 3.4.

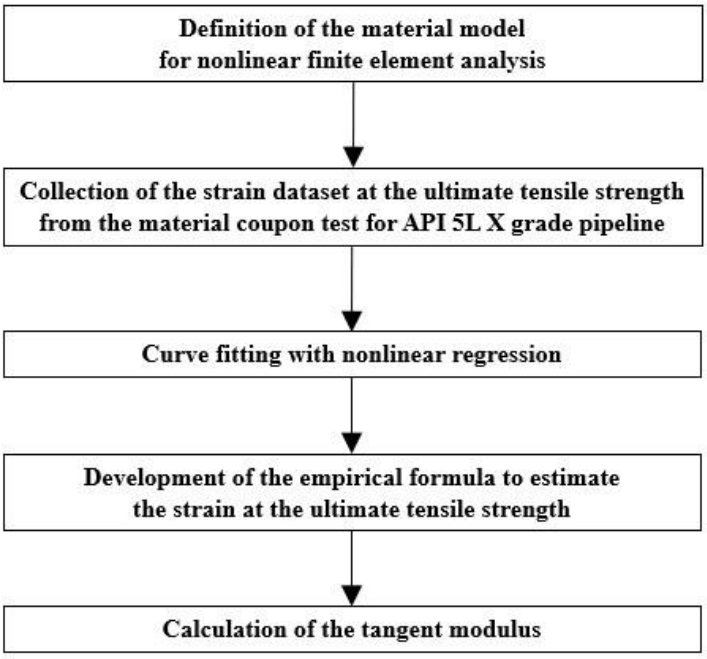

Figure 3.4 Procedure for the development of an empirical formula to estimate the strain at Ultimate Tensile Strength of pipelines.

In this study, a dataset of measurements of strain at UTS from material coupon test data for API 5L X52, X65, X70 and X80 grade pipeline has been used to derive an empirical formula to estimate ε_{UTS} using curve fitting with linear regression (Figure 3.5). The following exponential function (3.4) is assumed to predict ε_{UTS}:

$$\varepsilon_{UTS} = C_1 \times e^{-C_2 \omega} \tag{3.4}$$

where C_1 (=63.137) and C_2 (=2.574) are the fit coefficients, and ω is the σ_{yield} to σ_{UTS} ratio.

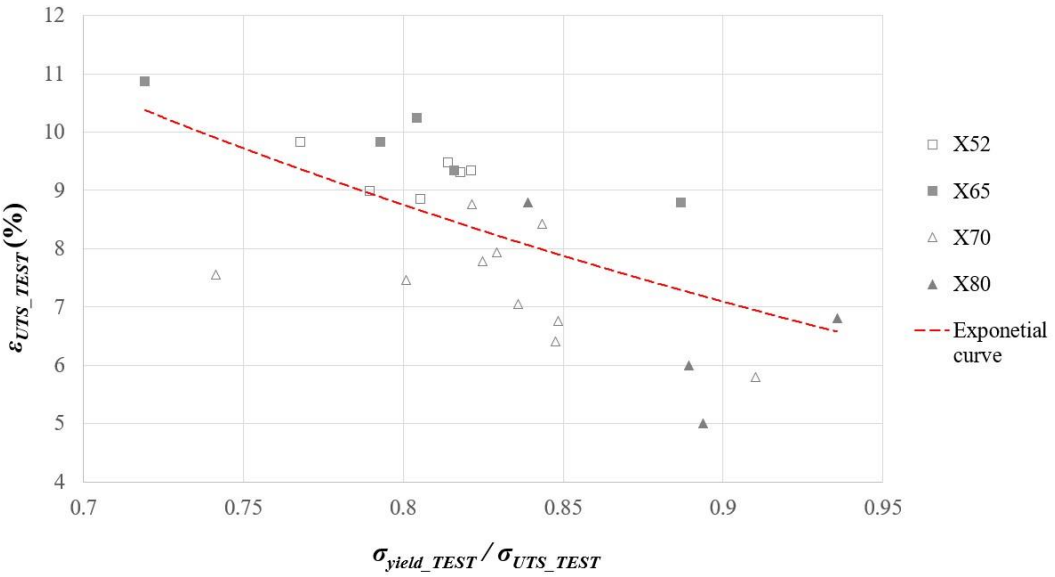

Figure 3.5 Material coupon test data plot and best-fit exponential curve using ε_{UTS_TEST} and the ratio of σ_{yield_TEST} to σ_{UTS_TEST}.

To validate the proposed formula, the Pearson Product-Moment Correlation Coefficient (PPMCC) was employed. The PPMCC is commonly used as a measure of the linear relationship between two quantitative variables and is calculated by the following formula (3.5):

$$PPMCC\ (r) = \frac{\sum(x - \bar{x})(y - \bar{y})}{\sqrt{\sum(x - \bar{x})^2 \sum(y - \bar{y})^2}} \tag{3.5}$$

Where x and y are the strain calculated by the proposed formula and from the material coupon test respectively and $\bar{x}$ and $\bar{y}$ are the average values of x and y groups of values, respectively.

Evans (1996) proposed guidance for the strength of the correlation expressed by the limit of the absolute *r*-value as shown in Table 3.1.

Table 3.1 The guidance for the strength of the correlation by Evans (1996).

Limit	Strength
0.00 – 0.19	very weak
0.20 – 0.39	weak
0.40 – 0.59	moderate
0.60 – 0.79	strong
0.80 – 1.00	very strong

Next, the *t*-value was calculated based on formula (3.6):

$$t_v = \frac{r\sqrt{n^* - 2}}{\sqrt{1 - r^2}} \tag{3.6}$$

Where t_v is the *t*-value and n^* is the number of observations (in here, n^* is 25).

According to the correlation analysis, as shown in Figure 3.6, the PPMCC between the strain calculated by the proposed formula and the strain from the material coupon test is 0.675 and the *t*-value is 4.39. The probability value ($P\_{probability}$) for a two-tailed test obtained by applying n^*-2 degree of freedom (=23) to the *t* distribution function in the Excel program is 0.0002, which is less than the 0.001 significance level (=99.9% confidence). Hence, the null hypothesis that there is no statistically significant relationship between the strain calculated by the proposed formula and strain obtained from the material coupon test (PPMCC=0) is rejected. Therefore, the relationship between the strain calculated by the proposed formula and from the material coupon test is statistically significant with r (23) = .675, and $P\_{probability} < .001$. In addition, the correlation strength is strong in accordance with Table 3.1.

Consequently, it can be concluded that the ε_{UTS} can be calculated using formula (3.4) for API 5L X-grade pipeline steels from X52 to X80, and that the tangent modulus E_t can be calculated by using formula (3.2) to consider the strain hardening effect. This bilinear material model, derived from the proposed methodology, is

used for nonlinear FEA in this study. The advantage of the proposed method is that it is possible to determine the strain at UTS using the basic material information of σ_{yield} to σ_{UTS} ratio. Consequently, the bilinear stress-strain model may be estimated without the need to perform the tensile tests, which may save time and cost at the early design stage.

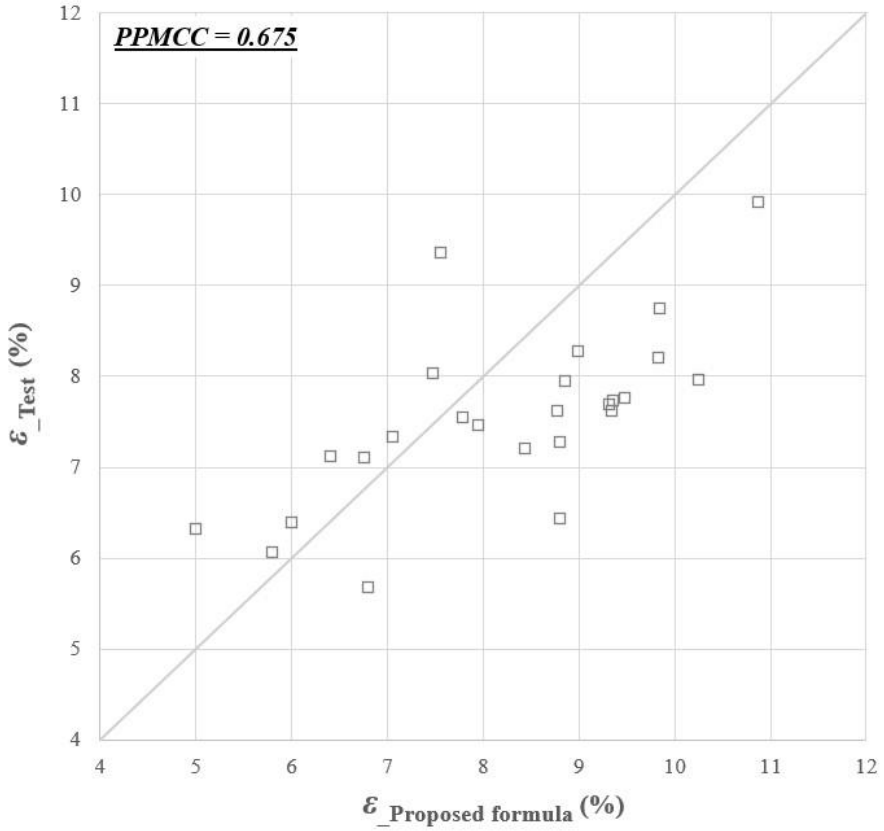

Figure 3.6 Pearson Product-Moment Correlation Coefficient between the strain calculated by the proposed formula and the strain from the material coupon test.

3.1.3. Determining Burst Pressure Using FEA

The bilinear material model as described in Section 3.1.2 is used in the FEA analysis as follows. Firstly, ε_{UTS} was estimated from the derived formula (3.4) and used to calculate the tangent modulus in order to consider the strain hardening effect in the plastic region.

The burst pressure is defined as the pressure that corresponds to be a point when the maximum von-Mises equivalent stress, determined using FEA, reaches the UTS at any node. Figure 3.7 depicts the plot of the von-Mises equivalent stress against the applied pressures from the FEA results. According to the burst pressure criterion defined in Section 3.1.1, the stress values determined before and after the UTS, indicated by the dotted circle in Figure 3.7 are used to obtain the burst pressure through linear interpolation or extrapolation of the UTS value.

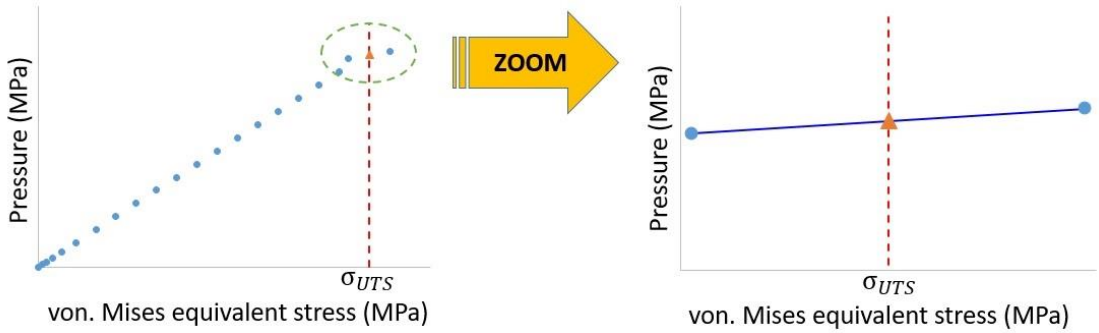

Figure 3.7 Determining busrt pressure of pipelines using Finite Element Analysis results.

3.1.4. Development of FEA Model for Flawless Pipelines.

The static nonlinear analysis for flawless pipelines under internal pressure is performed, and the following sections describe the setup of the ANSYS model used to perform the parametric study.

3.1.4.1. Geometric Information and Material Property

The geometric information and material properties for API X70 model used in the set-up of FEA are shown in Table 3.2 and Table 3.3, respectively.

Table 3.2 Geometric information of API X70 for the set-up of FEA model.

Outer diameter (mm)	Thickness (mm)	Model length (mm)
762	15.9	5 times of outer diameter (=3810)

Table 3.3 Material properties of API X70 for the set-up of FEA model (API 2004).

Young's modulus (MPa)	Tangent modulus (MPa)	Poisson's ratio	Yield strength (MPa)	Ultimate tensile Strength (MPa)
207,000	1220.1	0.3	482.63	565.37

3.1.4.2. Material Model

The bilinear material model as described in Section 3.1.2 is used in the FEA as follows. Firstly, ε_{UTS} was estimated from the derived formula (3.4) and used to calculate the tangent modulus in order to consider the strain hardening effect in the plastic region. The calculated tangent modulus is 1220.1 MPa as shown in Table 3.3.

3.1.4.3. Definition of Finite Element Type

The Plane 183 element has been selected to model the pipeline for two reasons. Firstly, this element can support axisymmetric analysis, that is, by using this element, the number of elements required to model the pipeline and the consequent computing time can be reduced. Secondly, this higher order 2-D and 8-node element can provide more accurate results than Plane 42 element.

3.1.4.4. Applied Loading and Boundary Condition

The applied loading and boundary conditions are shown in Figure 3.8. As a load condition, the internal pressure acts on the inside of the pipeline and is increased incrementally. Axisymmetry and symmetry boundary conditions are considered to simplify the model. First, the longitudinal direction of FE model should coincide with the global Y-axis to apply the axisymmetry boundary condition. In addition, it is assumed that the pipeline is a very long, thin-walled pipeline, so the shrinkage of the longitudinal direction due to the Poisson's ratio is negligible. For the above

reason, the symmetry boundary condition has been applied to both ends of the pipeline FE model.

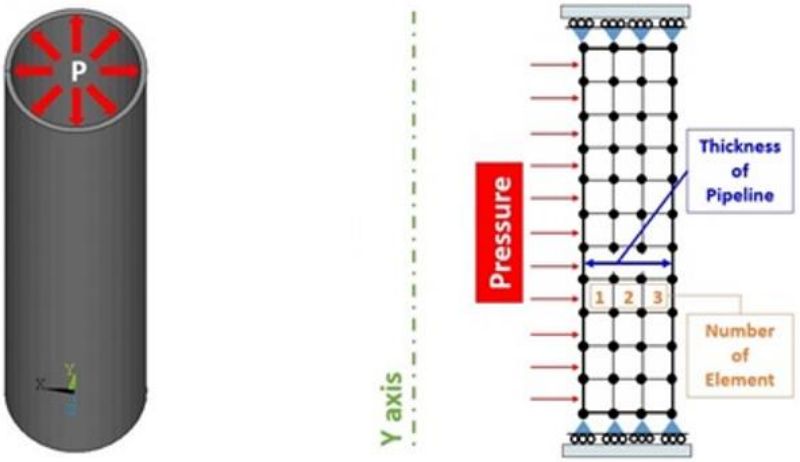

(a) (b)

Figure 3.8 Mesh size, loading and boundary condition of Finite Element Analysis model of flawless Pipeline: (a) loading condition, (b) mesh size, loading condition and boundary condition.

3.1.4.5. Convergence Study for Mesh Size and Model Length

A convergence study was conducted to identify the optimum number of elements in the model through the wall thickness as shown in Figure 3.8 (b). Four different models were created with between one and four elements in the pipe wall. The results for the von-Mises equivalent stress and the burst pressure for the four models at different number of elements are shown in Figure 3.9.

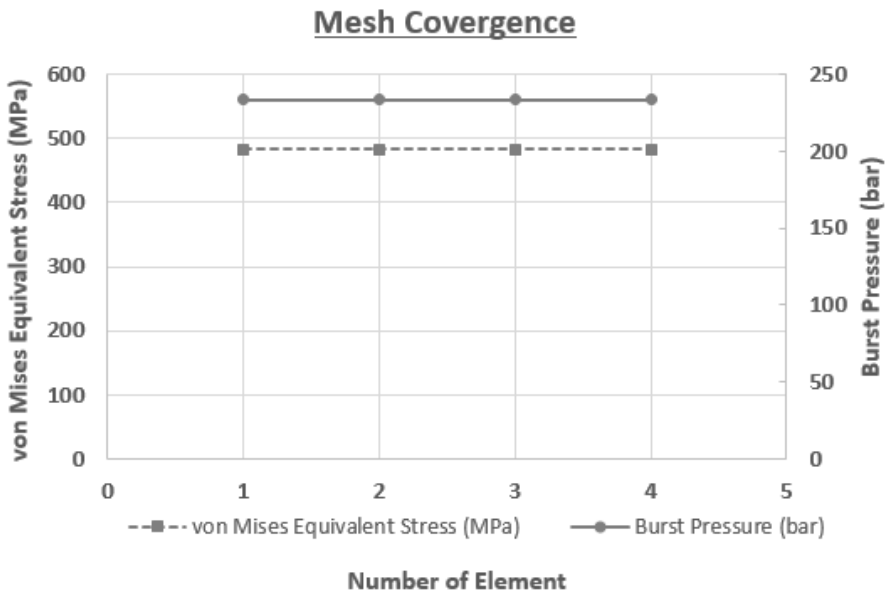

Figure 3.9 von-Mises equivalent stress and burst pressure according to the number of element.

It can be seen from this plot that the number of elements through the wall thickness does not affect the result. However, in order to be able to investigate the stress distribution through the wall thickness, three elements were chosen for this study.

In the case of FEA model length, it is recommended that at least one diameter of the pipeline should be included in the FE-model (DNV 2008). Consequently, the length of FEA model has conservatively been taken to be more than five times the pipeline outer diameter to avoid end effects.

3.1.5. Development of FEA Model for Pipelines with a Dent

3.1.5.1. Definition of Finite Element Type for Pipelines with a Dent

In order to perform a more accurate analysis, it is necessary to minimize the error when discretizing the target model geometry, which in turn leads to accurate results. SOLID186, a higher order 3D 20-node solid element, is an element with mid-nodes that can achieve a good mesh and eventually get more accurate results. Therefore, SOLID186 is selected for getting more precise answers.

In addition, to reduce the computational time, a fine mesh was applied to the area contacting the model with the indenter, and the mesh size was gradually increased in the other areas. Contact elements were applied to the surface between the indenter and the pipeline.

3.1.5.2. Applied Loading and Boundary Condition

As shown in Figure 3.10, the loading conditions for the nonlinear FEA of the burst pressure of pipelines with a dent are divided into three steps: indentation without internal pressure, removal of the indenter and application of internal pressure.

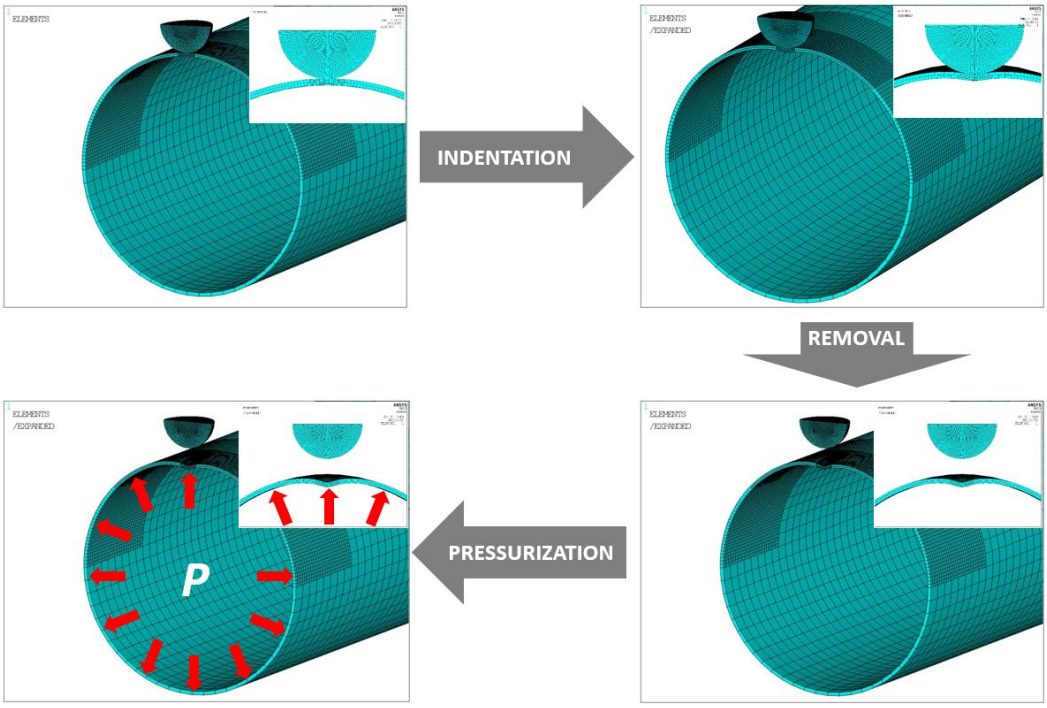

Figure 3.10 Loading condition of Finite Element Analysis model for the pipelines with a dent.

Firstly, the pipeline is indented to the depth specified as a ratio of the pipeline outer diameter to a dent depth and secondly, removal of the indenter step is for the situation where the dent generated in the pipeline is rebounding elastically. This elastic recovery involves rebounding from the spheroidal-shaped deformation of the pipeline section as well as the local rebound in the dent. Finally, the internal

pressure is applied to predict the burst pressure of the pipeline. The internal pressure is increased stepwise by a defined increment until the burst pressure is reached.

The boundary conditions at all the edges of the pipeline FEA model are selected based on the loading condition as seen in Table 3.4 and Figure 3.11. In addition, to minimize the FEA time, a ¼-symmetry model (Y-Z plane symmetry; X-Y plane symmetry at centre of model) as illustrated in Figure 3.11 was employed. If an indenter acts on the surface of a buried pipeline locally and then there will be no displacement at the end of the pipeline ($Ux=Uy=Uz=0$) due to the constraining effect of the backfill. In addition, it is expected that there is no displacement at the bottom of the pipeline due to the resistance of the soil ($Uy = 0$). However, when the internal pressure is applied globally, the end of the pipeline is expected to expand in the outward direction ($Uz = 0$).

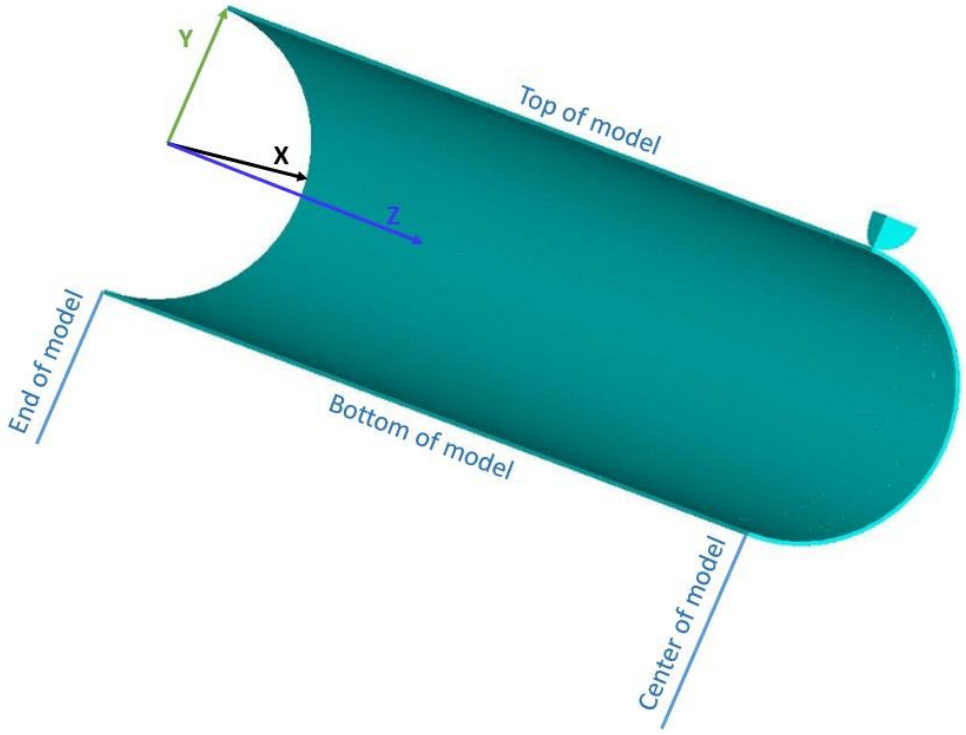

Figure 3.11 Boundary condition of Finite Element Analysis model for the pipelines with a dent.

Table 3.4 Boundary condition according to the loading condtion.

	Loading condition	End	Top, Center	Bottom
1	Indentation	All fixed (*Ux=Uy=Uz=0*)	Symmetry (*Ux=0, Uz=0*)	UY fixed + Symmetry (*Ux=Uy=0*)
2	Removal of the indenter	All fixed (*Ux=Uy=Uz=0*)	Symmetry (*Ux=0, Uz=0*)	UY fixed + Symmetry (*Ux=Uy=0*)
3	Application of internal pressure	Symmetry (*Uz=0*)	Symmetry (*Ux=0, Uz=0*)	UY fixed + Symmetry (*Ux=Uy=0*)

3.1.5.3. Convergence Study for Mesh Size and Model Length

Convergence studies were conducted to determine the optimum number of elements and model length for the nonlinear FEA model for pipelines with a dent. For verification, the dented pipeline was modelled with the material properties and geometric information from the FEA of a test model in API 1156 (Kiefner et al. 1997) (Table 3.5). The tangent modulus was defined using the formulae (3.2) and (3.4). A hemispherical indenter with a diameter of 219.075*mm* was used to construct an initial dent depth of 12% of the pipeline outer diameter.

Convergence studies were carried out for the number of elements and length of FE model. The number of elements under consideration was from one to eight in the thickness direction of the FEA model. The convergence of the FE model length was considered from 1.0 to 5.5 times of the pipeline diameter, and was examined while increasing by 0.5 times of the pipeline diameter.

As the results of convergence studies for the mesh size, the dent depth after removal of the indenter was almost the same regardless of the number of elements through the wall thickness between four and eight, so four was selected as the number of elements as shown in Figure 3.12 (a) below. In addition, based on the result of the number of elements, the convergence study regarding the model length for FEA was performed and a length multiplier of 5.5 was selected as shown in Figure 3.12 (b). This means that 5.5 times of the pipeline outer diameter is selected as the model length for FEA.

Table 3.5 Material properties and geometric information of Finite Element Analysis model from API 1156 (Kiefner et al. 1997).

Material properties						Geometric information	
Grade	Young's modulus (MPa)	Tangent modulus (MPa)	Poisson's ratio	Yield strength (MPa)	UTS (MPa)	Outer diameter (*mm*)	Thickness (*mm*)
X52	207,000	1550	0.3	371.60	529.50	323.85	4.7752

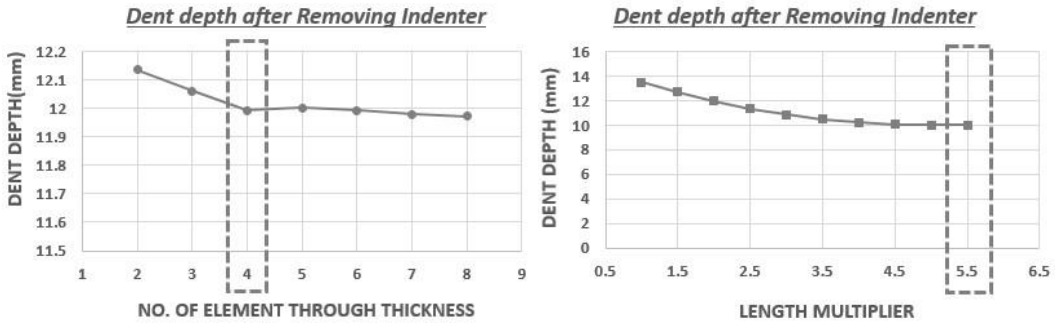

(a) (b)

Figure 3.12 Convergence study results of the mesh size and model length for Finite Element Analysis: (a) number of elements through thickness, (b) length multiplier.

Using the mesh size and FE model length derived above, the dent shape results from this study (Applied FEA) were compared with FEA results (API 1156 FEA) and test results (API 1156 TEST) from API 1156 (Kiefner et al. 1997) as illustrated in Figure 3.13.

From comparison of results, the maximum dent depth after indenter removal was 19.05*mm* for API 1156 FEA and API 1156 TEST and 20.75*mm* for Applied FEA. The dent depth from API 1156 FEA and TEST is 91.8% of the Applied FEA. From this result, it can be confirmed that the Applied FEA shows conservative results. In addition, the dent depth tendency is quite similar all together as shown in Figure 3.13, and it can be said that the selected loading and boundary conditions are appropriate for further research.

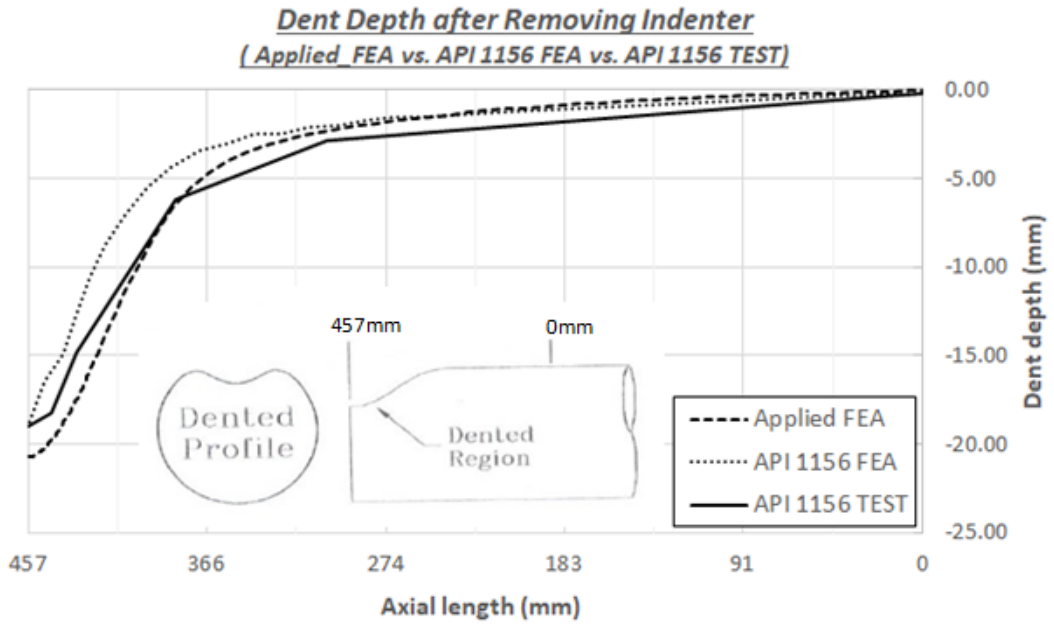

Figure 3.13 Comparison of the dent depth after removing indenter.

3.2. Deep Neural Network

Since artificial intelligence (AI) has a role as a key technology of the fourth industrial revolution, this state-of-the-art technology is used as a very popular and useful method in many areas. In addition, this phenomenon leads the robust growth of interest towards artificial neural network (ANN) that is an idea inspired from neural networks in the human brain and are one of the methods in machine learning. The relation between AI, machine learning and neural networks is shown in Figure 3.14 and the comparison to the biological neural network and the ANN is illustrated in Figure 3.15.

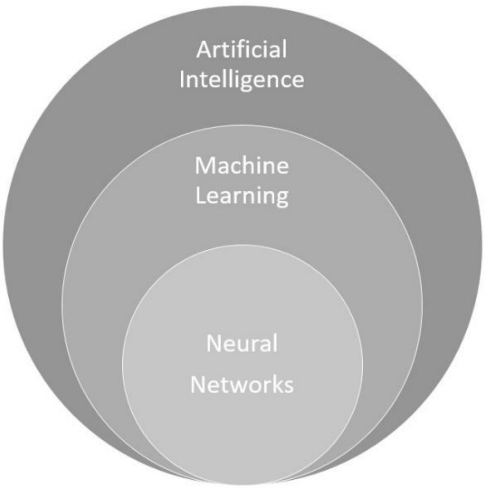

Figure 3.14 Relations between artificial intelligence, machine learning and neural networks.

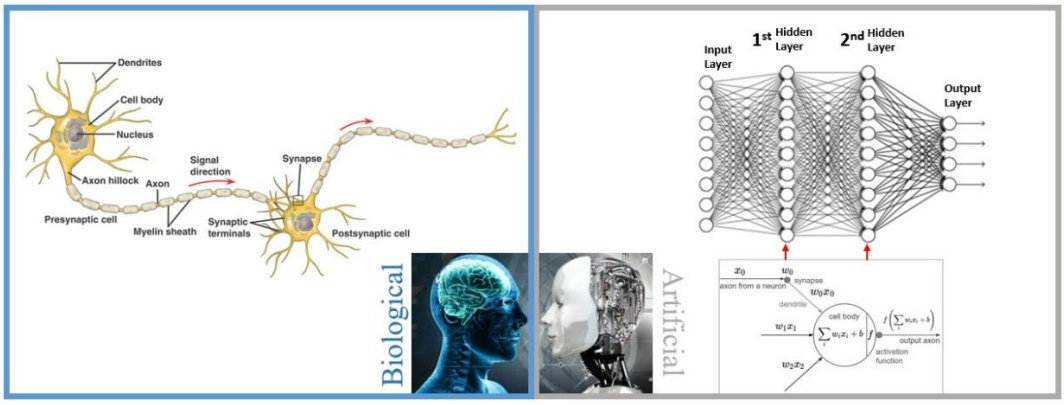

Figure 3.15 Comparison with biological neural network and artificial neural network.

Accordingly, the ANN is expected to be another solution to solve the problems relating to the pipelines.

A DNN, which is on the basis of ANN algorithm and is a method amongst various machine learning methods, is applied in this study. The application of DNN to the pipeline industry as a new solution to evaluate the structural integrity of pipelines with or without dent seems to be a worthwhile subject to review.

To develop the DNN model to predict the burst pressure of flawless pipelines, the dataset from the FEA based Parametric Study results and the results of experiments for the flawless pipeline are used for the *training*, *validation*, and *test dataset*.

In case of the pipelines with a dent, the DNN model to predict the burst pressure of pipelines with a dent is developed based on the dataset from the FEA based Parametric Study results for the hemispherical dent and the results of experiments. In addition, the developed DNN model for pipelines with a dent is employed to conduct the *test* against the dataset from the FEA based Parametric Study results and the result of the experiment of the pipelines with a spheroidal dent.

3.2.1. Development of Deep Neural Network

An ANN architecture as shown in Figure 3.16 is composed of an input layer, hidden layers and output layer. In particular, when there are two or more hidden layers, the neural network is termed a Deep Neural Network (DNN).

In here, the input layer is where the data comes in and the output layer is where the model infers. The hidden layer is located between input and output layers, because the output of one layer is to be the input of the next layer. In the hidden layer, a net input is calculated, and the net input produces the actual output through an activation function, then the output transfers to the next layer. In addition, the neural network has a form connected to each neuron by the weighted link, and the multi-layer perceptron that has multi-hidden layers between input layer and output layer is used widely.

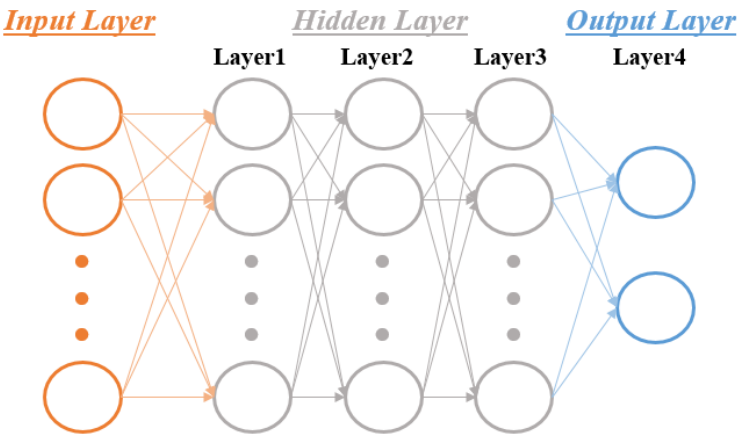

Figure 3.16 Diagram of the artificial neural networks.

In particular, the purpose of the use of activation functions is to calculate the weight (*w*) and bias (*b*) to minimize the errors in the output and decides the activation of the neuron based on the calculated weight and bias. The use of activation function (*f(Z)*) can impart nonlinearity to the output of neurons (P_o), and the relationship between the output of the neuron and the activation function is given in Equation (3.7).

$$P_O = f(Z(x)) = f\left(\sum_{i=1}^{N} w_i x_i + b\right) \tag{3.7}$$

Where $Z(x) = \sum_{i=1}^{N} w_i x_i + b$, x_i is input and *N* is the number of neurons in layer.

3.2.2. Deep Neural Network Architecture

Machine learning can be divided into supervised learning, unsupervised learning, and reinforcement learning. In this study, supervised learning is applied. In particular, it focuses on the DNN amongst supervised learning algorithms, and the neural network uses the fully connected layer.

3.2.2.1. Definition

It is necessary to define the terms used in research related to a DNN, and the definitions of the terms related to the DNN are as follows:

Supervised learning	an algorithm that learns with given correct answers. In this case, learning is conducted in a paired form (relationship) between input and output.
Unsupervised learning	an algorithm that learns without given correct answers. In this case, learning is conducted only by the input itself.

Reinforcement learning	a method of finding the optimal method by strengthening learning through trial and error after providing only an environment with a specific purpose or rule.
Fully connected layer	all node activations on one layer move to each and every node on the next layer
Hyper-Parameter	a value that is specified by the user before starting the machine learning process.
Training dataset	a dataset to train the model, adjust the parameters like weight and bias
Validation dataset	a dataset to evaluate a model that is fit on the training dataset while tuning model.
Test dataset	a dataset to evaluate a final model.
Weight	strength of the connection between nodes.

3.2.2.2. Activation Function

An activation function is used to determine whether the sum of the input causes activation or not. The widely used ReLU activation function in recent years is adopted as an activation function due to the benefits of this function like faster computation and avoiding the vanishing gradient problem (Cent et al. 2018, Pedamonti 2018, Kim et al. 2020). The ReLU activation function is expressed as an equation (3.8) and plotted as shown in Figure 3.17.

$$ReLU(x) = \begin{cases} max\ (0, x), & x \geq 0 \\ 0, & x < 0 \end{cases} \tag{3.8}$$

Where, *x* is the input to the neuron.

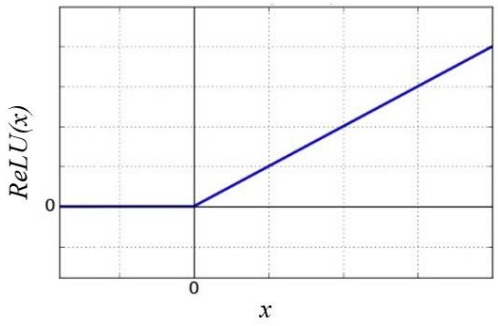

Figure 3.17 ReLU activation function.

3.2.2.3. Optimization

Furthermore, the broadly adopted and known as an alternative solution of the classical stochastic gradient descent method, Adam optimization algorithm (Kingma et al. 2015) was selected for the optimization of the weight and bias.

3.2.2.4. Weight Initialization

In addition, for the initiation of the weight, He initialization (He et al. 2015) was chosen, and this initialization method is widely known to be specialized for the ReLU function, and is the most popular method recently.

3.2.2.5. Cost Function

The cost function is used to measure the error of learning, that is, how well the neural network has learned the *training dataset*. In this study, the Mean Absolute Percentage Error (MAPE) that is commonly used to evaluate the accuracy of forecasting (Chen et al. 2003, Shen et al. 2009) is employed as the cost function. The MAPE formula (3.9) is given by as follows:

$$MAPE = \frac{100\%}{n^*} \sum_{i=1}^{n^*} \left| \frac{y_i - x_i}{y_i} \right| \tag{3.9}$$

Where x_i is the burst pressure calculated by learning and y_i is the burst pressure from the learning data.

The interpretation of MAPE results is based on the evaluation method proposed by Lewis (1982), and is explained in Table 3.6.

Table 3.6 The guidance for the interpreting of MAPE results by Lewis (1982).

MAPE	Interpretation
Less than 10%	Highly accurate
Between 10% and 20%	Good
Between 20% and 50%	Reasonable
Greater than 50%	Inaccurate

3.2.2.6. Feature Normalization

The scale of all features is needed be the same scale, and normalization is the method to make all features to be the same scale. In this study, MinMaxScaler has been adopted to normalise the features and this scaler can change the features to be between 0 and 1 using equation (3.10).

$$x_{norm} = \frac{x - x_{min}}{x_{max} - x_{min}} \tag{3.10}$$

Where x is a raw data (before normalization) from a feature and x_{norm}, x_{min} and x_{max} are the normalized data, maximum and minimum value of the feature, respectively.

3.2.2.7. Number of Neuron

The number of neurons in the hidden layer has been tuned by trial and error method. For the flawless pipelines, 124×64×8 neurons were set for 3 hidden layers, and for the dented pipeline, 64×16×4 neurons were set for 3 hidden layers. According to Panchal et al. (2014), the number of neurons in hidden layers might effect on the

overfitting or underfitting problem. To handle the overfitting problem, there are some ways like controlling the number of layers or neurons, regularization and dropout. In this research, the number of layers and neurons have been adjusted properly.

3.2.3. Application to Burst Pressure Prediction for Flawless and Dented Pipelines

The parametric study results described in chapter 4 and 5, and experimental results from open-sources are used to build DNN models to predict the burst pressure for flawless and dented pipelines. In addition, the considered parameters to develop the DNN model is described as follows:

(a) Flawless pipelines

For Input diameter, thickness, the ratio of outer diameter to thickness and UTS.

For Output the ratio of burst pressure to UTS of the pipeline material.

(b) Pipelines with a Dent

For Input diameter, thickness, dent depth, the ratio of dent depth to diameter, dent length after removal of indenter, the ratio of dent length after removal of indenter to diameter and UTS.

For Output the ratio of the burst pressure to UTS of the pipeline material.

3.2.3.1. Selection of Hyper-Parameters

Next, it needs to define hyper-parameters for the DNN model. Based on the above-mentioned functions and the defined hyper-parameter, the DNN model can be finally developed. In this study, the number of hidden layers, size of epoch, and learning rate are taken into account and the values are defined through the trade-off studies as listed in Table 3.7.

Table 3.7 Subject to trade-off studies for defining hyperparameters for flawless and dented pipelines.

Hyper-Parameters	Sample
Number of hidden layers	2, 3, and 4
Epoch size	10, 100, 1000, 2000, 3000, and 4000
Learning rate (10^{-3})	50, 10, 5, 1, 0.9, 0.8, 0.7, 0.6, 0.5, and 0.1

3.2.3.2. For Flawless Pipelines

(a) Number of Hidden Layers

The study of selecting the number of hidden layers in DNN model was targeted at two, three and four in the case of flawless pipelines. From the results of trade-off studies as seen in Figure 3.18, the MAPE for two, three and four hidden layers was 10.59%, 3.5% and 3.64%, respectively. According to Table 3.6, MAPE for two hidden layers indicates good accuracy, and three and four hidden layers are interpreted as highly accurate. Finally, three hidden layers with the lowest MAPE was observed were employed in the DNN model.

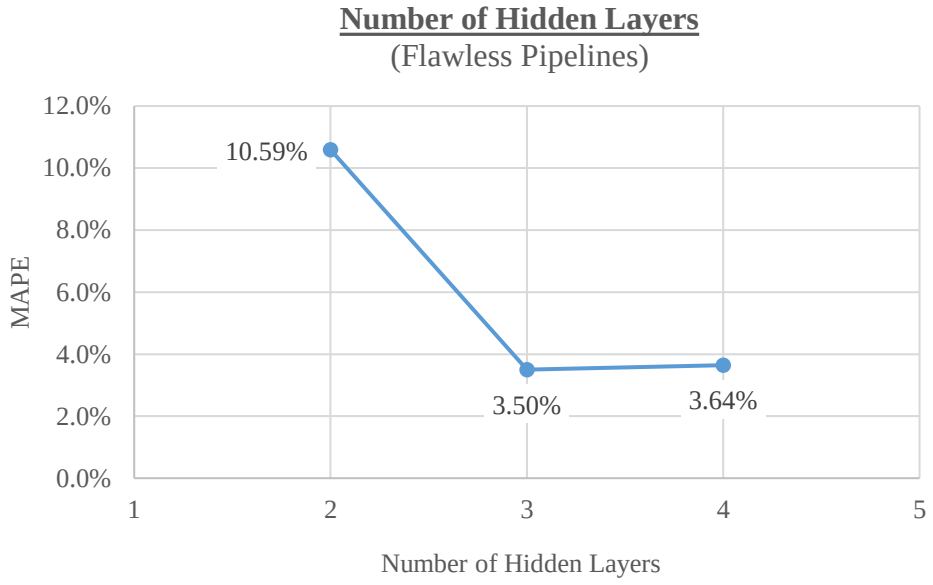

Figure 3.18 Selection of the number of hidden layers of the Deep Neural Network model to predict the burst pressure of flawless pipelines.

(b) Size of Epoch

An epoch is defined as the status that the learning is completed through the forward propagation and backward propagation over the entire *training dataset*, and the selection of the proper size of epochs is critical against preventing the under-fitting or over-fitting problems. Therefore, for the DNN model epoch sized of 10, 100, 1000, 2000, 3000, and 4000 were considered. The findings of the trade-off studies are shown in Figure 3.19, which show that MAPE converges between 3% and 4%. In particular, the lowest MAPE (=3.29%) was observed at an epoch size 3000 and therefore this size was selected for the DNN model. According to Table 3.6, the MAPEs for all cases indicate high accuracy.

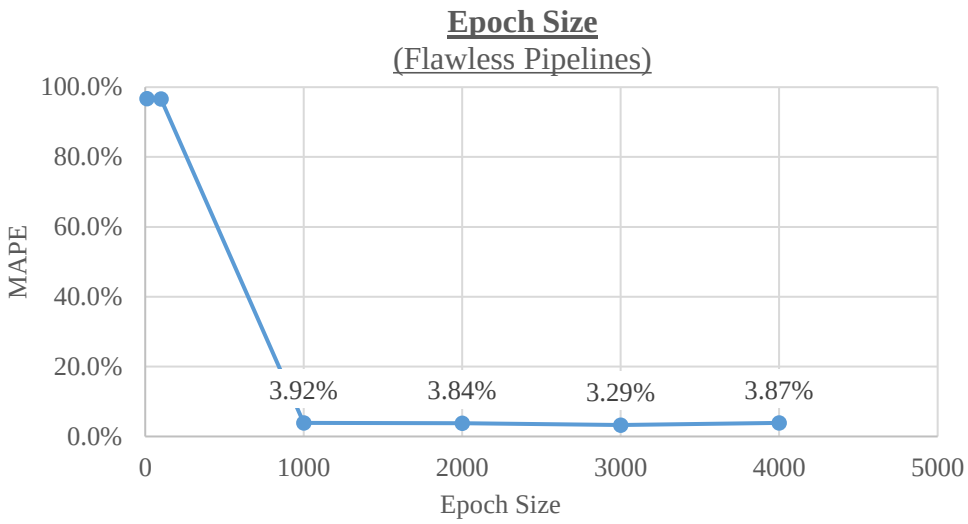

Figure 3.19 Selection of the epoch size for the Deep Neural Network model to predict the burst pressure of flawless pipelines.

(c) Learning Rate

The learning rate is related to the determination of the update of weight. If the learning rate is too small, it may lead to long learning times. On the other hand, a too high learning rate may result in non-convergence. Therefore, the learning rate needs to be appropriately adjusted according to the DNN model. To determine the learning rate, ten different learning rates were taken into consideration. The resultant MAPE from each of the learning rates considered is illustrated in Figure 3.20 and Table 3.8. According to the results, the learning rate with the lowest is

0.0008 and the resultant MAPE, 3.39%, can be interpreted as highly accurate based on Table 3.6.

Table 3.8 Mean Absolute Percentage Error according to the learning rate for the flawless pipelines.

Learning rate (10^{-3})	50	10	5	1	0.9	0.8	0.7	0.6	0.5	0.1
MAPE (%)	14.16	17.15	19.05	3.65	3.53	3.39	3.54	3.77	3.62	8.51

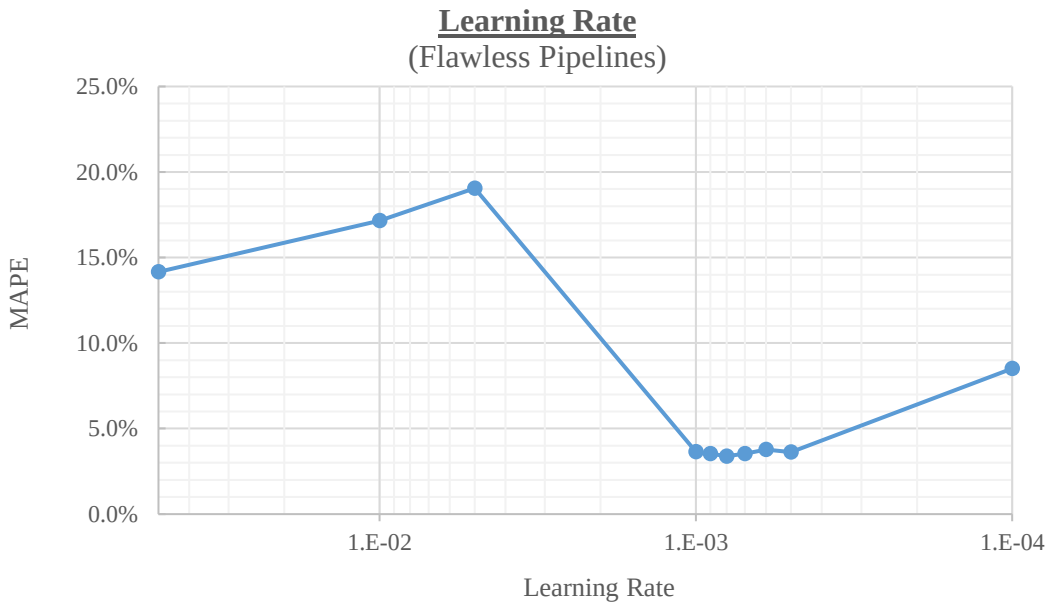

Figure 3.20 Selection of the learning rate for the Deep Neural Network model to predict burst pressure for the flawless pipelines.

3.2.3.3. For Pipelines with a Dent

(a) Number of Hidden Layers

The number of hidden layers of the DNN model was examined for two, three and four in the case of pipelines with a dent. In the results of trade-off study shown in Figure 3.21, the MAPE according to the number of hidden layers, two, three and four, are 0.12%, 0.027% and 0.048%, respectively. According to Table 3.6, the MAPEs for all cases indicate high accuracy, therefore, whatever amongst three cases is selected, it is expected not to effect on the output. However, it has to be

chosen one of the three options, so three hidden layers with lower errors are adopted in this DNN model.

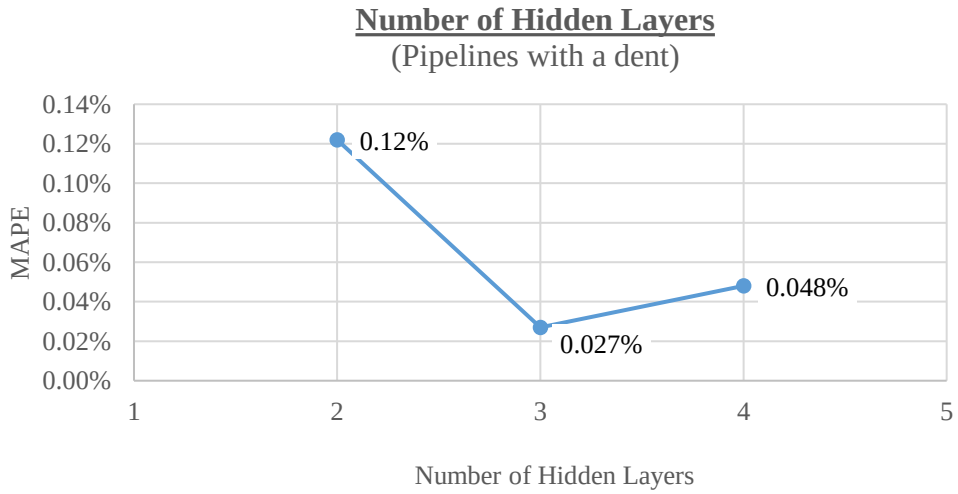

Figure 3.21 Selection of the number of hidden layers for the Deep Neural Network model to predict the burst pressure of pipelines with a dent.

(b) Size of Epoch

For the sizes of epoch for the DNN model, 10, 100, 1000, 2000, 3000, and 4000 were considered. As seen in Figure 3.22, the MAPE was observed to converge 0% from epoch size 1000. The lowest MAPE (=0.03%) was observed at epoch size 1000, 3000 and 4000. According to Table 3.6, MAPEs for all cases indicate high accuracy, and finally epoch size 1000 was employed for the DNN model.

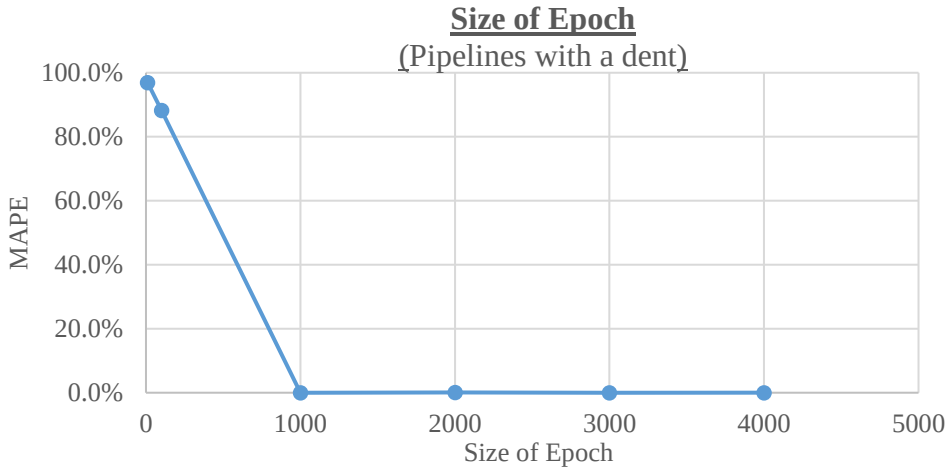

Figure 3.22 Selection of the epoch size for the Deep Neural Network model to predict the burst pressure of pipelines with a dent.

(c) Learning Rate

In total, ten different learning rates as illustrated in Table 3.9 were considered to determine the learning rate. The resultant MAPE, according to the learning rate, is presented in Table 3.9 and Figure 3.23, and this can be interpreted as highly accurate based on Table 3.6. According to the results, the learning rate with the lowest is 0.001.

Table 3.9 Mean Absolute Percentage Error according to the learning rate for pipelines with a dent.

Learning rate (10^{-3})	50	10	5	1	0.9	0.8	0.7	0.6	0.5	0.1
MAPE (%)	0.63	0.36	0.91	0.08	0.10	0.16	0.08	0.14	0.63	9.39

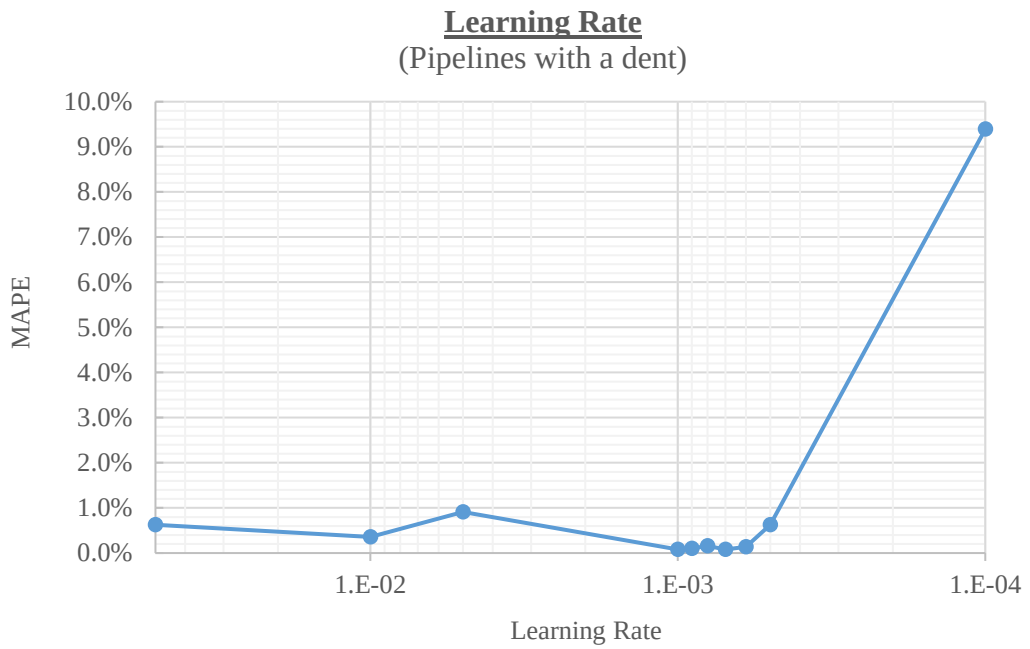

Figure 3.23 Selection of the learning rate for the Deep Neural Network model to predict the burst pressure of pipelines with a dent.

The summary of the hyper-parameters for DNN model is described in

Table 3.10 and the defined DNN diagram is depicted in Figure 3.24.

Table 3.10 Summary of the defined hyper-parameters for Deep Neural Network model.

	Number of Hidden Layer	Size of epoch	Learning rate
Flawless pipelines	3	3000	0.0008
Pipelines with a dent	3	1000	0.001

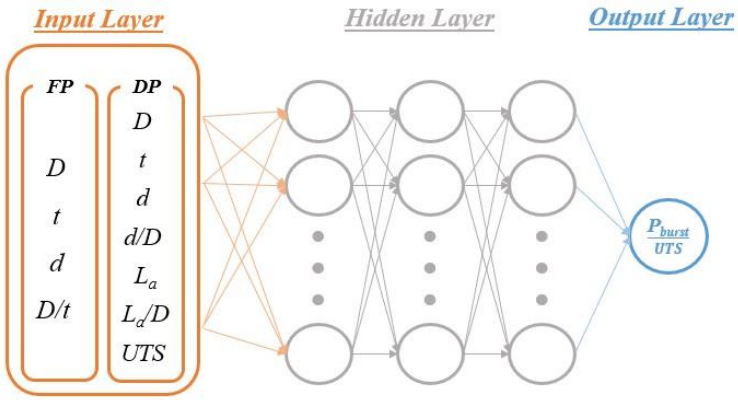

	Input Layer	Hidden Layer			Output Layer
	Features	Nodes			Features
Flawless Pipelines (FP)	*4*	*128*	*64*	*8*	*1*
Dented Pipelines (DP)	*7*	*64*	*16*	*4*	*1*

Figure 3.24 Defined Deep Neural Network diagram

3.2.4. Implementation

Selection of the programming language for the best use of AI is important, and especially for the DNN implementation. For AI development, there are programming languages such as Python, C ++, JVM language family, JavaScript, Lua, etc. Amongst them, Python is at the forefront of AI research and is widely used in machine learning and deep learning frameworks. Therefore, in this research, Python is used as a programming language to develop the DNN model to predict the burst pressure of pipelines with or without a dent. In addition, TensorFlow, which provides an open source library for neural networks, is adopted as a framework. For the last, Jupyter notebook, which is an integrated development and learning environment in Python, is selected as an interface.

3.3. Summary

In this chapter, the methodologies in terms of the FEA and the DNN for developing the burst pressure prediction model and deep neural network model for the flawless pipelines and the pipelines with an unconstrained, plain dent were described.

The burst pressure of the pipeline was defined when the von-Mises equivalent stress at one node or at all nodes allocated throughout the thickness direction in the numerical model reached the UTS.

For the flawless pipelines, the axisymmetry and symmetry boundary condition was employed, and internal pressure was adopted as a loading condition. On the other hand, for the pipelines with a dent, the loading conditions were divided into three steps as shown in Figure 3.10, and the boundary conditions were applied depending on the loading condition as seen in Table 3.4.

The proposed formula to calculate the strain at UTS was developed based on the data from the material coupon test, and the material model of FEA was defined, accordingly.

Mesh size and model length were specified by convergence study. Three were selected for the number of elements through the wall thickness. And, five and five and a half times of the diameter of pipelines were adopted for the model length of flawless pipelines and pipelines with a dent, respectively.

Finally, the DNN model to predict the burst pressure of the pipelines with or without a dent had characteristics like supervised learning, three hidden layers, fully connected layer, and ReLU activation function. In addition, epoch size and learning rate for flawless pipelines and pipelines with a dent were selected as 3000 and 0.0008, and 1000 and 0.001, respectively.

CHAPTER 4

4. DEVELOPMENT OF A BURST PRESSURE PREDICTION MODEL FOR FLAWLESS PIPELINES

To develop an empirical formula that can calculate the burst pressure of flawless pipelines, the parametric studies are conducted, yield strength and ultimate tensile strength of the material, and outer diameter and thickness of the pipeline are considered as variables. The parametric study results are used to derive an empirical formula to estimate the burst pressure of flawless pipelines. The derived empirical formula is validated by comparing with the experimental test results.

The procedure to develop an empirical formula that can estimate the burst pressure of flawless pipelines is as follows in Table 4.1.

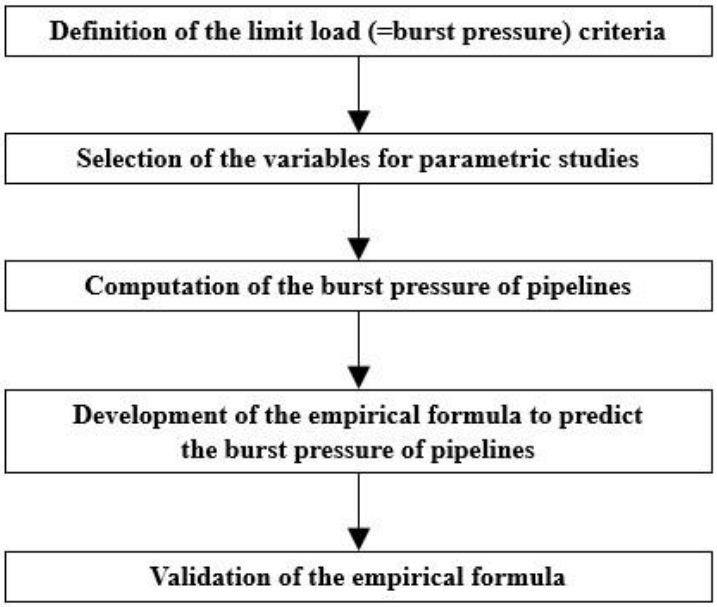

Figure 4.1 Procedure for the development of an empirical formula to predict the burst pressure of flawless pipelines.

4.1. FEA Based Parametric Study

To derive a reliable empirical formula for predicting the burst pressure of API 5L X grade pipelines (API 2004), pipelines that have different mechanical properties like yield strength and ultimate tensile strength, and various geometries like diameter and thickness of the pipeline, conforming to the ranges in API 5L pipeline code, were selected.

79 models for the X80 pipeline and 90 models per each grade from X52 to X70 were modelled with nonlinear FEA to determine the burst pressure. In total, 529 parametric studies were conducted as listed in Table A.1 in the Appendix A. The material properties and geometric information of the FEA models in the parametric study are listed in Table 4.1 and Table 4.2, respectively.

Table 4.1 Material properties of the FEA model for parametric study (API 2004).

Material	X52	X56	X60	X65	X70	X80
Poisson's ratio	0.3					
Young's modulus (MPa)	207,000					
Tangent modulus (MPa)	1186	1276	1317	1187	1220	1123
Yield strength (σ_{yield}, MPa)	358.53	386.11	413.69	448.16	482.63	551.58
Ultimate tensile strength (σ_{UTS}, MPa)	455.05	489.53	517.11	530.90	565.37	620.53
$\sigma_{yield} / \sigma_{UTS}$	0.788	0.789	0.800	0.844	0.854	0.889

Table 4.2 Geometric information and bounding cases of the FEA model for parametric study (API 2004).

	Bounding cases					
Material	X52	X56	X60	X65	X70	X80
Outer diameter (*D, mm*)	60.3 - 610					323.9 - 609.6
Thickness (*t, mm*)	3.9 - 50.8					4.775 - 15.875
D / t	10.0 - 64.08					25.5 - 96.0

The tangent modulus and the strain at ultimate tensile strength, to carry out nonlinear FEA with a bilinear material model, were defined using formula (3.2) and the proposed formula (3.4), respectively.

4.2. FEA Based Parametric Study Results

A typical von-Mises equivalent stress distribution from one of the parametric studies is plotted in Figure 4.2, expressed using the 2D Axisymmetric full expansion plotting option of ANSYS.

The von. Mises equivalent stress at point A has reached the UTS of X70, 565.37 MPa, and the burst pressure is obtained according to the method outlined in Section 3.1.3. The pipeline is considered to have failed when the von-Mises stress at any node has exceeded the UTS of the material.

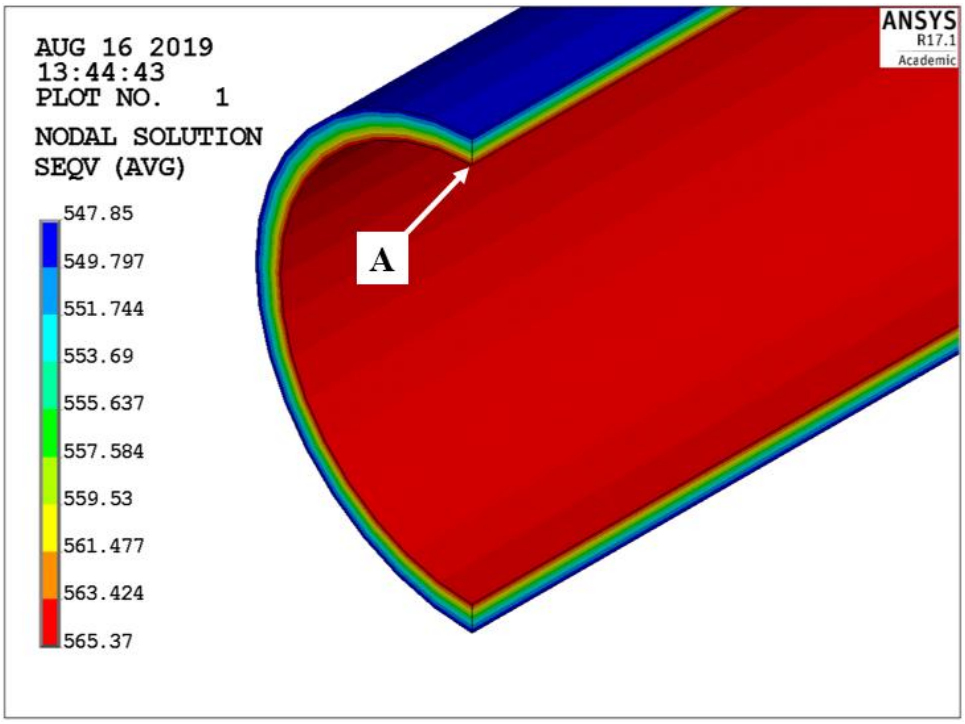

Figure 4.2 Sample of von-Mises equivalent stress distribution from Finite Element Analysis results (2D Axisymmetric full expansion plot).

The von-Mises equivalent stress ($\sigma_{equi.}$) is related to the principal stress by formula (4.1) and the principal stresses are defined by the three directional stresses as following; $\sigma_1 = \sigma_{hoop}$, $\sigma_2 = \sigma_{axial}$ and $\sigma_3 = \sigma_{radial}$.

$$\sigma_{equi.} = \left[\frac{(\sigma_1 - \sigma_2)^2 + (\sigma_2 - \sigma_3)^2 + (\sigma_3 - \sigma_1)^2}{2}\right]^{0.5} \quad (4.1)$$

The burst pressure (or limit load) determined for each FEA pipeline model, is related to the UTS of the applied material, the diameter and the thickness of the pipeline. Therefore, the FEA based Parametric Study results could be represented by a relationship between the burst pressure and the ratio between the diameter and the thickness of the pipeline for each material, as shown in Figure 4.3 below. According to Figure 4.3, it is demonstrated that the burst pressure increased as the ratio of diameter to thickness decreased, and/or as the material grade increased.

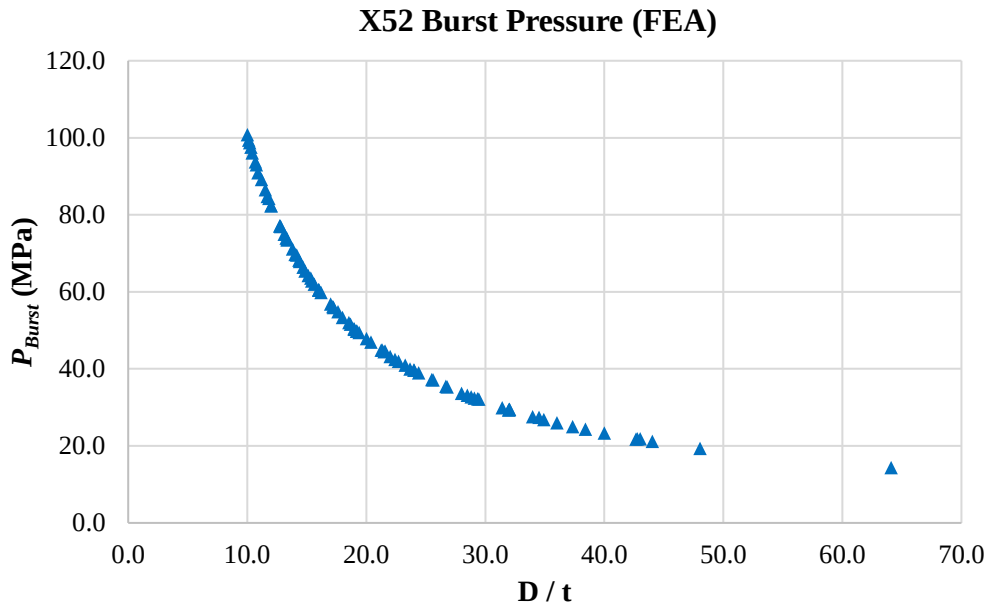

(a)

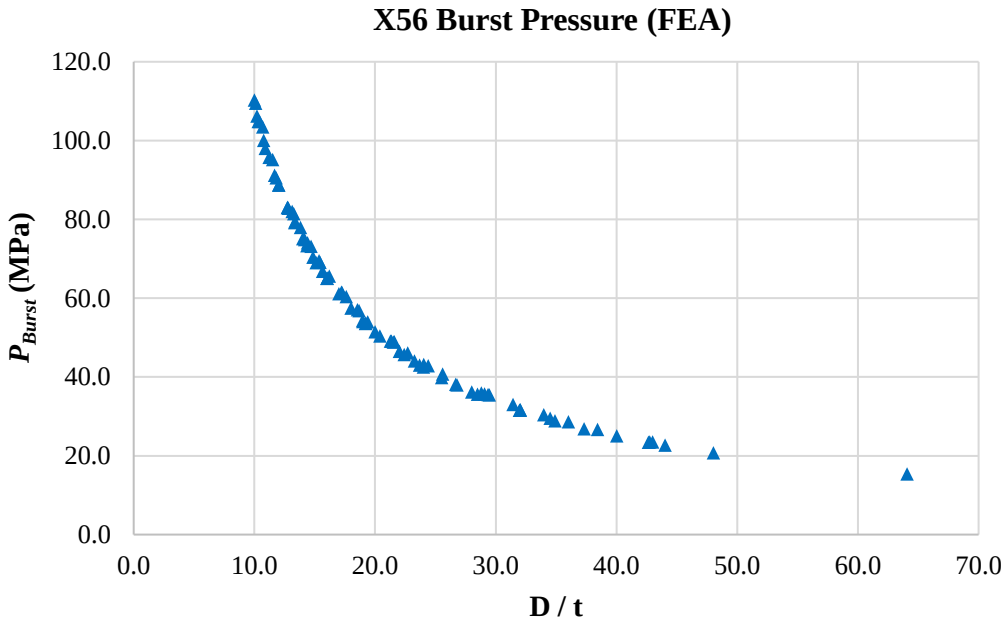

(b)

Figure 4.3 FEA based Parametric Study results summarized as the relationship between the burst pressure and the ratio between the diameter and the thickness of the pipeline for each material: Finite Element Analysis results for (a) X52 and (b) X56.

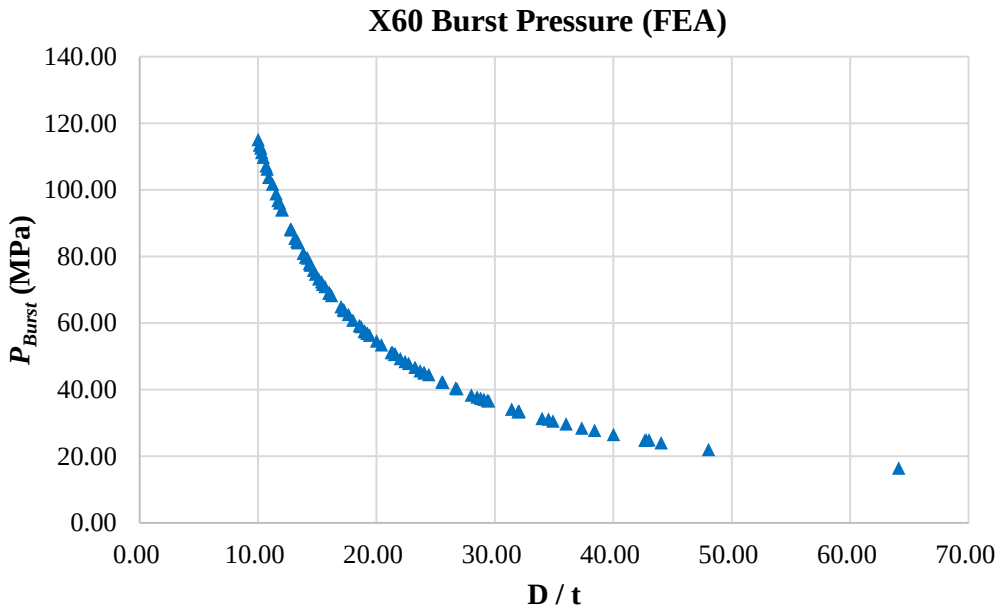

(c)

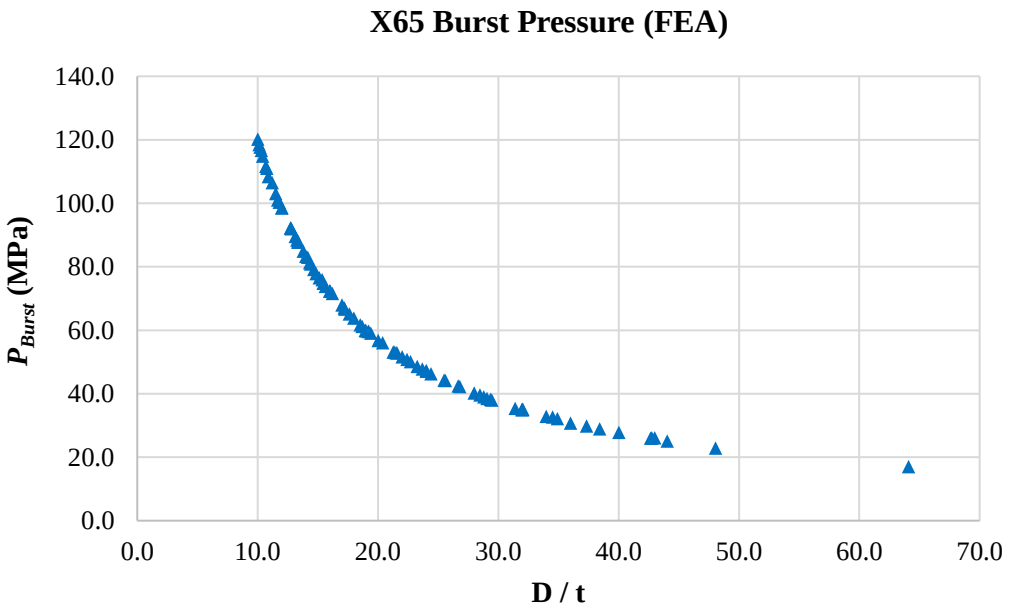

(d)

Figure 4.3 (*cont.*) FEA based Parametric Study results summarized as the relationship between the burst pressure and the ratio between the diameter and the thickness of the pipeline for each material: Finite Element Analysis results for (c) X60 and (d) X65.

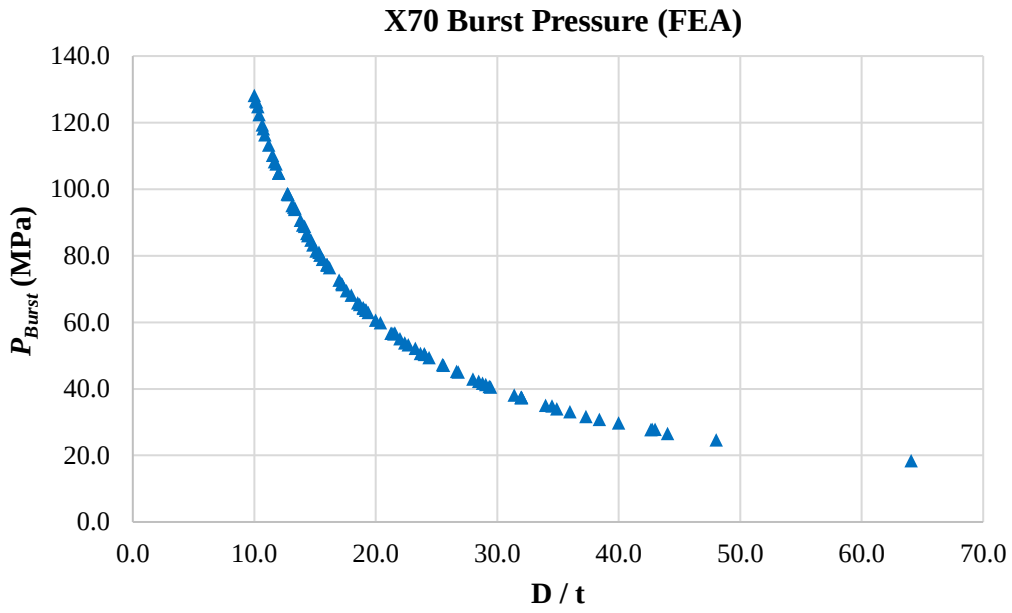

(e)

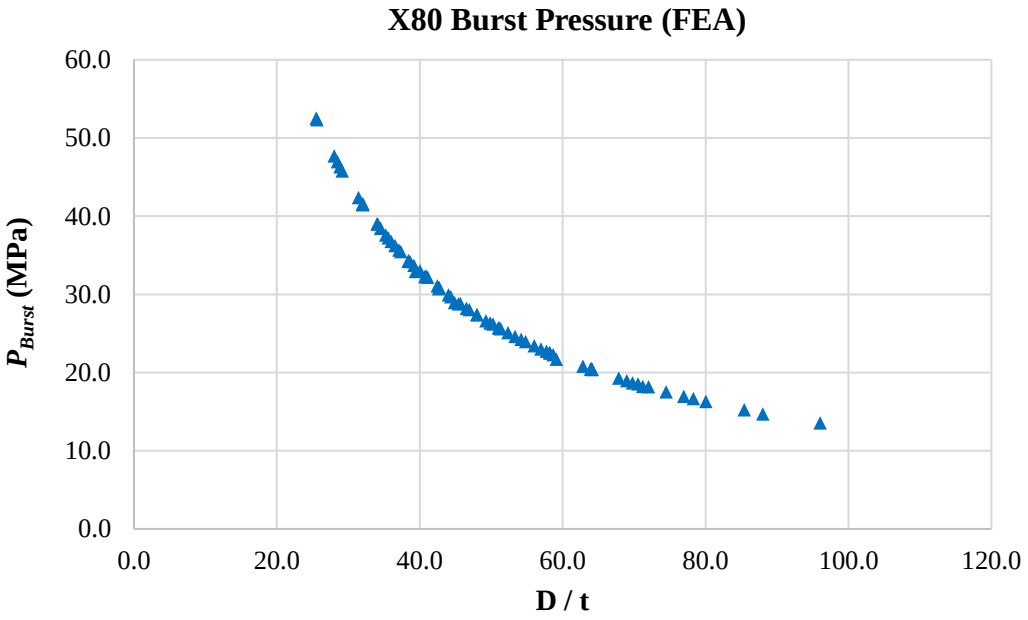

(f)

Figure 4.3 (*cont.*) FEA based Parametric Study results summarized as the relationship between the burst pressure and the ratio between the diameter and the thickness of the pipeline for each material: Finite Element Analysis results for (e) X70 and (f) X80.

4.3. Derivation of Empirical Formula

Based on the FEA based Parametric Study results of the burst pressure from the 529 individual cases, as listed in Table A.2 and Table A.3 in the Appendix A, a new empirical formula of the form of a power law for API 5L X grade material, was derived by curve fitting with nonlinear regression and expressed as formula (4.2). The FEA based Parametric Study results of the burst pressure for each material grade are plotted in Figure 4.4, and all of the data could be fitted to the power law curve with R squared (R^2 = 0.9992).

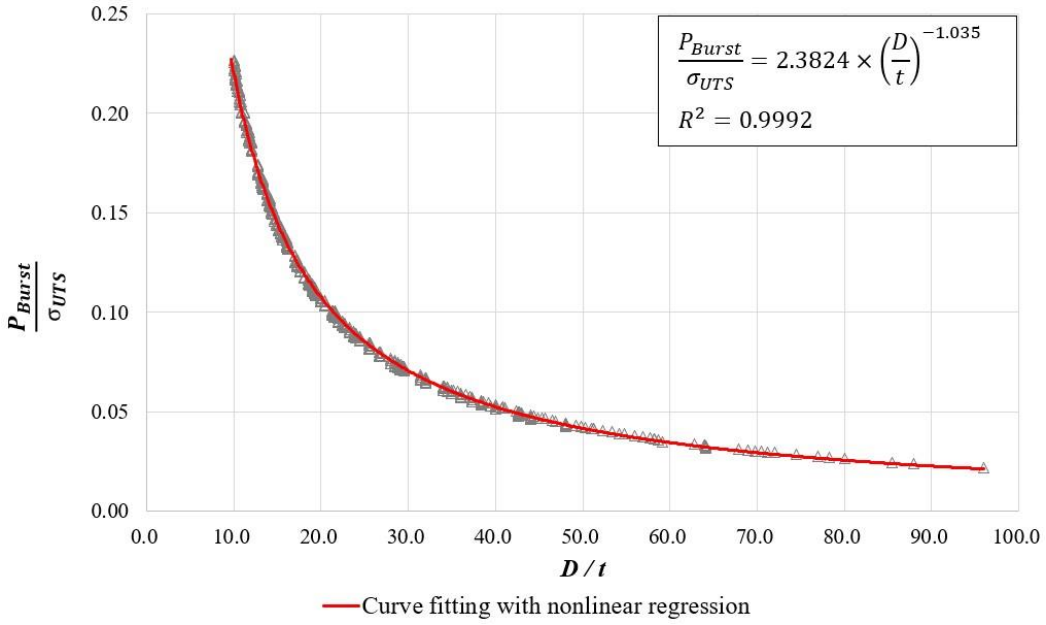

Figure 4.4 Correlation between P_{Burst}/σ_{UTS} and D/t and R squared (R^2).

$$\frac{P_{Burst}}{\sigma_{UTS}} = a\left(\frac{D}{t}\right)^{m} \tag{4.2}$$

where a (= 2.3824) and m (= -1.035) are the power function coefficients, D is the pipeline outer diameter and t is the pipeline thickness. Consequently, the empirical formula (4.2) to predict the burst pressure can be rewritten as follows:

$$P_{Burst} = \sigma_{UTS} \times 2.3824 \times \left(\frac{D}{t}\right)^{-1.035} \quad (4.3)$$

Formula (4.3) is only valid for the range of materials and geometries in the FEA based Parametric Study, i.e. for API 5L X grade flawless pipelines from X52 to X80 and the ratio of *D* to *t* of pipelines ranging from 10 to 96.

4.4. Validation of FD Formula

The newly derived empirical formula (4.3), hereafter termed the *FP formula*, has been validated by comparison with the experimental test data and analytical calculation results for the burst pressure of flawless pipelines. The 14 experimental results were taken from Zhu and Leis (2012); Law and Bowie (2007); Liessem et al. (2004); Zhang et al. (2014). The experimental specimens in Table 4.3 were selected to cover different API 5L X60, X65, X70 and X80 grades and a range of pipeline diameters and thicknesses.

The geometric information and material properties of the 14 test specimens are listed in Table 4.3 below.

Table 4.3 Geometric information and material properties of 14 specimens of the experiment: Zhu and Leis (2012), Law and Bowie (2007), Liessem et al. (2004) and Zhang et al. (2014).

Test No.	Material	Outer diameter (*D*, mm)	Thickness (*t*, mm)	*D* / *t*	Yield strength (σ_{yield}, MPa)	Ultimate tensile strength (σ_{UTS}, MPa)	$\frac{\sigma_{yield}}{\sigma_{UTS}}$	Burst pressure (MPa)
1	X60 (1)	762.00	14.40	52.92	501.0	543.0	0.923	20.90
2	X60 (2)	762.00	14.40	52.92	543.0	568.0	0.956	21.90
3	X65 (1)	273.14	7.10	38.47	587.0	662.0	0.887	36.33
4	X65 (2)	1016.00	16.90	60.12	641.0	683.0	0.939	23.60
5	X65 (3)	1016.00	16.90	60.12	668.0	695.0	0.961	24.30
6	X70 (1)	457.20	9.97	45.86	637.0	700.0	0.910	30.53
7	X70 (2)	914.40	19.10	47.87	534.0	553.0	0.939	23.10

Table 4.3 (*Cont.*) Geometric information and material properties of 14 specimens of the experiment: Zhu and Leis (2012), Law and Bowie (2007), Liessem et al. (2004) and Zhang et al. (2014).

Test No.	Material	Outer diameter (D, mm)	Thickness (t, mm)	D/t	Yield strength (σ_{yield}, MPa)	Ultimate tensile strength (σ_{UTS}, MPa)	$\frac{\sigma_{yield}}{\sigma_{UTS}}$	Burst pressure (MPa)
8	X70 (3)	914.40	19.10	47.87	562.0	570.0	0.986	23.50
9	X70 (4)	610.00	18.90	32.28	539.5	606.5	0.890	40.30
10	X70 (5)	1016.00	16.90	60.12	593.0	656.5	0.903	23.60
11	X80 (1)	356.90	6.96	51.28	568.0	677.0	0.839	27.44
12	X80 (2)	356.17	6.91	51.54	640.0	684.0	0.936	27.80
13	X80 (3)	1219.20	18.30	66.62	640.0	719.0	0.890	42.00
14	X80 (4)	1219.20	18.30	66.62	715.0	744.0	0.961	21.90

Furthermore, the predictions by the *FP formula* were compared with those of the 21 burst pressure formulae reviewed in Section 2.4 and detailed in Table 2.1. The detailed comparison results are listed in Table 4.4 and Figure 4.5. The burst pressure prediction was normalized by dividing the predictions by the experimental results.

To evaluate the accuracy of the burst pressure prediction models, the following statistical Standard Error (SE) formula (4.4) was applied to compare the results of experiments with the prediction results from the analytical models:

$$\text{Standard Error (SE)} = \sqrt{\frac{\sum\left(\frac{P_{FP\ formula}}{P_{exp.}} - 1\right)^2}{N(N-1)}} \tag{4.4}$$

where $P_{FP\ formula}$, $P_{exp.}$ and N denote the predicted burst pressure by the *FP formula*, the results of experiments and total number of data, respectively.

In addition, the smaller the standard error represents the more accurate model. Therefore, the SE ranking is defined to be higher as the smaller the standard error is smaller.

Table 4.4 Average Discrepancy, Standard Error and Standard Error ranking for the normalized burst pressures through dividing the predictions by experimental results.

Model		Test Number					
		1	2	3	4	5	6
No.	Name	X60 (1)	X60 (2)	X65 (1)	X65 (2)	X65 (3)	X70 (1)
Experimental Burst Pressure (MPa)		20.90	21.90	36.33	23.60	24.30	30.53
1	ASME (1962)	1.00	1.00	0.97	1.00	1.00	1.02
2	Barlow OD (1836)	0.98	0.98	0.95	0.98	0.98	1.00
3	Barlow ID (1836)	1.02	1.02	1.00	1.02	1.02	1.05
4	Barlow flow (1836)	0.98	1.00	0.94	1.00	1.02	1.00
5	Bailey-Nadai (1930)	1.00	1.00	0.97	1.00	1.00	1.02
6	DNV (2013)	1.00	1.00	0.98	1.00	1.00	1.03
7	Fletcher (2003)	1.00	1.01	0.99	1.03	1.05	1.03
8	Max. Shear Stress (2002)	1.00	1.00	0.97	1.00	1.00	1.02
9	Turner (1910)	1.00	1.00	0.97	1.00	1.00	1.02
10	Stewart et al. (1) (1994)	0.97	0.98	0.92	0.96	0.96	0.98
11	Bohm (1972)	1.11	1.11	1.04	1.10	1.10	1.12
12	Faupel (1956)	1.15	1.15	1.11	1.15	1.16	1.17
13	Marin and Rimrott (1958)	1.11	1.12	1.03	1.09	1.09	1.12
14	Marin and Sharma (1958)	1.15	1.16	1.10	1.14	1.14	1.17
15	Nadai (1931)	1.16	1.15	1.12	1.15	1.16	1.18
16	Nadai (1963)	1.15	1.15	1.12	1.15	1.15	1.18
17	Soderberg (1941)	1.16	1.15	1.12	1.15	1.16	1.18
18	Svensson (1958)	1.11	1.11	1.04	1.10	1.10	1.12
19	Stewart et al. (2) (1994)	1.13	1.13	1.07	1.12	1.12	1.14
20	Zhu and Leis (2006)	1.05	1.06	0.99	1.04	1.04	1.06
21	Zhu and Leis (2007)	1.04	1.05	1.00	1.06	1.07	1.06
22	Proposed equation	1.02	1.02	0.99	1.02	1.02	1.04

Table 4.4 (*Cont.*) Average Discrepancy, Standard Error and Standard Error ranking for the normalized burst pressures through dividing the predictions by experimental results.

Model		Test Number					
		7	8	9	10	11	12
No.	Name	X70 (2)	X70 (3)	X70 (4)	X70 (5)	X80 (1)	X80 (2)
Experimental Burst Pressure (MPa)		23.10	23.50	40.3	23.6	27.44	27.80
1	ASME (1962)	1.00	1.00	0.96	0.94	0.98	0.97
2	Barlow OD (1836)	0.98	0.98	0.93	0.93	0.96	0.95
3	Barlow ID (1836)	1.02	1.02	0.99	0.96	1.00	0.99
4	Barlow flow (1836)	0.99	1.00	0.94	0.91	0.92	0.96
5	Bailey-Nadai (1930)	1.00	1.00	0.95	0.94	0.98	0.97
6	DNV (2013)	1.00	1.00	0.97	0.94	0.99	0.98
7	Fletcher (2003)	1.03	1.04	1.01	0.97	0.96	1.00
8	Max. Shear Stress (2002)	1.00	1.00	0.96	0.94	0.98	0.97
9	Turner (1910)	1.00	1.00	0.96	0.94	0.98	0.97
10	Stewart et al. (1) (1994)	0.94	0.94	0.88	0.87	0.93	0.93
11	Bohm (1972)	1.07	1.07	0.99	0.98	1.05	1.06
12	Faupel (1956)	1.15	1.15	1.10	1.08	1.10	1.12
13	Marin and Rimrott (1958)	1.06	1.06	0.98	0.96	1.04	1.05
14	Marin and Sharma (1958)	1.12	1.12	1.07	1.03	1.10	1.11
15	Nadai (1931)	1.16	1.16	1.11	1.09	1.13	1.12
16	Nadai (1963)	1.15	1.15	1.10	1.08	1.13	1.12
17	Soderberg (1941)	1.16	1.16	1.11	1.09	1.13	1.12
18	Svensson (1958)	1.07	1.07	0.99	0.98	1.05	1.06
19	Stewart et al. (2) (1994)	1.10	1.10	1.04	1.02	1.08	1.08
20	Zhu and Leis (2006)	1.02	1.02	0.96	0.94	1.00	1.01
21	Zhu and Leis (2007)	1.05	1.05	0.99	0.98	1.00	1.02
22	Proposed equation	1.02	1.02	0.98	0.96	1.00	0.99

Table 4.4 (*Cont.*) Average Discrepancy, Standard Error and Standard Error ranking for the normalized burst pressures through dividing the predictions by experimental results.

Model		Test Number		AD	SE	SE Ranking
		13	14			
No.	Name	X80 (3)	X80 (4)			
Experimental Burst Pressure (MPa)		21.90	22.70	-	-	-
1	ASME (1962)	1.00	1.00	-1.439%	0.690%	6
2	Barlow OD (1836)	0.99	0.98	-2.998%	1.019%	9
3	Barlow ID (1836)	1.02	1.01	1.000%	0.612%	3
4	Barlow flow (1836)	0.96	0.99	-2.790%	1.175%	11
5	Bailey-Nadai (1930)	1.00	1.00	-1.324%	0.691%	7
6	DNV (2013)	1.00	1.00	-0.636%	0.587%	2
7	Fletcher (2003)	0.99	1.03	1.042%	0.756%	8
8	Max. Shear Stress (2002)	1.00	1.00	-1.041%	0.628%	5
9	Turner (1910)	1.00	1.00	-1.027%	0.626%	4
10	Stewart et al. (1) (1994)	0.96	0.95	-5.882%	1.877%	13
11	Bohm (1972)	1.09	1.09	6.975%	2.239%	15
12	Faupel (1956)	1.14	1.15	13.468%	3.809%	19
13	Marin and Rimrott (1958)	1.08	1.08	6.317%	2.160%	14
14	Marin and Sharma (1958)	1.13	1.13	12.075%	3.485%	18
15	Nadai (1931)	1.16	1.15	14.284%	4.014%	22
16	Nadai (1963)	1.15	1.15	13.941%	3.925%	20
17	Soderberg (1941)	1.16	1.15	14.268%	4.009%	21
18	Svensson (1958)	1.09	1.09	7.038%	2.253%	16
19	Stewart et al. (2) (1994)	1.11	1.11	9.812%	2.893%	17
20	Zhu and Leis (2006)	1.04	1.03	1.945%	1.097%	10
21	Zhu and Leis (2007)	1.03	1.05	3.241%	1.186%	12
22	Proposed equation	1.01	1.01	0.653%	0.587%	1

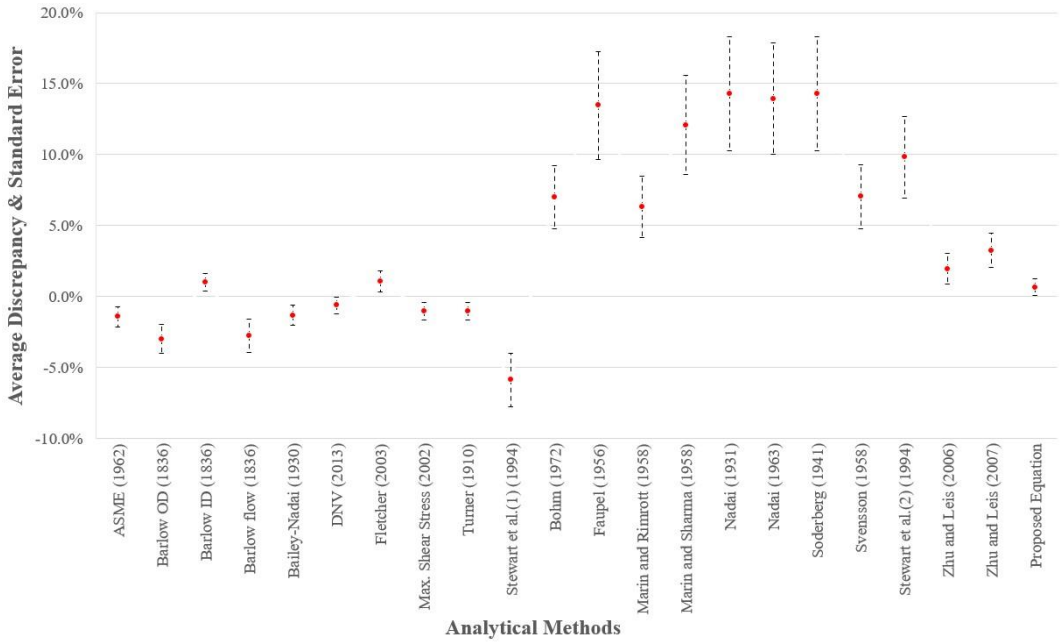

Figure 4.5 Average discrepancy and standard errors in association with the results of experiments and the prediction by analytical methods.

According to the results indicated in Table 4.4 and Figure 4.5, the predicted burst pressures calculated by the *FP formula* showed the best agreement with the results of the experiments with a standard error of 0.587% and average discrepancy of 0.653%.

It was observed from Figure 4.5 that in general, the error bounds of the pipeline burst pressure predictions using the formulae based on Tresca and the average shear stress criterion categories were lower than the error bounds based on the von-Mises criterion category. The results from the former category tended to predict the results of experiments better, and the latter category generally tended to overestimate the burst pressure. Nevertheless, the only exception in the latter category was the proposed formula, which produced similar results to those from DNV and Barlow ID formulae.

From the above results, it is confirmed that the proposed methodology, that is, the methodology of determining the burst pressure (or limit load) by performing nonlinear FEA based on the tangent modulus calculated using the strain at UTS determined by the proposed formula (4.3), is reliable.

4.5. Summary

In this chapter, an empirical formula was presented to predict the burst pressure for API 5L X grade flawless pipelines.

First, an empirical formula to estimate the strain at UTS has been derived using the material coupon test data, and used to define the tangent modulus for the FEA material model. This formula was applied to define the material model for FEA, and 529 parametric studies carried out with pre-defined material model. From the results of parametric studies, an empirical formula was developed to predict the burst pressure termed the *FP formula*, which has then been validated against 14 experimental results.

According to the validation of the proposed formula, it was found that the best agreement amongst 22 equations was achieved between the burst pressure calculated by the *FP formula* and the experimental burst test results.

CHAPTER 5

5. DEVELOPMENT OF A BURST PRESSURE PREDICTION MODEL FOR PIPELINES WITH A DENT

To develop an empirical formula that can calculate the burst pressure of pipelines with a dent, the parametric studies are conducted, and the dent depth, dent length, yielding and ultimate tensile strength of the material, outer diameter and thickness of the pipeline are considered as variables. The parametric study results are used to derive an empirical formula to estimate the burst pressure of pipelines with a dent. The derived empirical formula is validated by comparing with the experimental test results. In this chapter, the derived empirical formula does not consider the effect of the dent width to avoid the complexity of equation and to validate the proposed formula by comparing with the experimental test results. The effect of the dent width will be dealt in Chapter 6 through the further related FEA parametric studies.

The procedure to develop an empirical formula that can estimate the burst pressure of pipelines with a dent is as follows in Figure 5.1

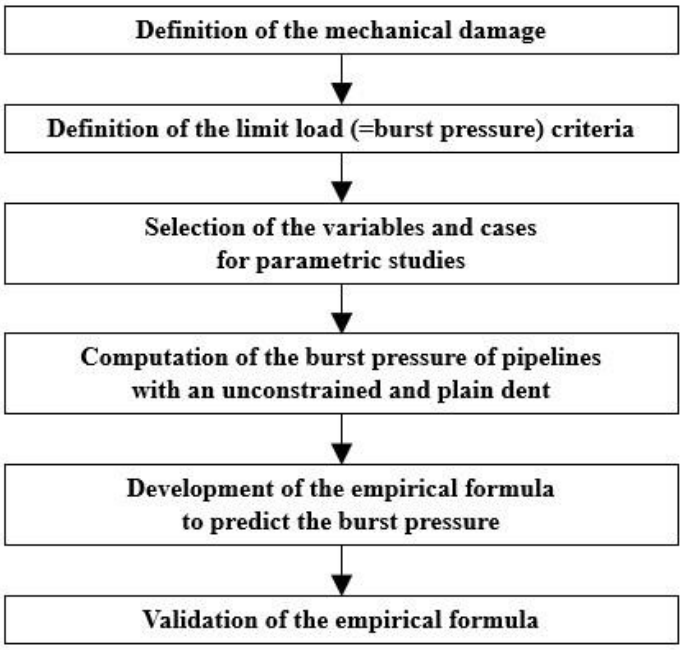

Figure 5.1 Procedure for the development of an empirical formula to predict the burst pressure of flawless pipelines.

5.1. FEA based Parametric Study

To develop an empirical formula for the assessment of the structural integrity of a pipeline with an unconstrained, plain dent, parametric studies were conducted using non-linear FEA to determine the burst pressure for API 5L X52, X65 and X80 grade pipelines with a dent. The type of dent modelled in the parametric studies is an unconstrained, hemispherical, plain dent with no pipeline thickness reduction in the dent region. As the dent is unconstrained, the dent can recover elastically or rebound, after indenter removal.

There are two aims of the FEA based Parametric Study, and therefore the study has been divided into separate parametric studies termed FEA based Parametric Study (I) and (II). In addition, the subscripts, PS(I) and PS(II), denote Parametric Study (I) and (II), respectively.

a) FEA based Parametric Study (I): The aim of this study is to derive a burst pressure prediction empirical formula. To this end, 50 case studies using nonlinear FEA have been conducted using the $X52\_{PS(I)}$ material properties in

Table 5.1. The burst pressure prediction formula has been derived based on the 150 data generated by linear interpolation from the 50 FEA based Parametric Study results.

b) FEA based Parametric Study (II): The purpose of this study is to validate the proposed formula developed in Parametric Study (I). To this end, the nonlinear FEA has been conducted using the $X52_{\_PS(II)}$, $X65_{\_PS(II)}$ and $X80_{\_PS(II)}$ material properties in Table 5.1. To validate the derived formula, the PPMCC and MAPE were used. Where PPMCC and MAPE were defined using the FEA based Parametric Study results and the results calculated by the proposed formula for $X52_{\_PS(II)}$, $X65_{\_PS(II)}$ and $X80_{\_PS(II)}$.

These parametric studies for $X52_{\_PS(I)}$, $X52_{\_PS(II)}$, $X65_{\_PS(II)}$ and $X80_{\_PS(II)}$ materials that have different yield strength and UTS performed 50, 30, 25 and 25 cases by FEA, respectively.

In this study, the strain hardening effect of the material and the effect of the structural geometric change caused by the dent were taken into account as the material nonlinearity and geometric nonlinearity, respectively.

The next sections describe in detail how the parametric studies were performed.

5.1.1. Definition of Dent Depth and Dent Length

The purpose of this study is to derive an empirical formula for predicting the burst pressure of pipelines with a dent, hereafter referred as the *PD formula*, and the prerequisite of this study is to define the dent depth and dent length. The dent depth, as shown in Figure 2.2, can be defined as the amount of deformation in the direction of the inside of the mathematically perfect pipeline. In the case of dent length (L) as shown in Figure 5.3, it can be defined as the distance between the cross-sections that are not affected by the dent before and after the location of the dent in the longitudinal direction. As shown in Figure 5.2, the initial dent depth and dent length before removal of the indenter are denoted D_b and L_b, respectively. R_{ind} represents the radius of the indenter and can be calculated by the following formula (5.1) using

the Pythagorean theorem.

$$R_{ind}{}^2 = \left(\frac{L_b}{2}\right)^2 + (R_{ind} - D_b)^2 \Rightarrow R_{ind} = \frac{1}{8}\frac{L_b{}^2}{D_b} + \frac{D_b}{2} \tag{5.1}$$

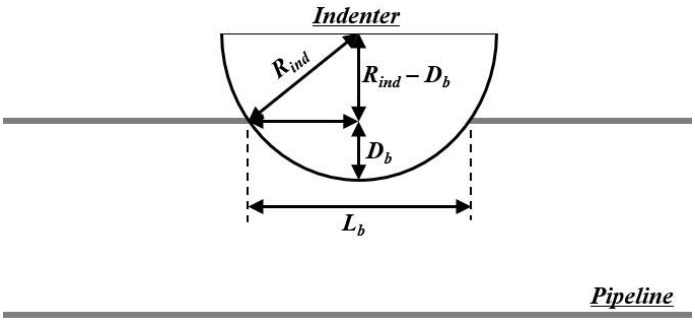

Figure 5.2 Definition of the indenter radius (R_{ind}), initial dent depth (D_b) and initial dent length (L_b) before removal of the indenter.

However, after removal of the indenter, that is, when the dent has already been formed, it is not easy to identify exactly the locations that are not affected by the dent in reality. According to Noronha et al. (2010), the dent length is defined as a distance measured at the half depth of the dent as shown in Figure 5.3. Using this method, it is easier to consistently define the dent depth (D_a) and dent length (L_a), where D_a and L_a are the dent depth and dent length respectively measured after removal of the indenter *i.e.* including the rebound effect. Using this method, the dent depth and the dent length can be obtained from the results of FEA. In addition, for field engineers, these values can be measured on-site using a special tool. Therefore, in this study, the dent length is defined as a distance measured at the half depth of the dent.

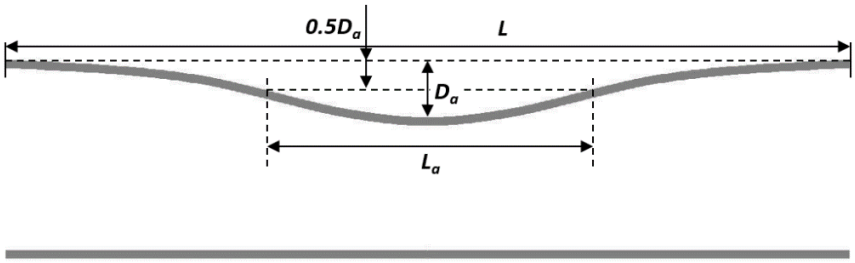

Figure 5.3 Definition of the dent depth (D_a) and dent length (L_a) after removal of the indenter.

5.1.2. Pipeline Material Properties and Geometric Information

The pipeline material properties used to derive the burst pressure prediction empirical formula for pipelines with a dent are listed in Table 5.1. The reason for choosing the pipeline of this specification is that there was already a burst pressure experimental data and FEA results for this pipeline in API 1156 (Kiefner et al. 1997). This information can be used not only to determine the element size and the length of FE model but also to verify the reliability of the formula for the prediction of the burst pressure of pipelines with a dent. The material properties of $X52_{\_PS(I)}$ are from API 1156 (Kiefner et al. 1997) and the other material properties are the minimum values of API 5L: Specification for Line Pipe (API 2004). In addition, the geometric information is same as the values stated in Table 5.1.

Table 5.1 Material properties and geometric information of the Finite Element Analysis model for parametric study (I) (Kiefner et al. 1997) and (II) (API 2004).

	Parametric study (I)	Parametric study (II)		
Outer diameter (*mm*)		323.85		
Thickness (*mm*)		4.7752		
Material	$X52_{\_PS(I)}$	$X52_{\_PS(II)}$	$X65_{\_PS(II)}$	$X80_{\_PS(II)}$
Poisson's ratio		0.3		
Young's modulus (MPa)		207,000		
Tangent modulus (MPa)	1550	1186	1187	1123
Yield strength ($\boldsymbol{\sigma_{yield}}$, MPa)	371.60	358.53	448.16	551.58
Ultimate tensile strength ($\boldsymbol{\sigma_{UTS}}$, MPa)	529.50	455.05	530.90	620.53
$\boldsymbol{\sigma_{yield}} / \boldsymbol{\sigma_{UTS}}$	0.702	0.788	0.844	0.889

5.1.3. Variables for FEA Based Parametric Study

For the parametric studies, the indenter radius (R_{ind}), the ratio of the initial dent depth (D_b) to initial dent length (L_b) and the ratio of the initial dent depth to pipeline outer diameter (D) are used for the variables of FEA based Parametric Study, and the bounding cases of variables are defined in Table 5.2 and Table 5.3. Where D_b and L_b are the initial indentation values of the dent before the rebound and these values are used only for creating the dent shape on the pipelines.

D_a and L_a as defined in Figure 5.3 are the dent depth and dent length respectively measured after removal of the indenter *i.e.* including the rebound effect and these results are used to derive an empirical formula to predict the burst pressure of pipelines with a dent.

R_{ind} for the FEA based Parametric Study (I) and (II) are defined using the formula (5.1) and listed in Table 5.4.

Based on the mentioned variables, parametric studies are conducted by the nonlinear FEA.

Table 5.2 Variables for the FEA based Parametric Study (I).

Material	$X52_{\_PS(I)}$
Design Variables	Bounding cases
D_b / D (%)	2.5, 5, 10, 15 and 20
D_b / L_b (%)	2.5, 5, 7.5, 10, 12.5, 25, 37.5, 50, 75 and 100

Table 5.3 Variables for the FEA based Parametric Study (II).

Material	$X52_{\_PS(II)}$	$X65_{\_PS(II)}$	$X80_{\_PS(II)}$
Design Variables	Bounding cases		
D_b / D (%)	2.5, 5, 10, 15 and 20		
D_b / L_b (%)	2.5, 5, 7.5, 10, 12.5 and 25	5, 7.5, 10, 12.5 and 25	

Table 5.4 Indenter radius (R_{ind}) according to the ratio of D_b to L_b and D_b to D.

R_{ind}		D_b/L_b (%)									
		2.5	5.0	7.5	10.0	12.5	25.0	37.5	50.0	75.0	100.0
D_b/D (%)	2.5	1623.3	408.9	184.0	105.3	68.8	20.2	11.2	8.1	5.8	5.1
	5.0	817.7	210.5	98.1	58.7	40.5	16.2	11.7	10.1	9.0	8.6
	10.0	421.0	117.4	61.2	41.5	32.4	20.2	18.0	17.2	16.6	16.4
	15.0	294.2	91.8	54.3	41.2	35.1	27.0	25.5	25.0	24.6	24.5
	20.0	234.8	83.0	54.9	45.0	40.5	34.4	33.3	32.9	32.6	32.5

5.2. FEA Based Parametric Study (I) Results

5.2.1. Variation in von-Mises Stress with Loading Condition

The von-Mises equivalent stress according to the loading condition from the results of parametric studies conducted by the nonlinear FEA shows the trend indicated in Figure 5.4 at the dented location. Figure 5.4 shows that the von-Mises equivalent stress is increasing during the indentation step and some parts are reaching the plastic zone beyond the elastic zone.

In the indenter removal step, the load by indentation is removed and the stress reflecting the spring-back effect remains as the residual stress. The residual stresses of the dented location on the outer (P1) and inner side (P5) of pipeline show the highest and the lowest value, respectively.

Finally, when the internal pressure acts on the inside of the pipe, the stress rises continuously. All the nodes (P1 to P5) in the thickness direction both within the dented area or in the location unaffected by the dent reach the UTS and result in a burst. The burst pressure was calculated according to the burst pressure defined in Section 3.1.1 and 50 burst pressure data were obtained as listed in Table B.1 in the Appendix B. In addition, the ratio of D_a to D and the ratio of L_a to D are calculated by deriving the dent depth (D_a) and dent length (L_a) data reflecting rebound after removal of the indenter.

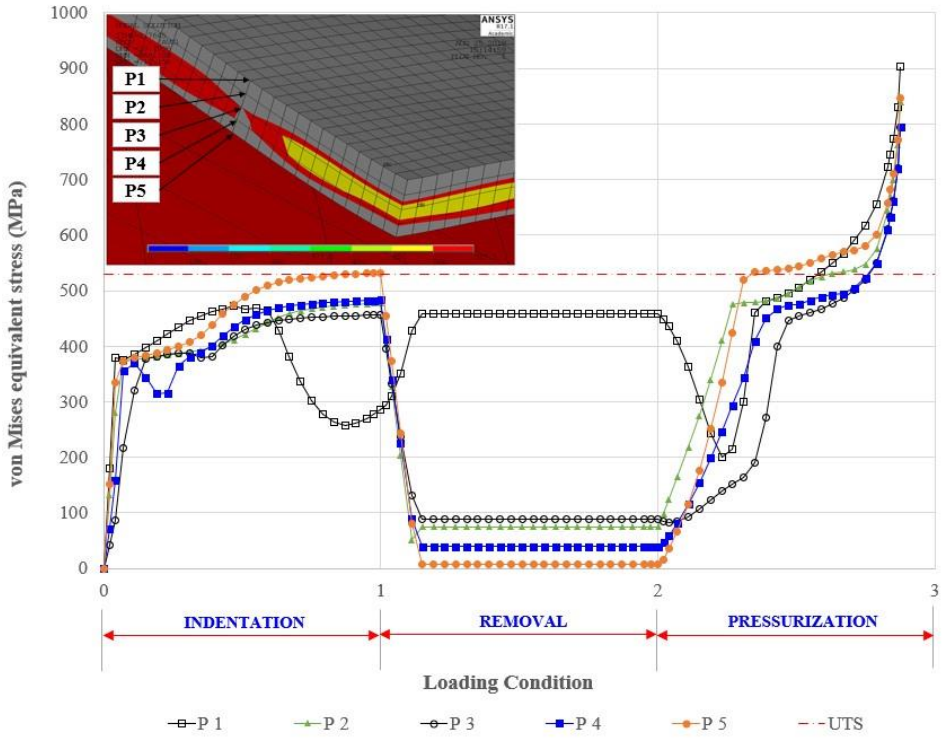

Figure 5.4 A schematic of von-Mises equivalent stress tendency at the burst section on the dented area with the loading conditions; where P1 to P5 are the nodes in the thickness direction within the dented area.

5.2.2. Burst Pressure according to Dent Depth and Dent Length

This section covers the effects of dent depth and dent length on the burst pressure of pipelines with a dent.

The ratio of the initial dent depth to the length and the initial dent depth to pipeline outer diameter is simple, while the obtained ratio after removal of the indenter is not simple as evident from Table B.1 in the Appendix B. This means that it is difficult to find out the relations between the burst pressure and the rebounded dent depth and length. For this reason, the initial dent depth (D_b) and dent length (L_b) are used for the convenience of analysing the results, although D_a and L_a will be used for the calculation. From the results of FEA based Parametric Study (I), (Figure 5.5) it can be seen that the burst pressure decreases with increasing dent depth at each dent length. In addition, as the ratio of dent depth to dent length increases, that is, the shorter the dent length at each dent depth, the burst pressure decreases.

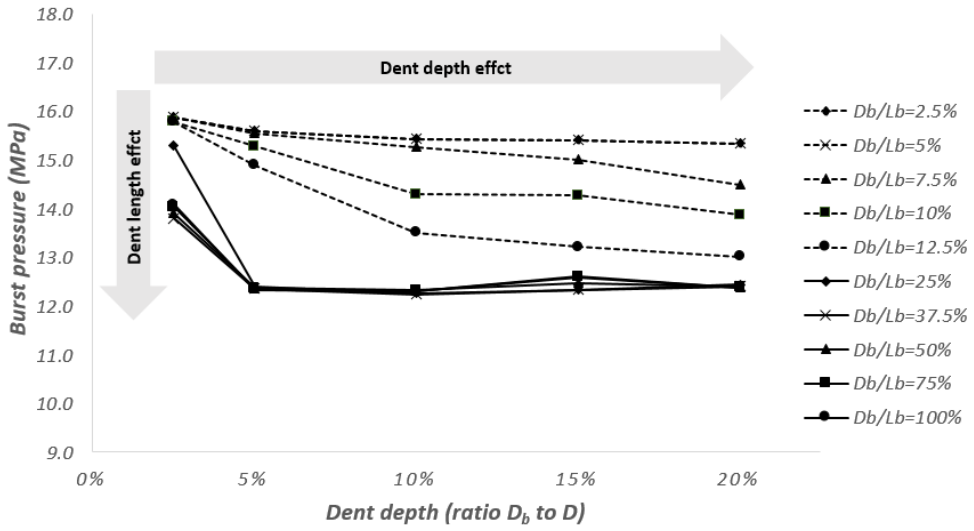

Figure 5.5 Effects of the dent depth and dent length on the burst pressure of pipelines with a dent.

5.2.3. Burst Location according to Dent Depth and Dent Length

Figure 5.6 illustrates the location of the burst in relation to the L_a/D ratio and the D/D_a ratio. The following formula (5.2) with conditions is used to determine where the burst occurs. If the condition is satisfied, the burst occurs in the dented area, otherwise, it occurs where there is no influence of the dent.

$$\frac{L_a}{D} \leq 2.3658 \times \left(\frac{D}{D_a}\right)^{-0.73} \quad for \ \frac{L_a}{D} \leq 0.681, \frac{D}{D_a} \leq 73.27 \tag{5.2}$$

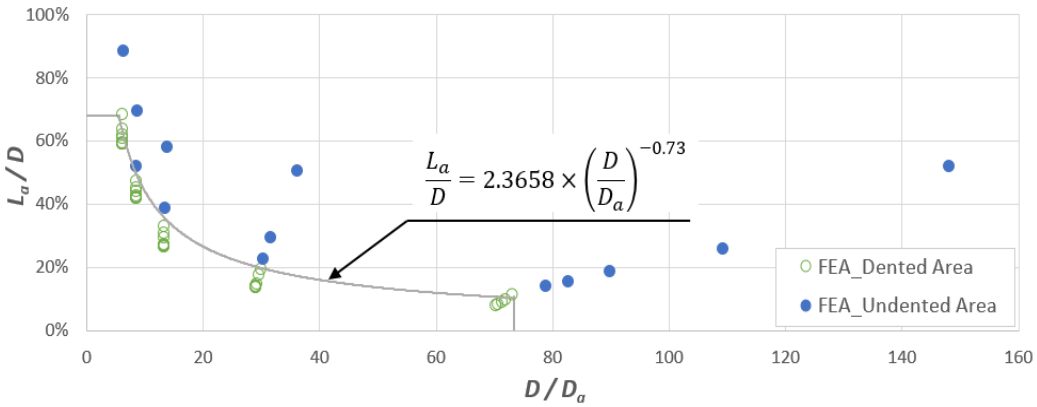

Figure 5.6 Location of the burst occurred in accordance with the ratio of L_a to D and D to D_a.

5.3. Derivation of Empirical Formula

As shown in Figure 5.7, from the results of the FEA based Parametric Study (I) taking into account the pipeline thickness, diameter, yield strength, UTS, dent depth and dent length based on the X52_PS(I), it can be seen that a relationship between the burst pressure and the ratio of L_a to D is similar to the dose-response relationship.

According to the results of Parametric Studies (I), the ratio of D_a to D and L_a to D varies between 0.67% to 15.96% and 7.79% to 88.50%, respectively. Using the obtained data, it is difficult to establish an intuitive relationship between the burst pressure and D_a/D and L_a/D. Therefore, a new dataset associated with the burst pressure and the L_a/D ratio according to the D_a/D ratio having a range of 1% to 15% incremented by 1% using the linear interpolation method was constructed and listed in Table B.2 in the Appendix B.

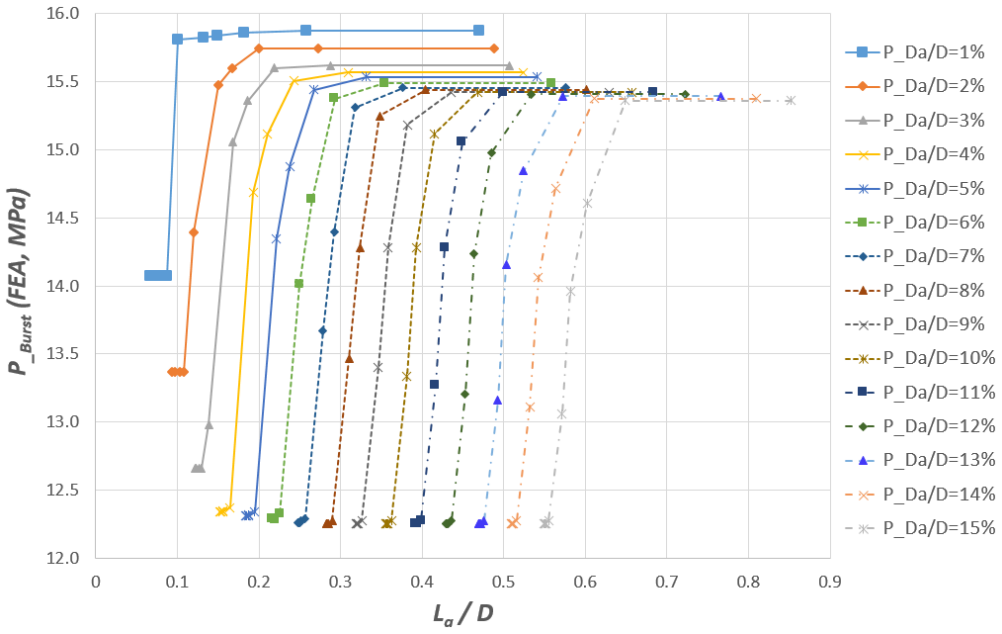

Figure 5.7 Burst pressure of pipelines with a dent in accordance with the ratio of L_a to D.

The occurrence of a dent in the pipeline can be understood as a decrease in the stiffness of the flawless pipeline due to the dent. In other words, an empirical

formula to predict the burst pressure of pipelines with a dent (P_{Burst}^{d}) can be expressed as the burst pressure of flawless pipelines (P_{Burst}^{f}) multiplied by a reduction factor (γ) governed by the dent depth and dent length.

Consequently, an empirical formula (5.3) was derived through logistic regression for the obtained new dataset and is expressed as follows:

$$P_{Burst}^{d} = \gamma \times P_{Burst}^{f} \tag{5.3}$$

Where, the formula (4.3) was used to predict the burst pressure of flawless pipelines (P_{Burst}^{f}), and written as follows:

$$P_{Burst}^{f} = 2.3824 \times \sigma_{UTS} \times \left(\frac{D}{t}\right)^{-1.035} \tag{5.4}$$

In addition, the reduction factor (γ) is written as a formula (5.5) that is expressed in terms of coefficients A_1, A_2, *and* x_0, exponent p and the L_a/D ratio. The relationship between each coefficient and the D_a/D ratio is shown in Figure 5.8 (a) ~ (d). The formulae (5.6a~d) to estimate coefficients are derived by a polynomial and logistic regression analysis and the R squared values are a range of 0.995 to 1.0. Where, the derived formulae (5.6a~d) consist of non-dimensional, geometric parameters like the D_a/D ratio (Race 2008) and/or the ratio of yield strength (σ_{yield}) to UTS (σ_{UTS}) that characterizes the strain hardening (Norman 2013).

$$\gamma = A_2 + (A_1 - A_2) \times \left\{1 + \left(\frac{L_a}{D \times x_0}\right)^{p}\right\}^{-1} \tag{5.5}$$

Consequently, the formula (5.3) can be rewritten as a following formula (5.6):

$$P_{Burst}^{d} = \left[A_2 + (A_1 - A_2) \times \left\{1 + \left(\frac{L_a}{D \times x_0}\right)^{p}\right\}^{-1}\right] \times \left\{2.3824 \times \sigma_{UTS} \times \left(\frac{D}{t}\right)^{-1.035}\right\} \quad (5.6)$$

Where

$$A_1 = 1885 \times \left(\frac{D_a}{D}\right)^4 - 872 \times \left(\frac{D_a}{D}\right)^3 + 138.6 \times \left(\frac{D_a}{D}\right)^2 - 9.1 \times \left(\frac{D_a}{D}\right) + 1 \quad (5.6a)$$

$$A_2 = -7230 \times \left(\frac{D_a}{D}\right)^5 + 3542 \times \left(\frac{D_a}{D}\right)^4 - 654 \times \left(\frac{D_a}{D}\right)^3 + 57 \times \left(\frac{D_a}{D}\right)^2 + \left(-6.71 \times \frac{\sigma_{yield}}{\sigma_{UTS}} + 2.27\right) \times \left(\frac{D_a}{D}\right) + 1 \quad (5.6b)$$

$$x_0 = 4.4 \times \left(\frac{D_a}{D}\right)^2 + 2.73 \times \left(\frac{D_a}{D}\right) + 0.068 \quad (5.6c)$$

$$p = 30 + 210 \times \left(1 + 10^{-500 \times (0.025 - \frac{D_a}{D})}\right)^{-1} \quad (5.6d)$$

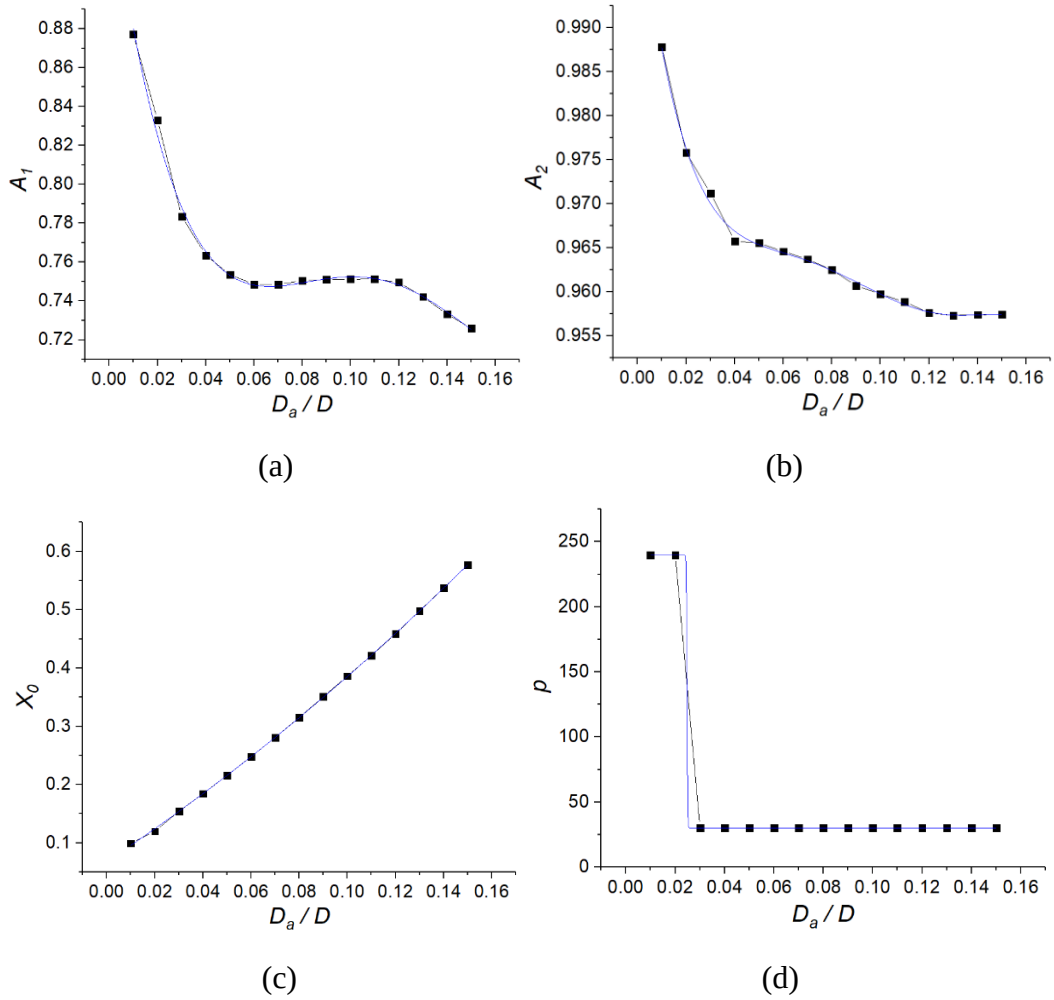

Figure 5.8 Coefficients and exponent as a function of the ratio of D_a to D: (a) coefficient A_1, (b) coefficient A_2, (c) coefficient x_0, (d) exponent p.

According to the results of Parametric Studies (I) as listed in Table B.2 in the Appendix B, the *PD formula* can be applicable for the D_a/D ratio less than 15.96%. Thus, the limit of the dent length (L_a) that varies depending on the dent depth (D_a) should be established. Using the results of Parametric Studies (I) as listed in Table B.2 in the Appendix B, the equation (5.7), the relationship between the L_a/D_a ratio and the D_a/D ratio, is derived by regression analysis of the logistic curve as shown in Figure 5.9 and the R squared value is 0.996. Consequently, the *PD formula* is applicable when the equation (5.7) is satisfied.

$$\frac{L_a}{D_a} - \left[3.566 + \left\{\frac{4.18}{1 + (\frac{D_a}{D}/0.01424)^{2.85}}\right\}\right] \geq 0 \quad (5.7)$$

This equation can be rewritten as formula (5.8):

$$L_a \geq D_a \times \left[3.566 + \left\{\frac{4.18}{1 + (\frac{D_a}{D}/0.01424)^{2.85}}\right\}\right] \quad (5.8)$$

The *PD formula* is comprised of the ratio of L_a to D and D_a to D. Therefore, both sides of the equation (5.8) can be divided by D. Finally, the applicable limit of the *PD formula* can be rewritten as formula (5.9) with a condition:

$$\frac{L_a}{D} \geq \frac{D_a}{D} \times \left[3.566 + \left\{\frac{4.18}{1 + (\frac{D_a}{D}/0.01424)^{2.85}}\right\}\right] \; for \; 0 \leq \frac{D_a}{D} \leq 15.96\% \quad (5.9)$$

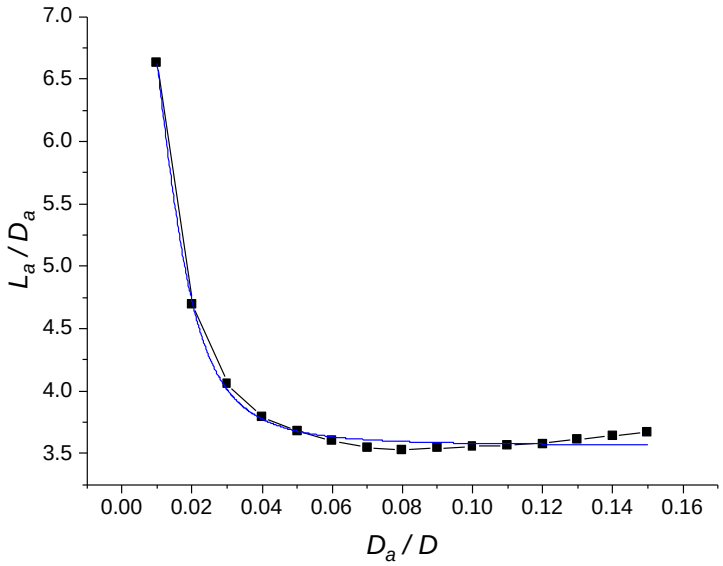

Figure 5.9 Limitation of the *PD formula* by the relationship between the ratio of L_a to D_a and D_a to D.

5.4. Validation of the PD Formula

There are two steps to validate the *PD formula*. Firstly, it is required to check how well the burst pressure calculated by the *PD formula* corresponds to the burst pressure results from the FEA based Parametric Study (I) as listed in Table B.1 in the Appendix B. Next, the reliability of the *PD formula* needs to be confirmed by comparing with the burst pressure calculated by the *PD formula* and the burst pressure results from the FEA based Parametric Study (II) as listed in Table B.3 to Table B.5 in the Appendix B. For this purpose, the correlation and statistical analysis are performed, and PPMCC and MAPE were used, respectively. This is for demonstrating that the *PD formula* can predict the burst pressure of dented pipelines using the results of the nonlinear FEA.

In case of the MAPE, this is one of the forecasting methods in statistics and used to measure the prediction accuracy between the actual value and predicted value. MAPE formula (3.9) in Section 3.2.2.5 is used and where x_i is the burst pressure calculated by *PD formula* and y_i is the burst pressure from the nonlinear FEA. The interpretation of MAPE results is based on the evaluation method proposed by Lewis (1982), and is explained in Table 3.6.

5.4.1. Comparison with FEA based Parametric Study (I) Results

To check the correlation between the burst pressure calculated by the *PD formula* and the burst pressure computed by the nonlinear FEA used to develop the formula, correlation and statistical analysis are conducted and PPMCC and MAPE are applied, respectively.

In accordance with the correlation analysis result as shown in Figure 5.10, the PPMCC is 0.991. The PPMCC is interpreted by the Evans guidance listed in Table 3.1, and indicates a very strong positive relationship between the burst pressure calculated by the nonlinear FEA and by the *PD formula*.

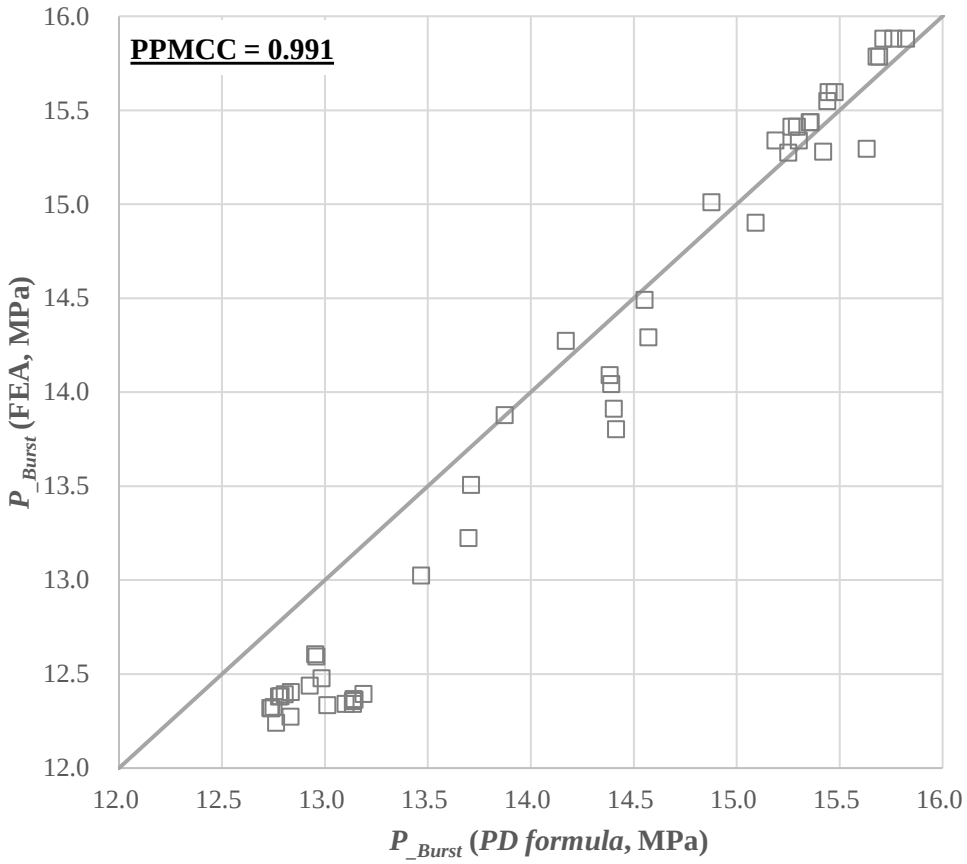

Figure 5.10 Pearson Product-Moment Correlation Coefficient between the burst pressure calculated by the *PD formula* and the FEA based Parametric Study (I) results.

In addition, MAPE is used to measure the prediction accuracy of the burst pressure between by the *PD formula* and the nonlinear FEA, and MAPE is 2.57%. Therefore, it can be concluded that the *PD formula* can substitute the nonlinear FEA to predict the burst pressure of dented pipelines for the FEA based Parametric Study (I).

5.4.2. Comparison with FEA based Parametric Study (II) Results

The reliability of the *PD formula* is validated by performing correlation and statistical analysis of the burst pressure between calculated by the *PD formula* and from the FEA based Parametric Study (II) results.

In accordance with the correlation analysis result as shown in Figure 5.11, the PPMCC, depending on the pipeline material, is distributed between 0.888 and

0.959. The PPMCC is interpreted by the Evans guidance listed in Table 3.1, and indicates a very strong positive relationship between the burst pressures from FEA based Parametric Study (II) results and the burst pressure by *PD formula*.

In addition, MAPE according to the pipeline material $X52_{\_PS(II)}$, $X65_{\_PS(II)}$, and $X80_{\_PS(II)}$ is 5.36%, 4.82%, and 5.86%, respectively. In addition, these values are used to evaluate the accuracy of the burst pressure using *PD formula*.

The results support the hypothesis that the *PD formula* is a reliable to nonlinear FEA for the prediction of the burst pressure of pipelines with a hemispherical dent.

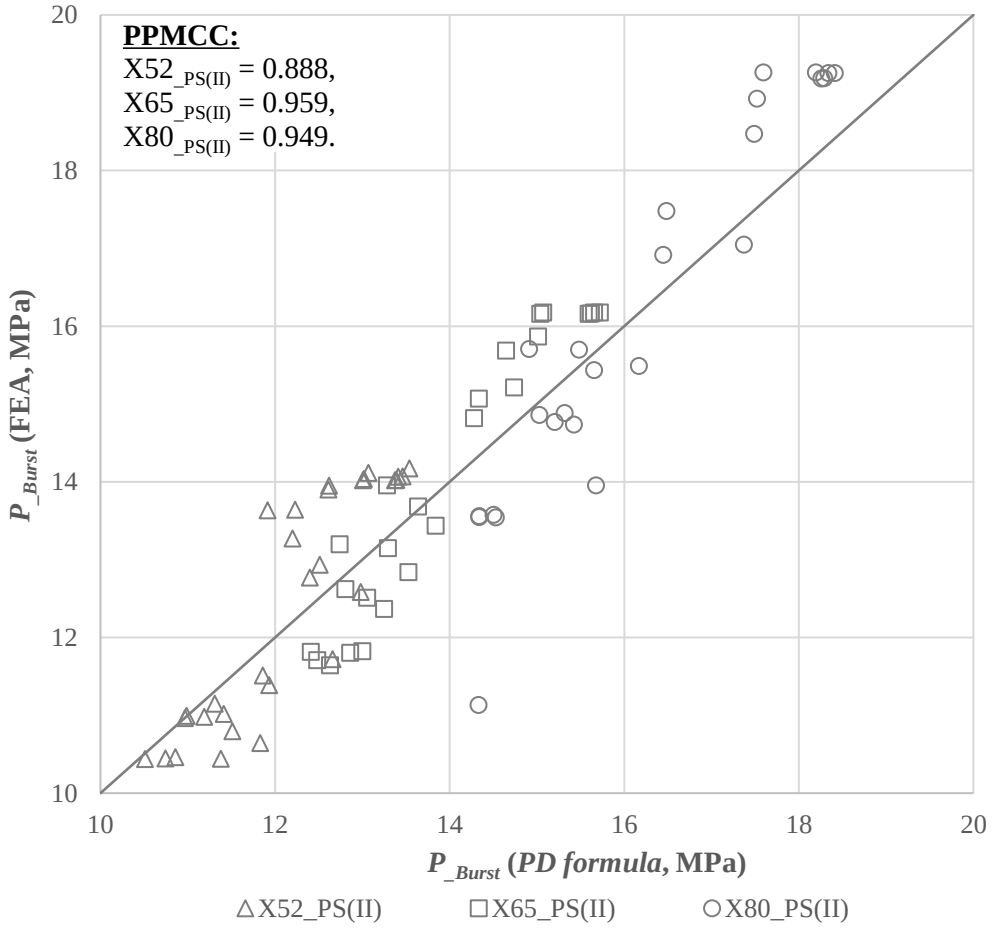

Figure 5.11 Pearson Product-Moment Correlation Coefficient between the burst pressure calculated by the *PD formula* and the FEA based Parametric Study (II) results.

5.4.3. Comparison with Experimental Results

The reliability of the *PD formula* was validated by performing correlation and statistical analysis between the burst pressure calculated by the *PD formula* and the three results of the experiment from the published papers (Kiefner et al. 1997, Shuai et al. 2018). The detailed information is as listed in Table 5.5.

Table 5.5 Validation information from the experimental result of the hemispherical dent: X52 (1) and (2) (Kiefner and Alexander 1997), X52 (3) (Shuai et al. 2018).

Characteristics	X52 (1)	X52 (2)	X52 (3)
Diameter (mm)	323.85	323.85	720
Thickness (mm)	4.7752	4.7752	8.1
Dent depth (mm)	34.773	25.654	48.68
Dent length (mm)	171.06	147.72	271.15
Yield strength (MPa)	371.6	371.6	375
Ultimate tensile strength (MPa)	529.5	529.5	468
Burst pressure, Experiment (MPa)	15.81	15.95	10.72
Burst pressure, *PD formula* (MPa)	15.30	15.35	9.78
Experiment / *PD formula*	1.034	1.039	1.096

In accordance with the correlation analysis result as shown in Figure 5.12, the PPMCC is 1.000. The PPMCC is interpreted by the Evans guidance listed in Table 3.1, and indicates a very strong positive relationship between the burst pressure calculated by the *PD formula* and from the experiment results. In addition, MAPE is obtained in a 5.27%. The obtained MAPE can be interpreted as highly accurate based on Table 3.6.

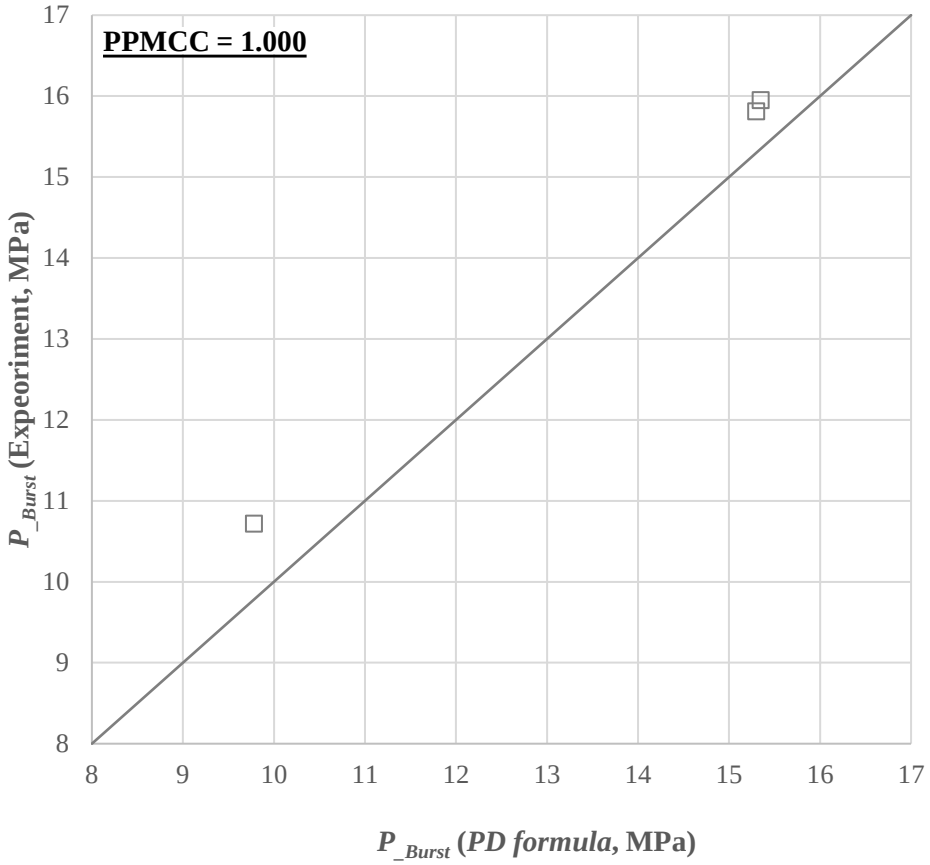

Figure 5.12 Pearson Product-Moment Correlation Coefficient between the burst pressure calculated by the *PD formula* and the experimental results.

The predicted burst pressure by the *PD formula* corresponded well with the results of experiments and showed a conservative tendency as shown in Figure 5.12. Therefore, it is confirmed that the developed *PD formula* is able to reliably predict the burst pressure of the pipeline with a dent.

5.5. Summary

In this chapter, an empirical formula has been developed to predict the burst pressure for API 5L X grade pipelines with an unconstrained, plain dent.

The proposed *PD formula* has been derived by regression analysis of the numerical analysis dataset, and validated by comparison with the 80 cases nonlinear FEA based Parametric Study results and three results of the experiment. The reliability

of the *PD formula* has been validated by performing the correlation and statistical analysis of the burst pressure between calculated by the *PD formula* and from the nonlinear FEA based Parametric Study results, and between by the *PD formula* and from the experimental results.

According to the validation results, the results of burst pressure calculated by the *PD formula* show good agreement with the nonlinear FEA based Parametric Study results and the burst pressure results of the experiment. Therefore, it can be concluded that the *PD formula* is able to reliably predict the burst pressure of pipelines with a dent.

CHAPTER 6

6. THE APPLICABILITY OF THE DEVELOPED FORMULA TO THE PIPELINES WITH SPHEROIDAL DENTS

As mentioned in Section 2.2, it is necessary to study on the influence of dent shape determined by the ratio of dent length and dent width on the burst pressure. To this end, a spheroidal indenter is employed to conduct this research. And, as seen in Table 6.1, the spheroidal indenter type is classified into a spheroidal indenter in the circumferential direction, *SWD*, and a spheroidal indenter in the axial direction, *SLD*, according to the ratio of the length and width. If the width is greater than the length, it is denoted as *SWD*, and for the width less than the length, it is denoted as *SLD*. In the case of the length equal to the width of the indenter is same as the hemispherical indenter as denoted *HSD*.

Table 6.1 Indenter types in accordance with the indenter length (L_I) and width (W_I).

Indenter		Length (L_I, mm)			
		50	75	100	150
Width (W_I, mm)	50	*HSD*	*SLD*	*SLD*	*SLD*
	75	*SWD*	*HSD*	*SLD*	*SLD*
	100	*SWD*	*SWD*	*HSD*	*SLD*
	150	*SWD*	*SWD*	*SWD*	*HSD*

Furthermore, the applicability of *PD formula* is validated by comparing the results from the *PD formula* with the results from the FEA and experimental test.

6.1. FEA Based Parametric Study

The first purpose of the study regarding a dent produced by the spheroidal indenter

on API 5L X52 pipeline is to investigate the effects of the pipeline longitudinal dent length and transverse dent length (=dent width) on the pipeline structural integrity. The second is to review whether the *PD formula* for predicting the burst pressure of pipelines with a hemispherical dent (Figure 6.1 (a)) is applicable to predicting the bursting pressure of pipelines with a spheroidal dent produced by the indenter shown in Figure 6.1 (b).

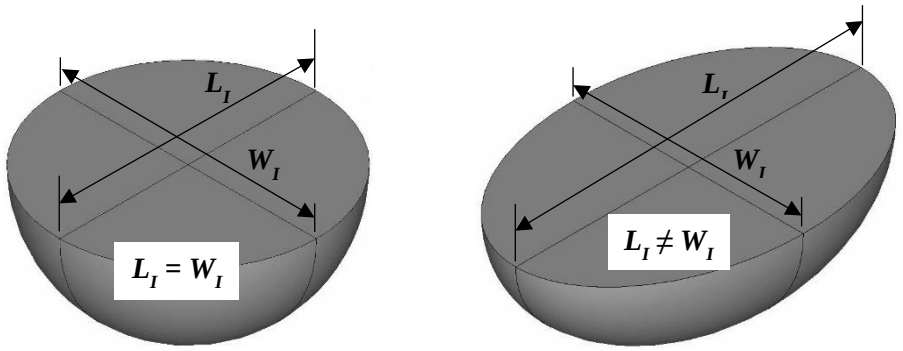

(a) (b)

Figure 6.1 Indenter types used in Finite Element Aanlysis based parametric study: (a) hemispherical indenter, (b) spheroidal indenter.

The basic methodology of using parametric studies to determine the burst pressure for a pipeline with a spheroidal dent follows the research methodology for pipelines with a dent produced by the hemispherical indenter as described in Section 3.1.1. To do this, the nonlinear FEA has been carried out using the X52 material properties and geometric information in Table 6.2 and the variables in Table 6.3.

In total, 48 case studies have been conducted for pipelines with a spheroidal dent. The burst pressure calculated using the *PD formula* is compared with the results of FEA based Parametric Study and experiment.

6.1.1. Definition of Spheroidal Indenter

To carry out the FEA based Parametric Study for the pipelines with a spheroidal dent, the length and width of the spheroidal indenter need to be defined. The length (L_I) and the width (W_I) of the spheroidal indenter are defined as the length in the

pipeline axial direction and the length in the circumferential direction, respectively, as shown in Figure 6.2.

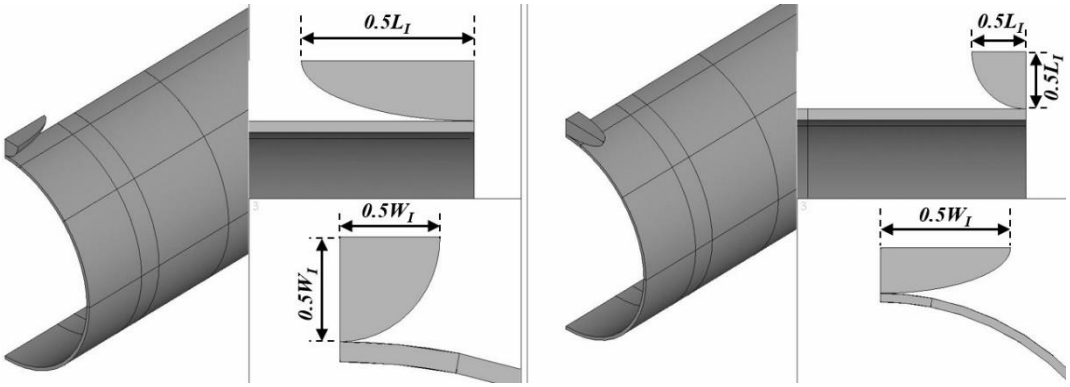

(a) **(b)**

Figure 6.2 Definition of the length (L_I) and width (W_I) of the spheroidal indenter: (a) L_I is greater than W_I, (b) L_I is less than W_I.

6.1.2. Definition of Dent Width

The purpose of this chapter is to review the effect of dent length and width on the structural integrity of pipelines. From the FEA based Parametric Study results, LOC_i^O, LOC_i^D and D_i as defined in Figure 6.3 (a) can be obtained, and the relation of them is expressed as the formula (6.1).

$$LOC_i^O = LOC_i^D + D_i \tag{6.1}$$

Where LOC_i^O is the coordinate of the original pipeline, LOC_i^D is the shifted coordinate of LOC_i^O due to the indentation, and D_i is the dent depth based on the LOC_i^O. The subscript i is the node number located in the circumferential direction of the FE model.

To investigate the effect of the dent length and width consistently, the dent width should be defined using the same construct as the dent length defined in Section 5.1.1. That is, the dent width should be defined as a value at the position of half the dent depth. To achieve this, the shape of the dented pipeline needs to be transformed

to the same shape used to define the dent length. As seen in Figure 6.3 (a), a dented shape transformed based on the outer diameter (D) of the pipeline can be defined using the formula (6.2).

$$LOC_i^{D'} = D - D_i \tag{6.2}$$

Where $LOC_i^{D'}$ is the transformed coordinate of LOC_i^D to normalize to the same shape used to define the dent length.

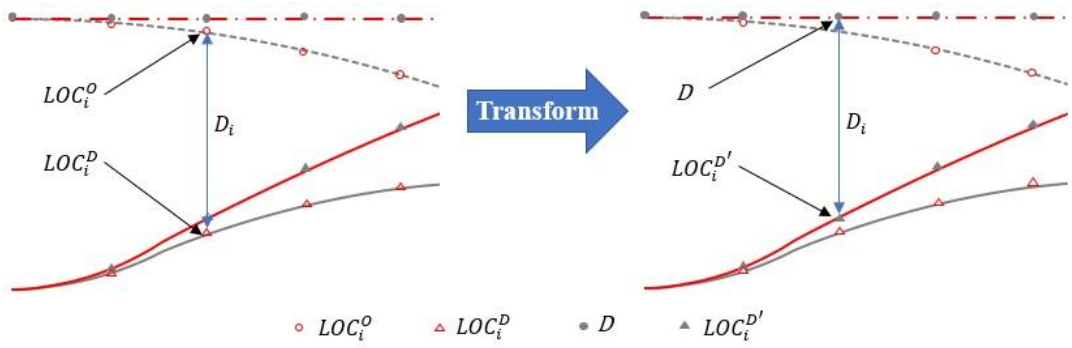

(a)

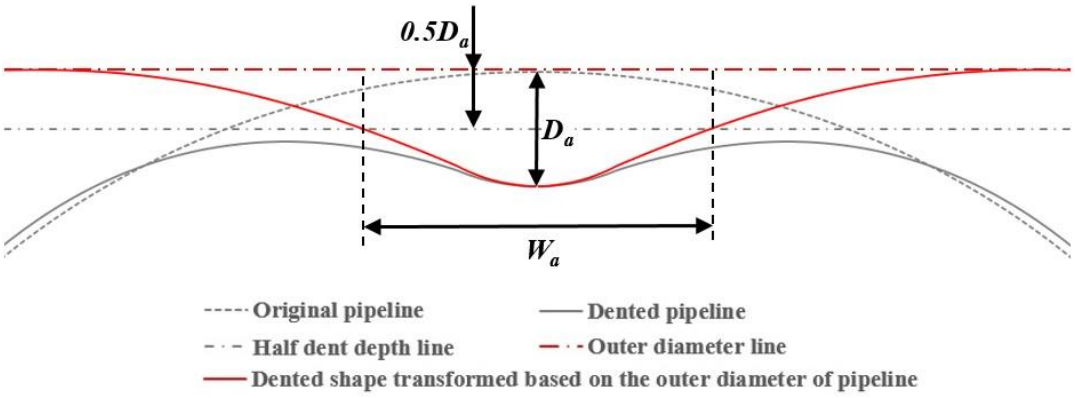

(b)

Figure 6.3 Definition of the dent width (W_a) after removal of the indenter: (a) the normalization of the LOC_i^D based on the LOC_i^O into the $LOC_i^{D'}$ based on the D, (b) definition of the dent width (W_a).

Consequently, the dent width is defined as the distance between the intersection points where the created curve meets the half dent depth line as shown in Figure 6.3 (b).

Where W_a as defined in Figure 6.3 (b) is the dent width measured after removal of the indenter *i.e.* including the rebound effect and this result is used to verify the applicability of the developed empirical formula to the pipeline with a spheroidal dent.

6.1.3. Pipeline Material Properties and Geometric Information

The pipeline material properties and the geometric information used for construction of the FEA model for the parametric study are listed in Table 6.2.

Table 6.2 Material properties and geometric information for Finite Element Analysis model of the pipeline with a spheroidal dent (API 2004).

Material properties						Geometric information	
Grade	Young's modulus (MPa)	Tangent modulus (MPa)	Poisson's ratio	Yield strength (MPa)	UTS (MPa)	Outer diameter (*mm*)	Thickness (*mm*)
X52	207,000	1186	0.3	358.53	455.05	323.85	4.7752

6.1.4. Variables for FEA Based Parametric Study

The variables considered in the parametric study are the ratio of the initial dent depth (D_b) to pipeline outer diameter (D), the length (L_I) and the width (W_I) of the spheroidal indenter as listed in Table 6.3. Where D_b is the initial indentation value of the dent before the rebound and this value is used only for creating the dent shape on the pipelines.

Based on the mentioned variables, 48 studies have then been conducted using nonlinear FEA.

Table 6.3 Variables for the FEA based Parametric Study of the spheroidal dented pipelines.

Material	X52
Design Variables	Bounding cases
D_b / D (%)	2.5, 5 and 10
L_I (*mm*)	50, 75, 100, and 150
W_I (*mm*)	50, 75, 100, and 150

6.2. FEA based Parametric Study Results

6.2.1. Burst Pressure according to Dent Depth, Length and Width

The ratio of the initial dent depth (D_b) to pipeline outer diameter (D), the length (L_I) and the width (W_I) of the spheroidal indenter is simple, while the obtained ratio of the dent depth (D_a) to pipeline outer diameter (D), the length (L_a) and width (W_a) of dent after removal of the indenter is not simple as evident from Table B.6 in the Appendix B.

Table 6.4 is a sample to explain the reasons for using the D_b/D ratio, the length (L_I) and the width (W_I) of the spheroidal indenter instead of the D_a/D ratio, the length (L_a) and the width (W_a) of the dent.

Table 6.4 Sample to explain the reasons for using the D_b/D ratio, the length (L_I) and the width (W_I) of the spheroidal indenter.

No.	D_b/D (%)	L_I (*mm*)	W_I (*mm*)	D_a (*mm*)	D_a/D (%)	L_a (*mm*)	L_a/D (%)	W_a (*mm*)	W_a/D (%)	Burst Pressure (MPa)		
										FEA	*PD formula*	
											L_a based	W_a based
1	2.5	50	50	4.41	1.36	33.74	10.42	29.05	8.97	13.2	12.43	12.41
2	2.5	75	50	4.25	1.31	41.36	12.77	31.64	9.77	13.57	13.36	12.45
3	2.5	100	50	3.99	1.23	49.72	15.35	34.16	10.55	13.58	13.38	13.38
4	2.5	150	50	3.58	1.11	67.4	20.81	37.9	11.7	13.6	13.42	13.42

If the values of the D_b/D ratio, the length (L_I) and the width (W_I) of the spheroidal indenter are used, it can be easily classified the group as "*Db/D=2.5%, WI=50mm and four different* L_I*".* However, once the D_a/D ratio, the length (L_a) and the width (W_a) of the dent are used, all values should be listed without classification. In other words, in the former case, the conditions are categorized on an obvious basis and easy to find out a trend. In the latter case, on the other hand, it means that it is difficult to find out the relationship between burst pressure and the dent depth, length, and width.

For this reason, the initial dent depth (D_b), dent length (L_I) and dent width (W_I) are used for the convenience of the analysis of the results.

The effects of the depth, length and width of the spheroidal dent have been investigated based on the FEA based Parametric Study listed in Table B.6 in the Appendix B. The burst pressure of the pipelines with a spheroidal dent according to the ratio of the initial dent depth (D_b) to pipeline outer diameter (D), the length (L_I) and width (W_I) of dent is illustrated in Figure 6.4, and the burst pressure is lower with deeper dent depth, shorter dent length and shorter dent width.

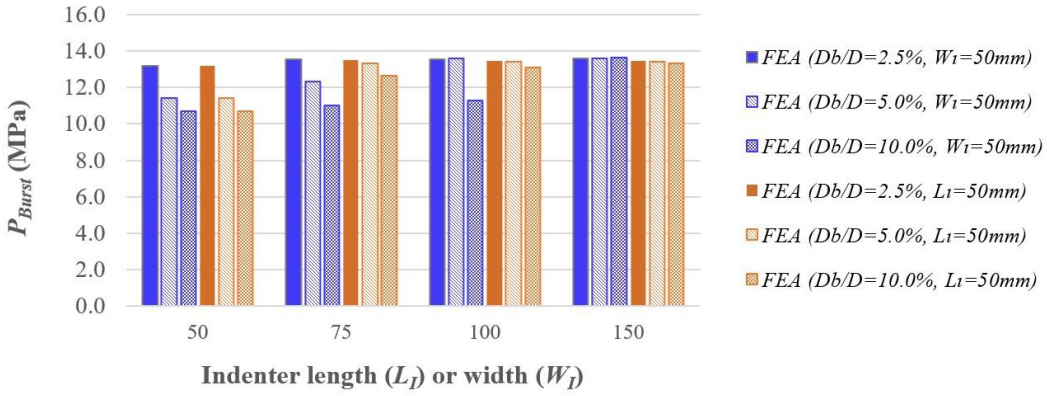

(a)

Figure 6.4 Burst pressure according to the dent depth, length and width: (a) at 50mm of L_I or W_I.

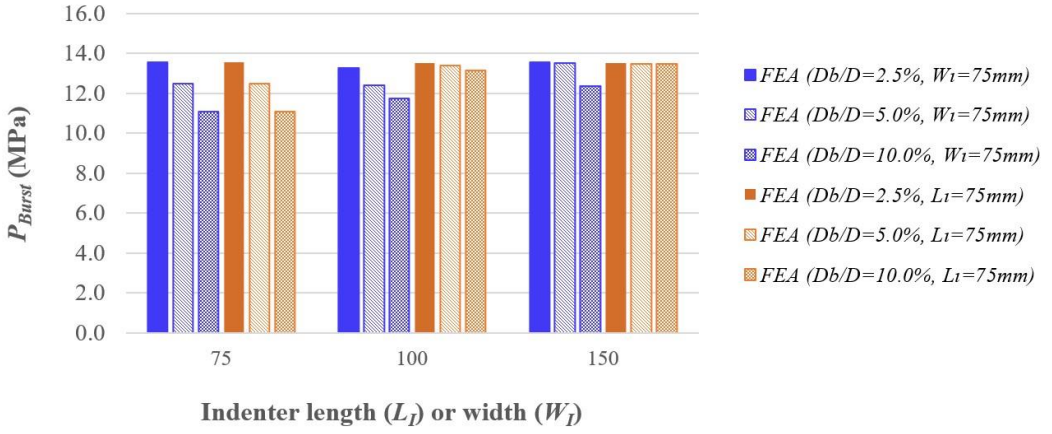

(b)

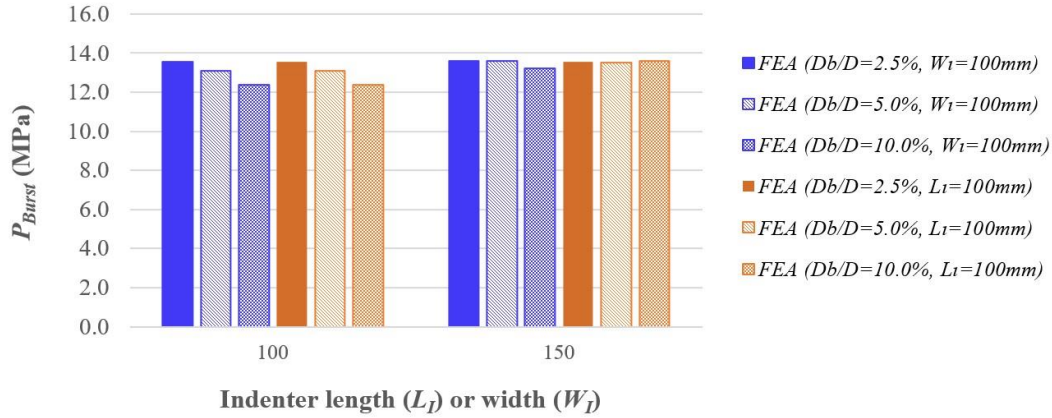

(c)

Figure 6.4 (*cont.*) Burst pressure according to the dent depth, length and width: (b) at 75mm of L_I or W_I and (c) at 100mm of L_I or W_I.

Figure 6.5 shows the burst pressure when the HSD (L_I=W_I) shapes are 50*mm*, 75*mm*, 100*mm* and 150*mm*. As the larger values of L_I and W_I at the same dent depth indicates the higher burst pressure. And the burst pressure is lower with deeper values of dent depth at the same values of L_I and W_I.

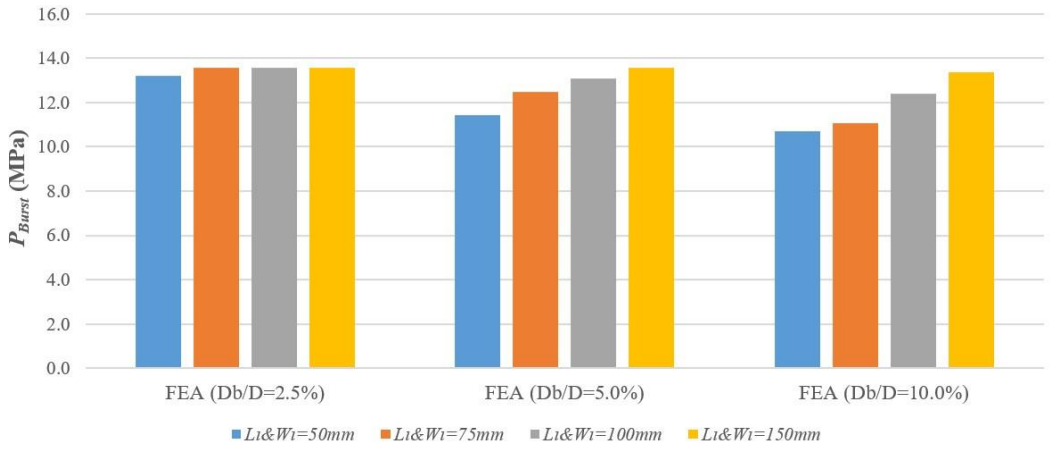

Figure 6.5 Burst pressure to the same dent length (L_1) and dent width (W_1).

Consequently, Figure 6.6 shows that the burst pressure of the pipelines with a spheroidal dent increases in the direction indicated by the arrow. In other words, as the longer indenter length (or dent length) shows the higher burst pressure at the same dent width, and the burst pressure is higher with the longer indenter width (or dent width) at the same dent length. This result is similar with the research results conducted by Wu et al. (2016).

Indenter		Length (mm)			
		50	75	100	150
Width (mm)	50	HSD	SLD	SLD	SLD
	75	SWD	HSD	SLD	SLD
	100	SWD	SWD	HSD	SLD
	150	SWD	SWD	SWD	HSD

Figure 6.6 Tendency of the burst pressure of pipelines with a spheroidal dent.

6.3. Validation of Applicability of Developed Empirical Formula

6.3.1. Comparison with FEA Based Parametric Study Results

A spheroidal dent is expressed in terms of both the dent length and the dent width. Therefore, to calculate the burst pressure of the pipelines with a spheroidal dent using the *PD formula* proposed in Section 5.3, it is necessary to choose either the dent length (L_a) or the dent width (W_a) as the L_a alternative to the *PD formula*. In the case of the using dent length (L_a), it is denoted as L_a based approach, and in the case of the using dent width (W_a), it is denoted as W_a based approach. The burst pressure results from FEA, La based approach and Wa based approach are listed in Table B.6 in the Appendix B.

As depicted in Figure 6.7, the W_a based approach is more conservative than the L_a based approach.

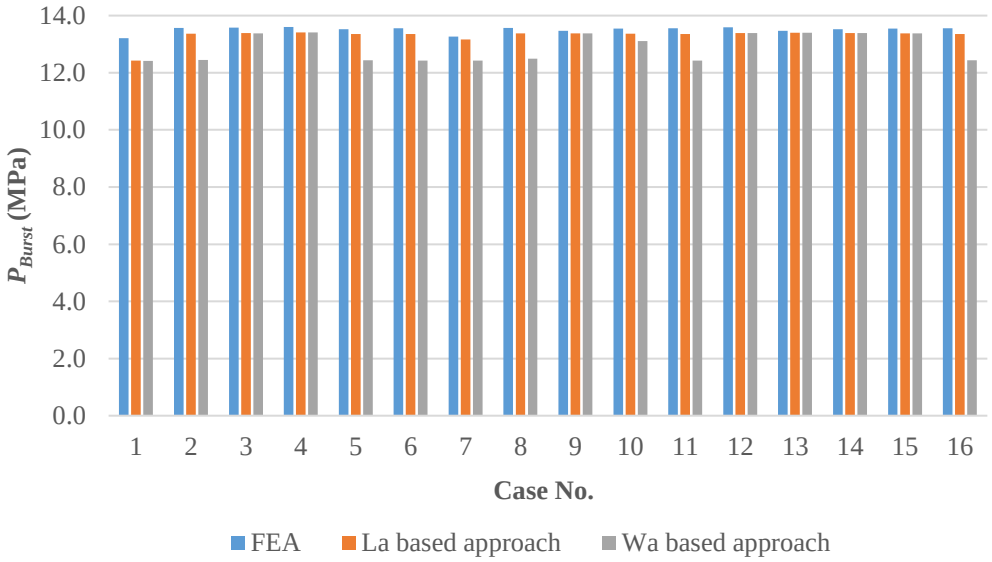

(a)

Figure 6.7 Comparison with the Finite Element Analysis and *PD formula*: for the ratio of initial dent depth to pipeline diameter, (a) 2.5%.

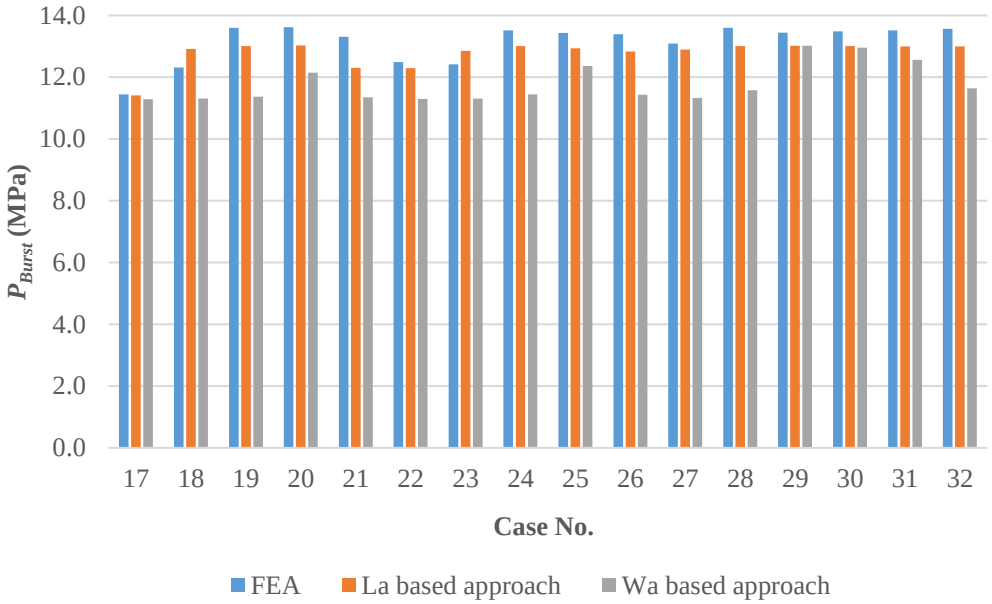

(b)

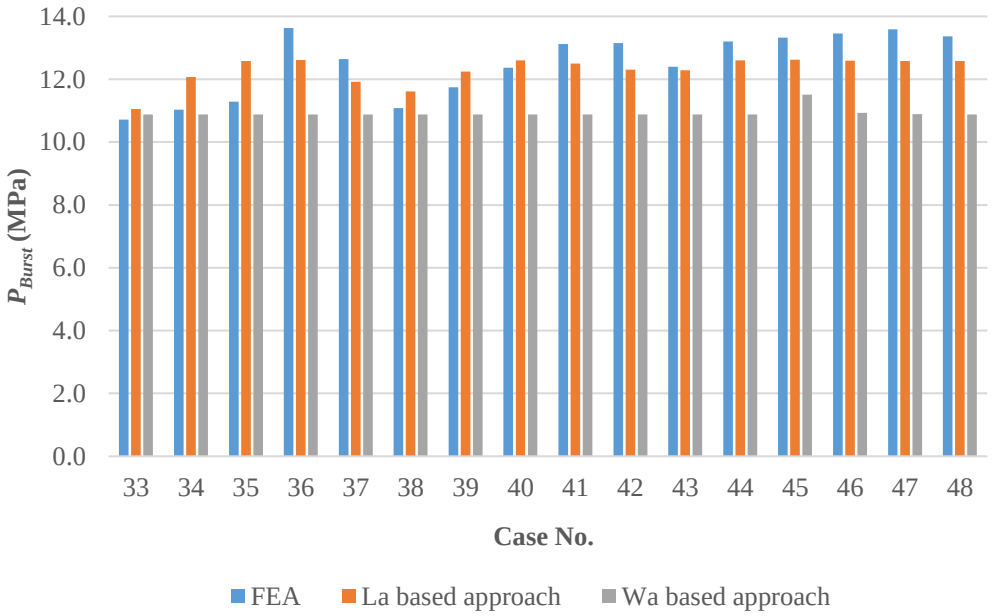

(c)

Figure 6.7 (*cont.*) Comparison with the Finite Element Analysis and *PD formula*: for the ratio of initial dent depth to pipeline diameter, (b) 5.0% and (c) 10.0%.

Figure 6.8 (a) shows the scatter plot between the burst pressure calculated by the proposed formula and the burst pressure computed using nonlinear FEA. According to the correlation analysis result, the PPMCC between FEA and the W_a based approach as demonstrated in Figure 6.8 (b) is 0.546, and the PPMCC between FEA and the L_a based approach as indicated in Figure 6.8 (c) is 0.784. The PPMCC for 0.546 and 0.784 is decoded by the Evans guidance listed in Table 3.1, and indicates a moderate and strong positive relationship, respectively. Therefore, it is reasonable to estimate the burst pressure of the pipeline with a spheroidal dent using the *PD formula* based on the L_a based approach. Moreover, measuring the dent length in the field is easier than measuring the dent width.

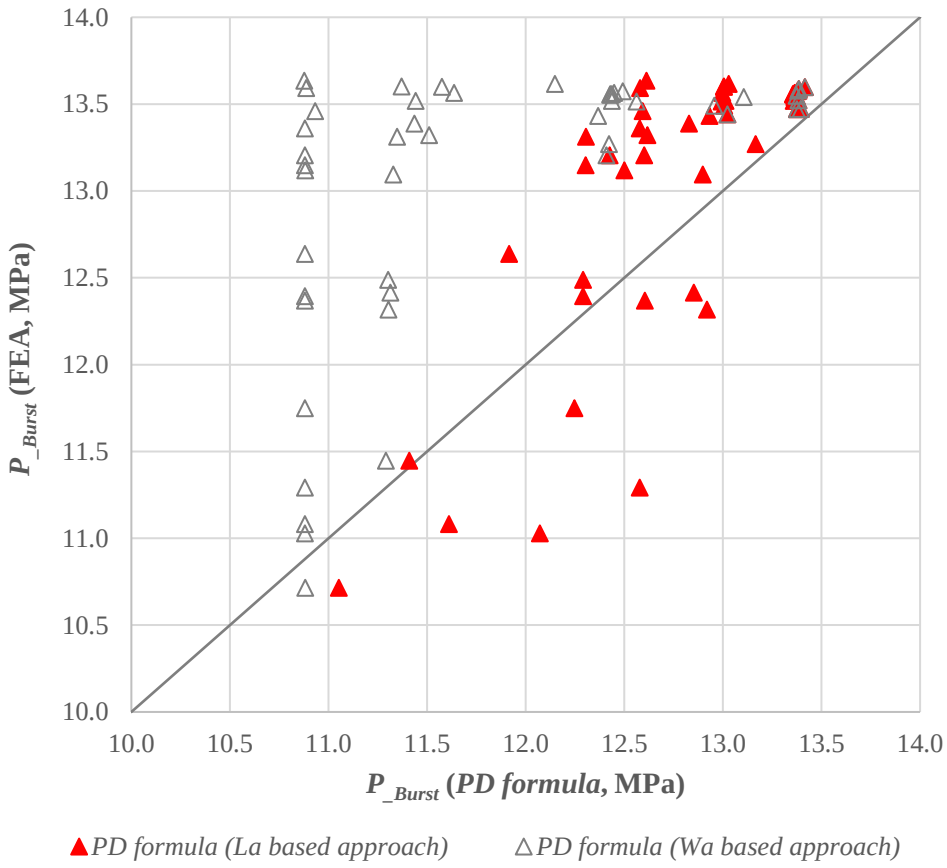

(a)

Figure 6.8 Scatter plot of the burst pressure by the *PD formula* and Finite Element Analysis: (a) L_a and W_a based approach.

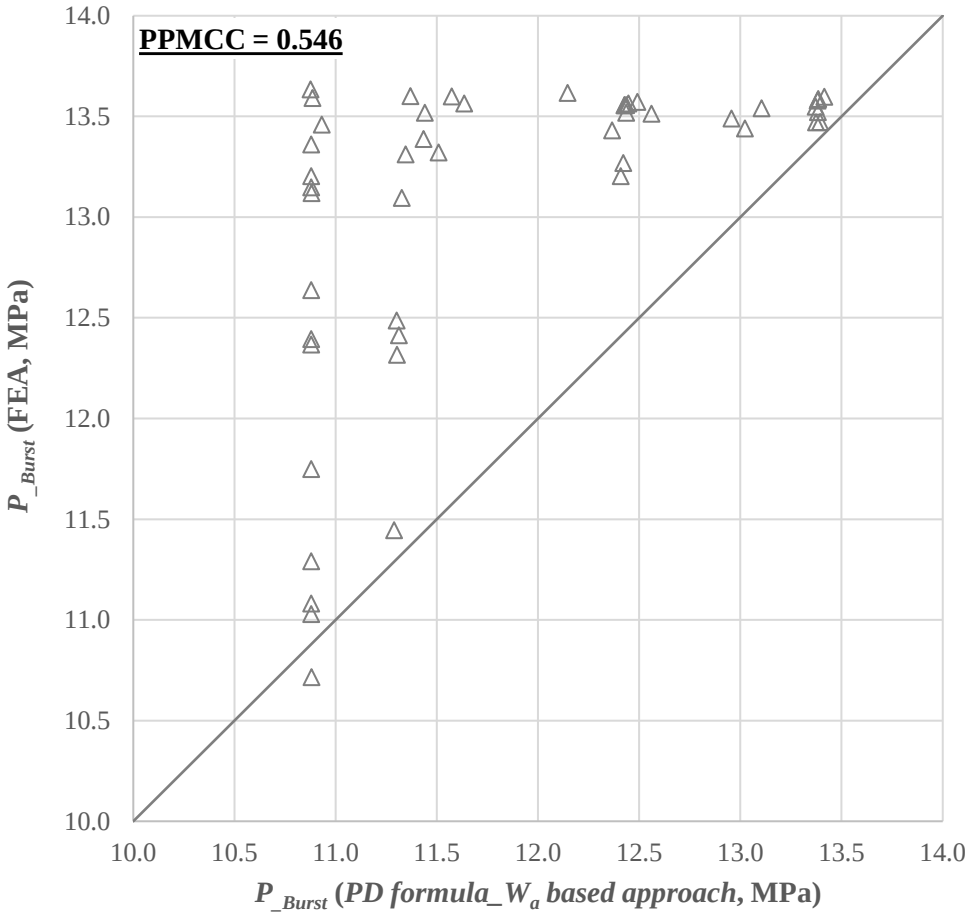

(b)

Figure 6.8 (*cont.*) Scatter plot of the burst pressure by the *PD formula* and Finite Element Analysis: (b) W_a based approach with Pearson Product-Moment Correlation Coefficient.

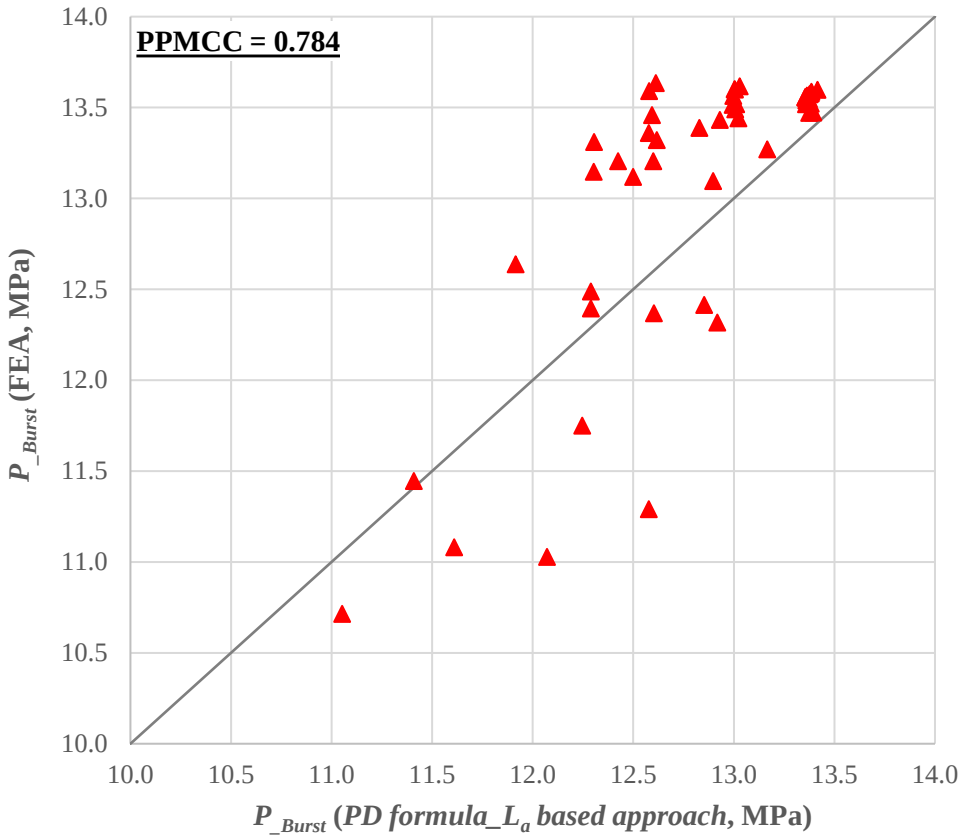

(c)

Figure 6.8 (*cont.*) Scatter plot of the burst pressure by the *PD formula* and Finite Element Analysis: (c) L_a based approach with Pearson Product-Moment Correlation Coefficient.

6.3.2. Comparison with Experimental Results

The reliability of the *PD formula* was validated by comparison between the burst pressure calculated by the *PD formula* and the one result of the experiment from the published paper (Bjørnøy et al. 2000). The detailed information is as listed in the Table 6.5.

Table 6.5 Validation information from the experimental result of the spheroidal dent (Bjørnøy et al., 2000).

Characteristics	X52
Diameter (mm)	273
Thickness (mm)	10.2
Dent depth (mm)	32.76
Dent length (mm)	247.52
Yield strength (MPa)	404
Ultimate tensile strength (MPa)	556
Burst pressure, Experiment (MPa)	42
Burst pressure, *PD formula* (MPa)	41.14
Experiment / *PD formula*	1.021

According to the Table 6.5, the predicted burst pressure (41.14 MPa) using the *PD formula* corresponded well with the conservatively predicted the result (42 MPa) of the experiment. Therefore, it is further confirmed that the *PD formula* is confirmed to be able to reliably predict for the burst pressure of the pipeline with a spheroidal dent.

6.4. Summary

In this chapter, the effects of the pipeline longitudinal dent length and transverse dent length (=dent width) on the pipeline structural integrity are investigated. In addition, the applicability to pipelines with a spheroidal dent of the *PD formula* that can predict the burst pressure of pipelines with a hemispherical dent is reviewed.

According to the FEA based Parametric Study results, the burst pressure of pipelines with a spheroidal dent is lower with deeper dent depth, shorter dent length and shorter dent width. In addition, based on the validation results, the burst pressure calculated using the *PD formula* is in good agreement with the nonlinear FEA based Parametric Study results and the burst pressure result of the experiment. Therefore, it can be concluded that the *PD formula* is able to reliably predict the burst pressure of the pipeline with a spheroidal dent.

CHAPTER 7

7. DEVELOPMENT OF A DEEP NEURAL NETWORK MODEL FOR BURST PRESSURE PREDICTION

In this research, DNN models have been developed to predict the burst pressure of flawless pipelines and pipelines with a dent using the FEA based Parametric Study results and the experimental results. The FEA based Parametric Study results and the experimental results for the flawless pipeline, the pipelines with a hemispherical dent and the pipelines with a spheroidal dent have been discussed in Chapters 4, 5, and 6, respectively and these results are used for the *training*, *validation*, and *test dataset* to develop the DNN. As explained in Section 3.2.2.5, the MAPE is utilized as the cost function of the *training* and *validation* of the DNN model.

Finally, the burst pressure computed by the developed DNN model is compared with the results calculated by the FEA and the experimental test results.

7.1. DNN Model for Flawless Pipelines

To develop the DNN model to predict the burst pressure of flawless pipelines, 450 data amongst the 529 data from the FEA based Parametric Study results of the flawless pipeline listed in Table A.2 and Table A.3 in the Appendix A have been used for the *training* and *validation dataset*, and 93 data including the remaining 79 data and 14 experimental data have been used for the *test dataset*. The proportion of the *training* and *validation* and the *test* in the total data is 80% and 20%, respectively. In here, the *training* and *validation dataset* is randomly split at a ratio of 80% to 20%.

According to Figure 7.1, the cost function of the *training* and *validation* stages in terms of the MAPE of the DNN model for the flawless pipelines converged on

0.90% and 8.26%, respectively, and stabilized.

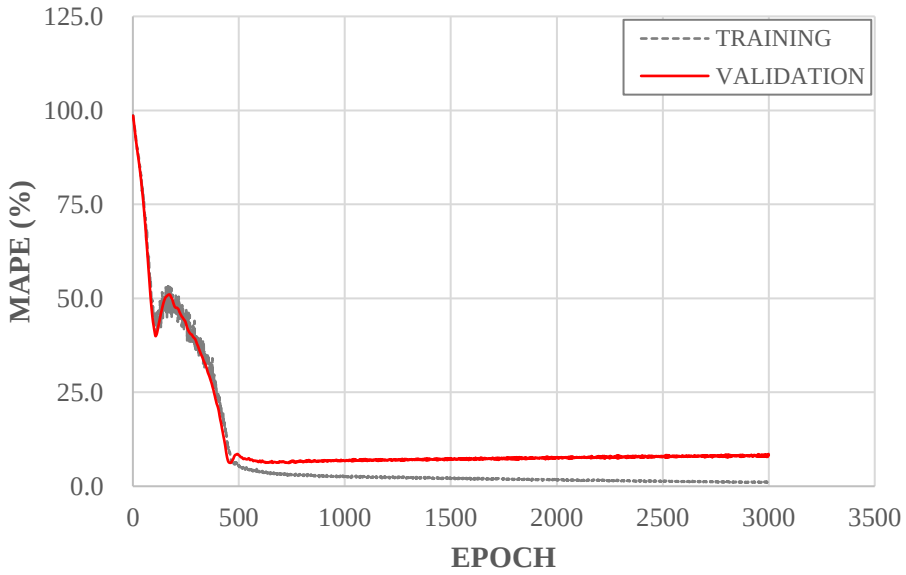

Figure 7.1 Cost function (MAPE) per EPOCH for the flawless pipelines.

7.1.1. Comparison with FEA Based Parametric Study Results

For the validation of the DNN model for the flawless pipelines, the burst pressure computed by the DNN model has been compared with the test dataset of 93 burst pressure results determined by the FEA and experiments. The comparison of results was performed by correlation analysis to examine the relationship as well as by statistical analysis to determine the accuracy of prediction, and PPMCC and MAPE were used, respectively.

As indicated by the correlation analysis result, shown in Figure 7.2, the PPMCC is 0.986. Compliant with the Evans guidance listed in Table 3.1, this value designates a very strong positive relationship between the burst pressure calculated by the DNN model and by the FEA.

In addition, the resultant MAPE from the burst pressure calculated by DNN and by FEA is 9.61%, which can be interpreted as highly accurate based on Table 3.6.

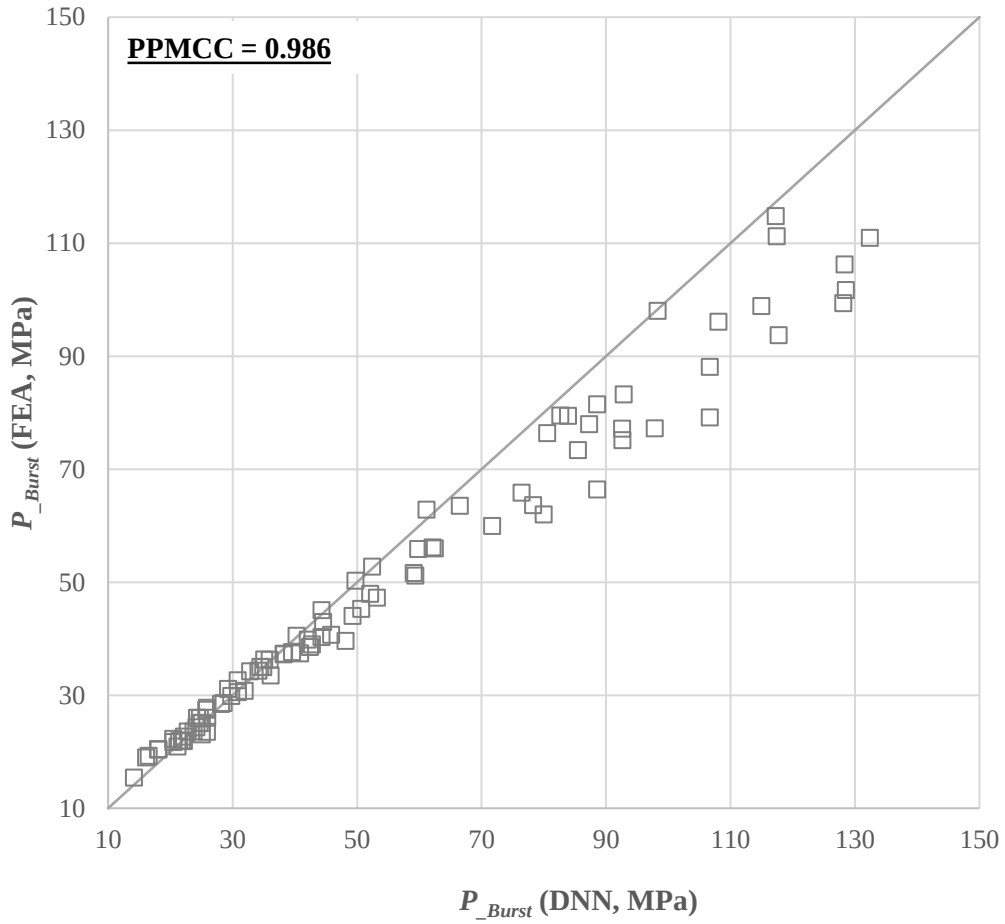

Figure 7.2 Pearson Product-Moment Correlation Coefficient between the burst pressure computed by the Deep Neural Network model and the FEA based Parametric Study results for the flawless pipelines.

7.1.2. Comparison with Experimental Results

The reliability of the DNN model was validated by performing correlation and statistical analysis between the burst pressure calculated by the DNN model and the 14 results of the experiment from the published paper (Law et al. 2007). The detailed information is as listed in Table 4.3.

In accordance with the correlation analysis results between the DNN model and experiment and between the *FD formula* and experiment as shown in Figure 7.3, the PPMCCs are 0.969 and 0.993 and the MAPEs are 4.1% and 2.14%, respectively. The PPMCCs interpreted by the Evans guidance listed in Table 3.1 and MAPEs

interpreted by the Lewis guidance listed in Table 3.6 indicate a very strong positive, highly accurate relationship between the burst pressure computed by the DNN model and the experimental test results and between the burst pressure calculated by the *FD formula* and by the experimental test results.

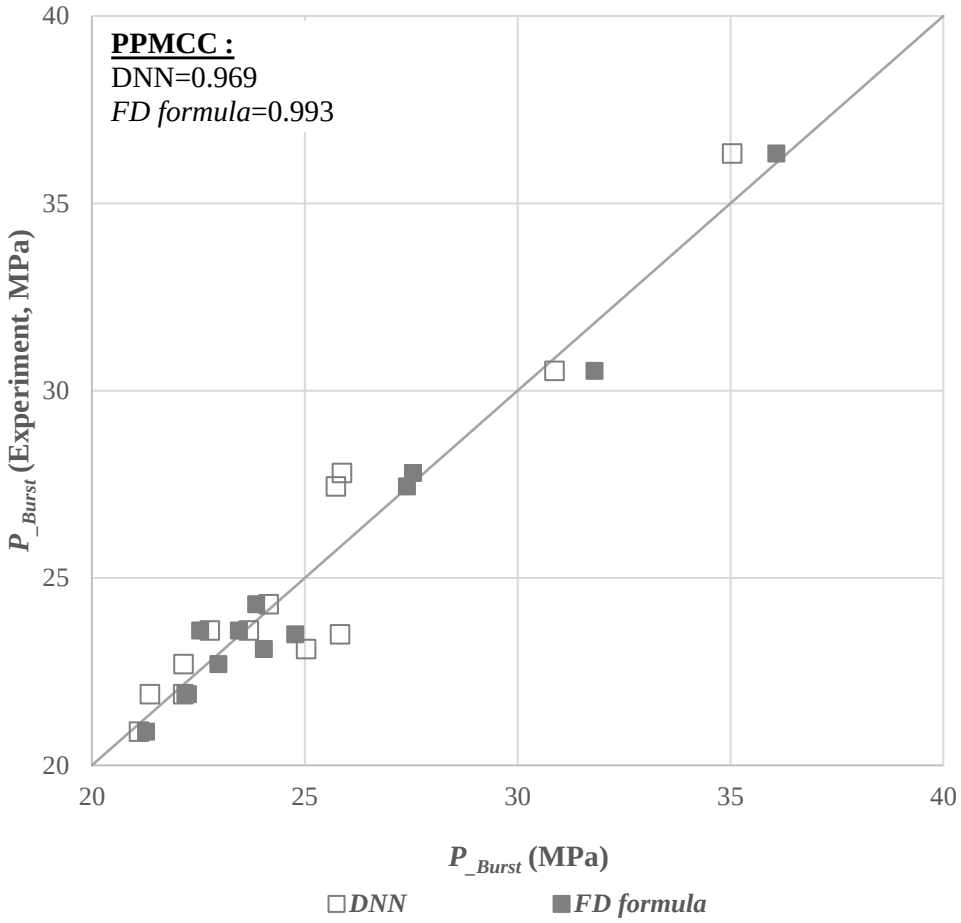

Figure 7.3 Pearson Product-Moment Correlation Coefficient: (open square) between the burst pressure computed by the Deep Neural Network model and the experimental results, (closed square) between the burst pressure caclulated by the FD formula and the experimental results.

From the above results handled in Section 7.1.1 to 7.1.2, it can be concluded that the DNN model can reliably predict the burst pressure of the flawless pipeline. In addition, it is confirmed that the FD formula predicts the burst pressure test results of the flawless pipelines as robust as the DNN model.

7.2. DNN Model for Pipelines with a Hemispherical Dent

In the case of pipelines with a hemispherical dent, the DNN model has been developed based on the 150 data from the FEA based Parametric Study results as listed in Table B.2 in the Appendix B, the *test* stage has been conducted using the $X52_{PS(I)}$ as listed in Table B.1 in the Appendix B to prove the DNN model. If a DNN model is well developed, it is no doubt that the burst pressure computed by the DNN model will have a good agreement with the $X52_{PS(I)}$ data. This is because the 150 data used to develop the DNN model was generated by linear interpolation of the $X52_{PS(I)}$ data. The proportion of the *training* and *validation dataset* and the *test dataset* in the total data is 75% and 25%, respectively. In here, the *training* and *validation dataset* is randomly split at a ratio of 80% to 20%.

As well, $X52_{PS(II)}$ as listed in Table B.3, $X65_{PS(II)}$ as listed in Table B.4, $X80_{PS(II)}$ as listed in Table B.5 in the Appendix B, and three results of the experiment as listed in Table 5.5 were used for the *test* of the developed DNN model.

Figure 7.4 represented the cost function of the *training* and *validation* in terms of MAPE of the DNN model for the pipelines with a hemispherical dent, and the decrease in the MAPE is visualized across the epoch. In addition, the values congregated between 0.04% and 0.42%, and between 0.08% and 0.30% as listed in Table 7.1, respectively, and it shows the converging and stabilizing of the DNN model. In addition, the resultant MAPEs from the *training* and *validation* stages can be interpreted as highly accurate based on Table 3.6.

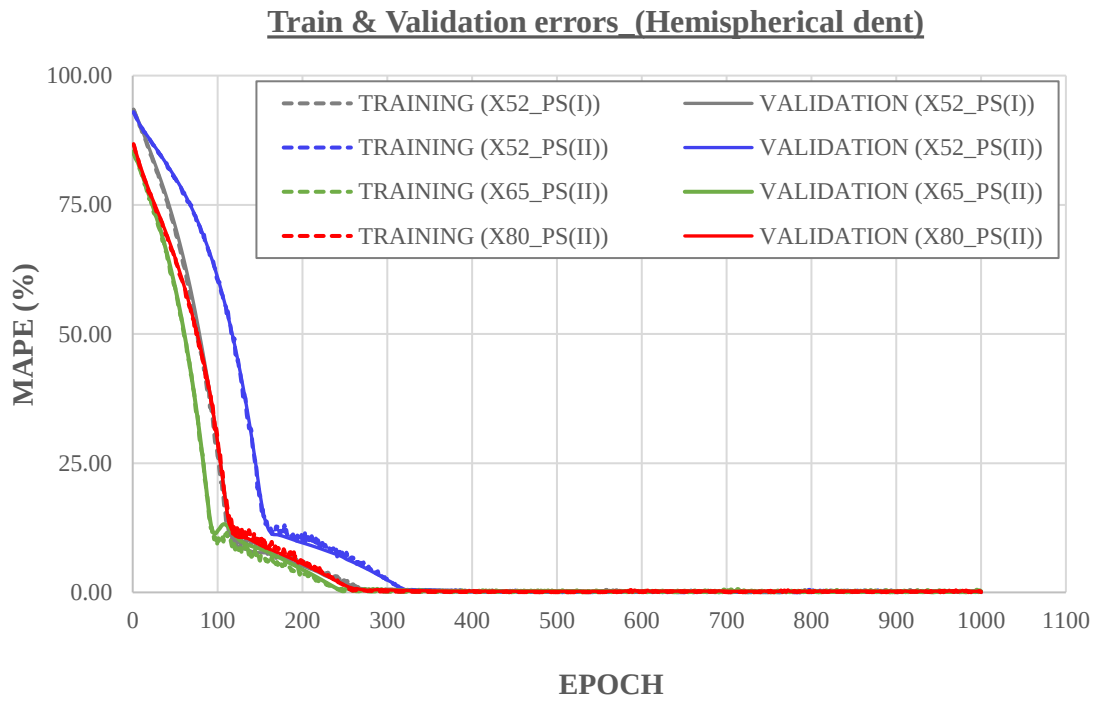

Figure 7.4 Cost function (MAPE) per EPOCH for the pipelines with a hemispherical dent.

Table 7.1 Cost function in terms of Mean Absolute Percentage Error in accordance with the applied material of pipelines.

		MAPE (%)	
		Train	Validation
Hemispherical dent	$X52_{PS(I)}$	0.16	0.30
	$X52_{PS(II)}$	0.14	0.08
	$X65_{PS(II)}$	0.42	0.25
	$X80_{PS(II)}$	0.04	0.22

7.2.1. Comparison with FEA Based Parametric Study Results

For the validation of the DNN model for the pipeline with a hemispherical dent, the burst pressure computed by the DNN model has been compared with the burst pressure determined by the FEA.

As indicated by the correlation analysis result as shown in Figure 7.5, the PPMCC

depending on the pipeline material is distributed between 0.959 and 1.0. Based on the Evans guidance listed in Table 3.1, these values indicates a very strong positive relationship between the burst pressure calculated by the DNN model and by the FEA.

The prediction accuracy (measured using MAPE) of the burst pressure from the DNN model and FEA for the $X52_{\_PS(I)}$, $X52_{\_PS(II)}$, $X65_{\_PS(II)}$, and $X80_{\_PS(II)}$ dataset is 0.28%, 2.17%, 2.81%, and 5.55%, respectively. The obtained MAPEs can be interpreted as highly accurate based on Table 3.6. According to the results, it can be said that DNN is able to reliably estimate the burst pressure of the pipeline with a hemispherical dent.

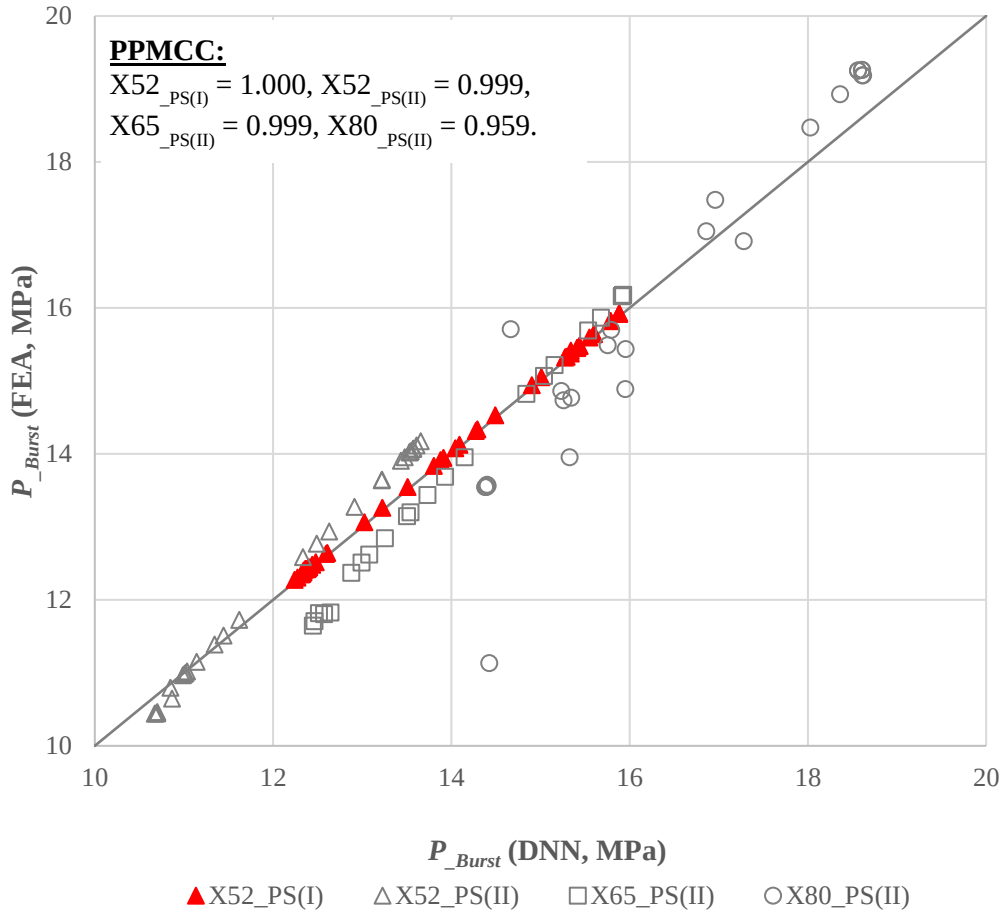

Figure 7.5 Pearson Product-Moment Correlation Coefficient between the burst pressure computed by the Deep Neural Network model and the FEA based Parametric Study results for the pipeline with a hemispherical dent.

7.2.2. Comparison with Experimental Results

The reliability of the DNN model was validated by performing correlation and statistical analysis between the burst pressure calculated by the DNN model and the three results of the experiment from the published papers (Kiefner et al. 1997, Shuai et al. 2018). The detailed information is as listed in Table 5.5.

In accordance with the correlation analysis results between the DNN model and experiments and between the *PD formula* and experiments as shown in Figure 7.6, the both PPMCCs are 1.000 and the MAPEs are 1.52% and 5.27%, respectively. The PPMCCs interpreted by the Evans guidance listed in Table 3.1 and MAPEs interpreted by the Lewis guidance listed in Table 3.6 indicate a very strong positive, highly accurate relationship between the burst pressure computed by the DNN model and the experimental test results and between the burst pressure calculated by the *PD formula* and by the experimental test results.

From the above results presented in Section 7.2.1 to 7.2.2, the predicted burst pressure by the DNN model corresponded well with the results of the FEA, the *PD formula* and the experimental test. In addition, it is confirmed that the *PD formula* can predict the burst pressure of the pipelines with a dent as robust as the DNN model.

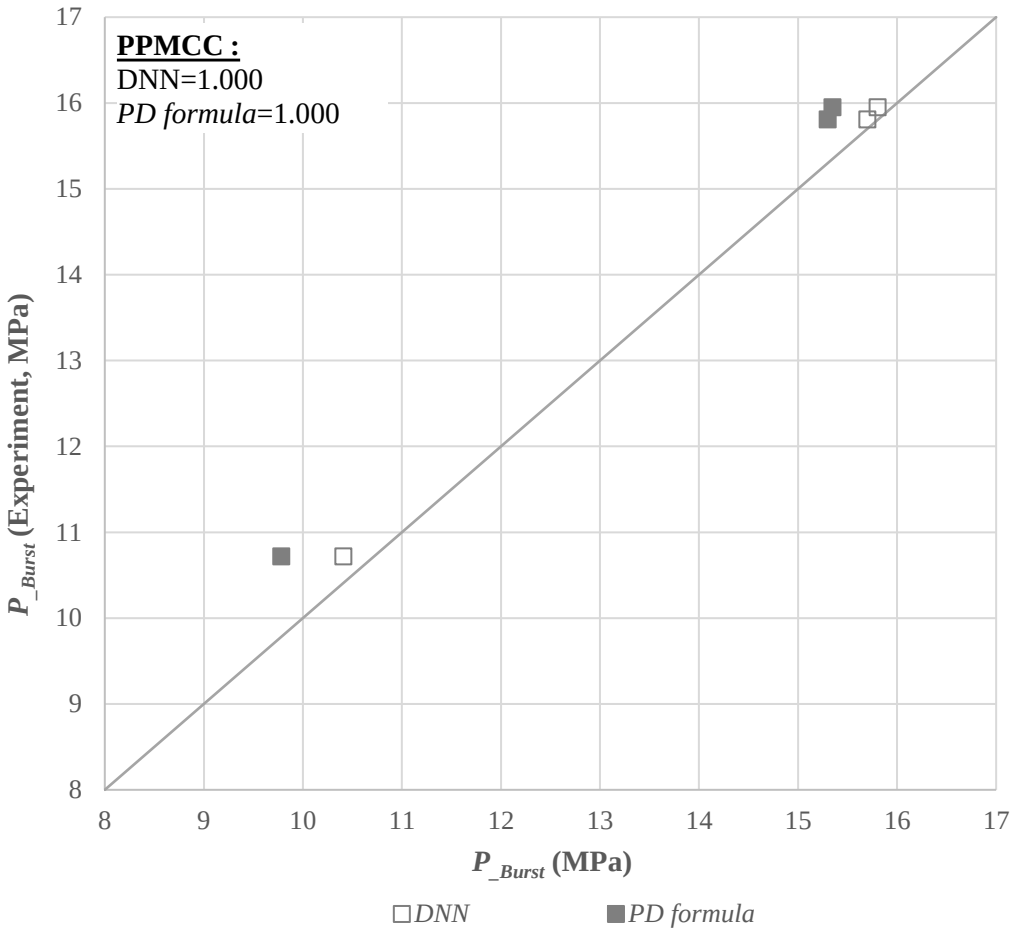

Figure 7.6 Pearson Product-Moment Correlation Coefficient between the burst pressure computed by the Deep Neural Network model and the experimental results for the pipeline with a hemispherical dent.

7.3. Application of DNN Model to Pipelines with a Spheroidal Dent

Additionally, the developed DNN model for the pipelines with a hemispherical dent has been applied to conducting the *test* against 48 data from the FEA based Parametric Study results of the pipelines with a spheroidal dent as listed in Table B.6 in the Appendix B and one experiment data (Bjørnøy et al. 2000) as listed in Table 6.5. The proportion of the *training* and *validation dataset* and the *test dataset* in the total data is 75% and 25%, respectively.

Figure 7.7 represented the cost function of the *training* and *validation* in terms of the MAPE of the DNN model for the pipelines with a spheroidal dent, and the values converged on 0.13% and 0.23%, respectively, and stabilized. The obtained MAPEs can be interpreted as highly accurate based on Table 3.6.

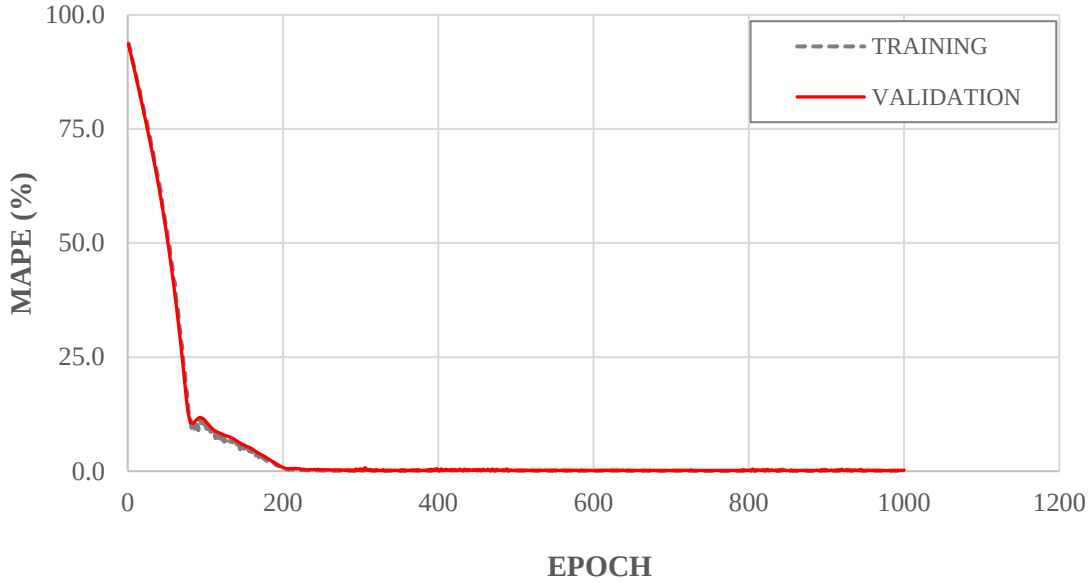

Figure 7.7 Cost function in terms of the Mean Absolute Percentage Error for the pipelines with a spheroidal dent.

7.3.1. Comparison with FEA Based Parametric Study Results

For the validation of the DNN model, the burst pressure computed by the DNN model has been compared with the burst pressure by the FEA. The results of comparison expressed as PPMCC for the correlation analysis and MAPE for the statistical analysis.

As said by the correlation analysis result as shown in Figure 7.8, the PPMCC is 1.000. Compliant with the Evans guidance listed in Table 3.1, this value designates a very strong positive relationship between the burst pressure calculated by the DNN model and by the FEA.

Besides, MAPE is used to measure the prediction accuracy of the burst pressure between by the DNN model and by the FEA, and which is 0.32%. The obtained

MAPE can be interpreted as highly accurate based on Table 3.6. Based on which, it can be said that DNN can reliably estimate the burst pressure of the pipeline with a spheroidal dent.

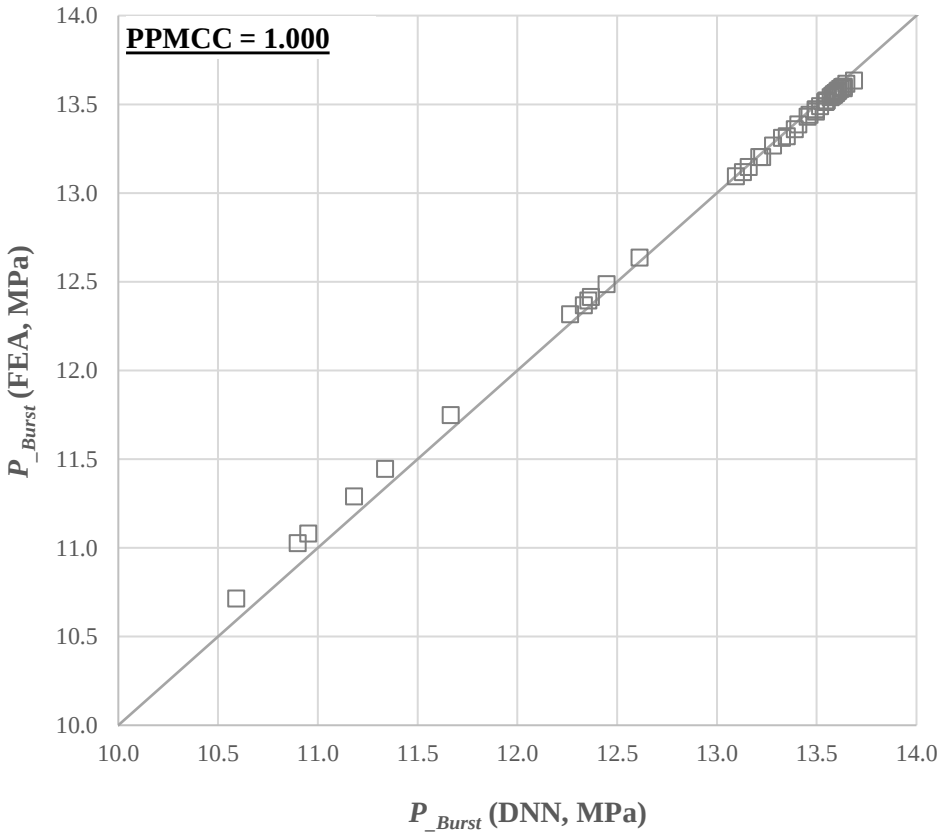

Figure 7.8 Pearson Product-Moment Correlation Coefficient between the burst pressure computed by the Deep Neural Network model and the FEA based Parametric Study results for the pipeline with a spheroidal.

7.3.2. Comparison with Experimental Result

The reliability of the DNN model for the pipeline with a spheroidal dent was validated by comparison between the burst pressure calculated by the DNN model and the one result of the experiment from the published paper (Bjørnøy et al., 2000). The detailed information is as listed in Table 6.5.

The burst pressure predicted by the DNN model showed a very poor agreement with the results of experiments, as shown in Figure 7.9, with an error of 58.1%.

The material properties and geometric information between the training data to develop the DNN model and the experiment are specified in Table 5.1 and Table 6.5, respectively, and it can be seen that there are significant differences. This means that DNN model developed using insufficient data has limitations in the application and can cause such a large error. Therefore, to improve the reliability of the DNN model, it is necessary to use a sufficient dataset to develop the DNN model.

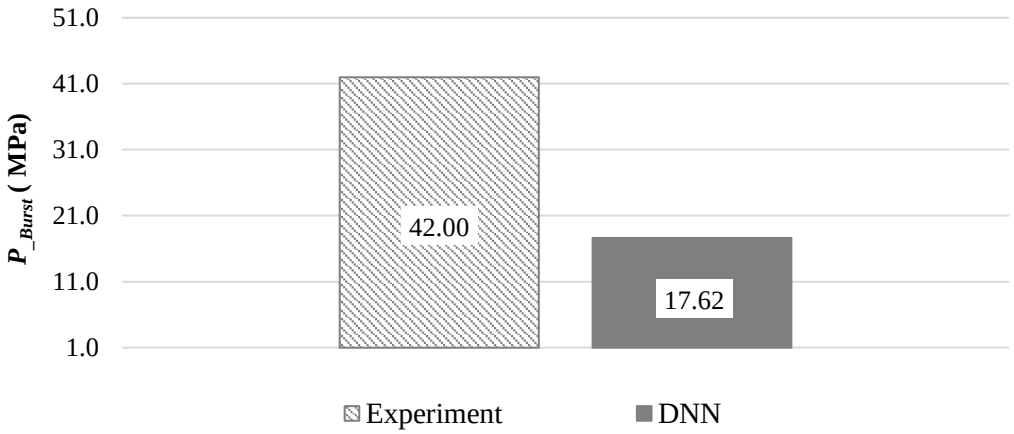

Figure 7.9 Pearson Product-Moment Correlation Coefficient between the burst pressure computed by the Deep Neural Network model and by the experiment for the pipeline with a spheroidal.

7.4. Summary

In this chapter, DNN models have been developed to estimate the burst pressure for API 5L X grade flawless pipelines and pipelines with an unconstrained, plain dent.

The developed DNN models used the FEA based Parametric Study results and validated by comparison with the FEA based Parametric Study results and the experimental test results. The reliability of the DNN models has been investigated by performing the correlation and statistical analysis between the burst pressure computed by the DNN model and the FEA based Parametric Study results and by the experimental results.

According to the validation results, the results of burst pressure computed by the DNN model corresponded well with the nonlinear FEA based Parametric Study results, and the burst pressure results of the experiment excluding the spheroidal dent.

CHAPTER 8

8. SUMMARY AND CONCLUSIONS

8.1. Summary

The aim of this research is the development of the validated, pragmatic and usable model that can be used by the operators and field engineers to examine the structural integrity for API 5L X grade pipelines with a dent instead of FEA and experiment. Based on the research works discussed in this thesis to achieve this aim, the following conclusions can be drawn:

8.1.1. Flawless Pipelines

An empirical formula to estimate the strain at UTS and an empirical formula to predict the burst pressure of API 5L X grade flawless pipelines have been developed.

(1) An empirical formula to estimate the strain at UTS was derived from API 5L X52, X65, X70 and X80 grade material coupon test data. This formula was then used to predict the strain at UTS and the calculated strain at UTS was employed to calculate the tangent modulus in order to consider the strain hardening effect within the FEA material model.

(2) Based on the defined material model using the calculated strain at UTS, a comprehensive nonlinear FEA was performed on 529 pipelines of different material properties and geometries that were subject to an internal pressure load. The results of the FEA based Parametric Study were used to derive a new empirical formula (*FP formula*) that predicts the burst pressure of a flawless

pipeline. This formula consists of σ_{UTS}, σ_{yield} to σ_{UTS} ratio, and the outer diameter to wall thickness ratio.

(3) The predictions of burst pressure for flawless pipelines using the *FP formula* were compared with the results of 14 pipeline burst pressure results of the experiment together with the results based on the conventional formulae. It was found that the best agreement was achieved between the burst pressure calculated by the proposed formula and the burst pressure results of the experiment. In addition, the proposed formula is shown to give the most accurate predictions of the 22 formulae reviewed in the literature based on the standard error criteria.

(4) Therefore, it can be concluded that the burst pressure prediction formula (*FP formula*) based on the von-Mises criterion derived by following the proposed methodology can accurately calculate the burst pressure for API 5L X grade flawless pipelines from X52 to X80 and D/t range from 10 to 96.

8.1.2. Pipelines with a Hemispherical Dent

The purpose of this study was to derive a practical formula to predict the burst pressure of pipelines with a hemispherical dent.

(1) An empirical formula termed as the *PD formula* that has been derived using the regression analysis of the FEA dataset can predict the burst pressure of pipelines with a dent as a function of the dent geometries like dent depth and dent length, pipeline geometries like diameter and thickness and material properties like yield strength and UTS.

(2) The *PD formula* is applicable for API 5L X52, X65, X70 and X80 grade pipelines where the ratio of dent depth to pipeline diameter is less than or equal to 15.96% and the ratio of dent length to pipeline diameter should be satisfied with the requirement calculated by the formula (5.9).

(3) The reliability of the *PD formula* was validated by performing the correlation and statistical analysis of the burst pressure between calculated by *PD formula* and by the nonlinear FEA, and between by the *PD formula* and experimental data. Here, the 80 cases of FEA based Parametric Study results and three experimental results were used.

(4) According to the validation results, the results of burst pressure calculated by the proposed formula are good agreement with the nonlinear FEA based Parametric Study results and the burst pressure results of the experiment.

8.1.3. Pipelines with a Spheroidal Dent

The effects of the pipeline dent length and dent width on the pipeline structural integrity has been investigated, and the applicability of the *PD formula* to predict the burst pressure of pipelines with a spheroidal dent has been determined.

(1) The *PD formula* is able to predict the burst pressure of pipelines with a dent as a function of the dent geometries like dent depth and dent length (or dent width), pipeline geometries like diameter and thickness and material properties like yield strength and UTS.

(2) It has been shown by FEA that the burst pressure of the pipelines with a spheroidal dent is lower with the deeper dent depth, the shorter dent length and the shorter dent width.

(3) The applicability of the *PD formula* has been conducted on API X52 pipelines with the ratio of dent length to dent width of 1.00 to 1.97 and the ratio of dent depth to pipeline outer diameter less than 7.52 and examined using correlation and statistical analysis using the 48 nonlinear FEA based Parametric Study results and the one experimental result. It was demonstrated that the burst pressure using the *PD formula* showed good agreements with the FEA based Parametric Study results and the burst pressure results of the experiment.

(4) Therefore, the *PD formula* for the pipelines with a hemispherical dent is applicable for the burst pressure prediction of the pipeline with a spheroidal dent.

8.1.4. DNN Model

The applicability of the DNN as a new solution to predict the burst pressure of flawless pipelines and pipelines with a dent has been studied.

(1) The FEA based Parametric Study results and the experimental results for the flawless pipelines, the pipelines with a hemispherical dent, and the pipelines with a spheroidal dent have been used to develop the DNN model.

(2) The reliability of the DNN model was investigated by performing the correlation (PPMCC) and statistical (MAPE) analysis of the burst pressure computed using the DNN model and using the nonlinear FEA and the experimental test results.

(3) According to the PPMCC and MAPE as summarized in Table 8.1, all figures indicate that the results of burst pressure computed by the DNN model corresponded well with the nonlinear FEA based Parametric Study results and the burst pressure results of the experiment excluding the spheroidal dent.

(4) However, the burst pressure predicted by the DNN model showed very poor agreement with the experimental test result for the pipelines with a spheroidal dent, and the error was 58.1%. It is determined that the occurrence of such a large error is due to a large difference between the learning data of the DNN model and the information of the experimental group.

8.1.5. Summary of PPMCC and MAPE

According to the PPMCCs and the MAPEs in the Table 8.1, it can be seen that *the FD formula* and *PD formula* can reliably predict the burst pressure of the flawless pipelines, the pipelines with a hemispherical dent and the pipelines with a spheroidal dent. Notably, from the PPMCCs and the MAPEs between the *PD formula* and the DNN model, it is further confirmed that *PD formula* is confirmed to be able to reliably predict for the burst pressure of the pipeline with a spheroidal dent.

Table 8.1 Summary of PPMCCs and MAPEs for all parametric studies.

Dent shape	(A)	(B)	Between (A) and (B)		Remarks
			PPMCC	MAPE (%)	
Flawless	FEM	*FD formula*	1.000	1.30	
		DNN	0.986	9.61	
	Experiment	*FD formula*	0.993	2.14	
		DNN	0.969	4.10	
Hemi-Spherical	FEM	*PD formula*	0.991	2.57	$X52_{PS(I)}$
		DNN	1.000	0.28	
	FEM	*PD formula*	0.888	5.36	$X52_{PS(II)}$
		DNN	0.999	2.17	
	FEM	*PD formula*	0.959	4.82	$X65_{PS(II)}$
		DNN	0.999	2.81	
	FEM	*PD formula*	0.949	5.86	$X80_{PS(II)}$
		DNN	0.959	5.55	
	Experiment	*PD formula*	1.000	5.27	
		DNN	1.000	1.52	
Spheroidal	FEM	*PD formula*	0.784	3.60	
		DNN	1.000	0.32	
	Experiment	*PD formula*	-	2.05	Error
		DNN	-	58.06	Error

8.2. Conclusions

Operators and field engineers working in the oil and gas industry have been looking forward to evaluating the structural integrity of pipelines with a dent for safe and economical operation. However, to date, there is no empirical formula to accurately and efficiently predict the burst pressure of a dented pipeline. To solve this problem, an empirical formula that can predict the burst pressure for API 5L X grade pipelines with an unconstrained, hemispherical or spheroidal, plain dent is developed and using the developed formula, the structural integrity of the dented pipelines can be evaluated. This is the key achievement of this research.

In addition, an empirical formula to predict the burst pressure of pipelines with a dent can be defined as the burst pressure of flawless pipelines multiplied by a reduction factor. Therefore, accurate prediction of the burst pressure of flawless pipelines is critical to improving the accuracy of the formula for dented pipelines. Therefore, an empirical formula to predict the burst pressure for API 5L X grade flawless pipelines has been developed, and which can predict the burst pressure more precisely than any other developed formula.

Furthermore, the conventional method for performing a nonlinear FEA considering the strain hardening effect of material has been to use a bilinear material model or a multiple linear material model. However, the disadvantage of using these material models is that material coupon test should be conducted. In this thesis, an empirical formula developed using material coupon test data to estimate the strain at UTS for API 5L X grade has been introduced. Using this formula, there is no need to perform a material coupon test, which saves time and cost due to a material coupon test. The strain at UTS calculated using the proposed formula is used to define the tangent modulus of the FEA material model.

Studies on the application of a DNN model to assess the structural integrity of pipelines with or without a dent has not been conducted. Accordingly, in this thesis, a DNN model has been developed and reviewed to evaluate the structural integrity of pipelines with or without a dent.

Consequently, based on the findings in this research, operators and field engineers can not only calculate the capacity of the dented pipelines without carrying out the expensive FEA on every dent but also can make efficient repair decisions.

8.2.1. Suggestion for the Future Work

To increase the reliability and range of applicability of the developed formulae, further research is required as below:

First, to improve the reliability of the developed formulae, it is required to conduct the validation of each developed formula by comparing with more experimental test data that is gathered from industry and research institutes about accidents or experiments related to the pipeline burst.

This research was performed with an unconstrained, plain dent, and related formulae were derived. To apply the derived formulae and DNN model, it is needed to update the In Line Inspection tools or to develop a simple tool to gauge the dent width and length which are defined in section 5.1.1 and 6.1.2. As well, in order to expand the range of applicability of the developed formulae, it is necessary to investigate whether the developed formula is applicable to a constrained dent and various dent shapes.

In addition, the research to develop the method for prediction of pipelines with a dent has been conducted on the specification of limited pipelines. Therefore, it is necessary to expand the range of materials and dimensions applied to the pipeline to carry out the research to obtain data. Especially, it is worth to further develop the proposed formula and DNN model for the dented pipelines by including the dent width term to improve the prediction accuracy.

Notably, the FEA for the flawless and the dented pipeline have been conducted with the bilinear material model based on the engineering stress and strain data. To improve the accuracy and the reliability of the proposed formulae, it is necessary to perform the FEA using a multi-linear material model based on the true stress-strain

curve, unfortunately, it is not often available.

Finally, a DNN model predicted well the burst pressure of the flawless pipelines and the pipelines with a hemispherical dent. However, the burst pressure of the pipeline with a spheroidal dent predicted by a DNN model showed a large error with the experimental test result. Therefore, it is necessary to develop a DNN model based on various material properties and geometric information to improve reliability and expand the range of applicability.

REFERENCE

About Pipelines, 2012. Oil and gas on the move: it's what pipelines do best, https://www.aboutpipelines.com/en/blog/oil-and-gas-on-the-move-its-what-pipelines-do-best/

API, 2004. API 5L: Specification for Line Pipe, Washington, DC, USA: American Petroleum Institute.

API, 2016. API 579-1 / ASME FFS-1, Fitness-For-Service, Washington, DC, USA: American Petroleum Institute.

ASME, 1962. ASME Boiler and Pressure Vessel Code, New York, NY, USA: American Society Mechanical Engineers.

ASME, 1971. ASME Boiler and Pressure Vessel Code; Section III. Division 1, New York, NY, USA: American Society Mechanical Engineers.

ASME, 1974. ASME Boiler and Pressure Vessel Code; Section III. Division 1 Par. 1430, New York, NY, USA: American Society Mechanical Engineers.

ASME, 1986. ASME Boiler and Pressure Vessel Code; Section XI. Division 2, New York, NY, USA: American Society Mechanical Engineers.

ASME, 2012. ASME B31G. Manual for Determining the Remaining Strength of Corroded Pipelines, New York, NY, USA: American Society Mechanical Engineers.

ASME, 2014. ASME B31.8, Gas transmission and distribution piping systems, New York, NY, USA: American Society Mechanical Engineers.

Arumugam, U., Kendric, D.Z., Sergi, L.T., Gao, M., 2010. An Approach for Evaluating and Prioritizing Dents for Remediation as Reported by ILI Tools. Proceedings of the 8th International Pipeline Conference, Calgary, Alberta, Canada

Allouti, M., Schmitt, C., Pluvinage, G., Gilgert, J., Hariri, S., 2012. Study of the influence of dent depth on the critical pressure of pipeline. Engineering Failure Analysis. 21, 40-51

Bailey, R.W., 1930. Thick-walled tubes and cylinders under high pressure and temperatures. Engineering. 129: 772-777.

Baker, M., 2004. Dent study, Final Report, TTO number 10, Integrity management program, Delivery order DTRS56-02-D-70036, DOT research and special programs administration, Office of pipeline safety.

Barlow, P. 1836. On the force excited by hydraulic pressure in Bramah press; the resisting power of the cylinder, and rules for computing the thickness of metal for presses of various powers and dimensions. Trans. Institution of Civil Engineers. 1: 133-139

Belanos, S.P., Ryan, R.S., 1958. Dents in pipe. Oil and Gas Journal, Vol. 56, pp 155-161.

Bjørnøy, O.H., Rengård, O., Fredheim, S., Bruce, P., 2000. Residual Strength of Dented Pipelines, DNV Test Results. Proceedings of the 10th International Offshore and Polar Engineering Conference. Seattle, USA.

Bohm, G.J., 1972. Pressure Vessels and Piping: Design and Analysis: A Decade of Progress, New York, USA: American Society Mechanical Engineers. 1: 23-32.

Cenk, B., Nafiz, A., 2018. A comparison of activation functions in artificial neural networks. 26th Signal Processing and Communications Applications Conference. IEEE.

Chen, X.H., Gao, B.J., Wang, X.G., 2016. Evaluation of limit load analysis for pressure vessels-Part I: Linear and nonlinear methods. Steel and Composite Structures. 22(6), 1391-1415

Chen, R.J.C., Bloomfield, P., Fu, J.S., 2003. An Evaluation of Alternative Forecasting Methods to Recreation Visitation, Journal of Leisure Research, 35:4, 441-454, DOI: 10.1080/00222216.2003.11950005.

Christopher, T., Rama Sarma, B.S.V, Govindan Potti, P.K., Nageswara, R.B., Sankarnarayanasamy, K., 2002. A comparative study on failure pressure estimations of unflawed cylindrical vessels. International Journal of Pressure Vessels and Piping. 79: 53-66.

Clevert, D.A., Unterthiner, T., Mayr, A., Hochreiter, S., 2015. Rectified factor networks. Advances in Neural Information Processing Systems.

Cosham, A., Kirkwood, M., 2000. Best practice in pipeline defect assessment. Proceedings of IPC: International Pipeline Conference.

Cosham, A., Hopkins, P., 2004. The effect of dents in pipelines-guidance in the pipeline defect assessment manual. International Journal of Pressure Vessels and Piping. 81(2), 127-139.

Cosham, A., Macdonald, M.A., 2005. Best practice for the assessment of defects in pipelines – gouges and dents. Engineering Failure Analysis. 12: 720-745.

Demir, H.H., Drueker, D.C., 1963. An experimental study of cylindrical shells under ring loading. In Progress in Applied Mechanics (the Prager Anniversary Volume), New York, 205-220.

Deolia, P., Shaikh, F.A., 2016. Finite element analysis to estimate burst pressure of mild steel pressure vessel using Ramberg-Osgood model., Perspectives in Science. 8, 733-735

De Weck, O., Kim, I.Y., 2004. Finite Element Method. Engineering Design and Rapid Prototyping.
Retrieved from http://web.mit.edu/16.810/www/16.810_L4_CAE.pdf

Dinovitzer, A., Bhatia, A., Walker, R., Lazor, R., 2000. A pipeline dent assessment model considering localized effects. International Pipeline Conference. ASME 2000. Volume 2

Dotson, R., Ginten, M., Alexander, C., Bedoya, J., Schröer, K., 2014. Combining high resolution in-line geometry tools and finite element analysis to improve dent assessments. Proceedings of Pipeline Pigging & Integrity Management Conference

DNV, 2008. Recommended Practice DNV-RP-F101. Norway: Det Norske Veritas.

DNV, 2013. Offshore Standard DNV-OS-F101. Norway: Det Norske Veritas.

EGIG, 2018. Gas pipeline incidents, 10th Report of the European Gas Pipeline Incident Data Group(period 1970 – 2016), EGIG: European Gas Pipeline Incident Data Group.

Elfwing, S., Uchibe, E., Doya, K., 2017. Sigmoid-Weighted Linear Units for Neural Network Function Approximation in Reinforcement Learning. arXiv. [Online]. Available: https://arxiv.org/abs/1702.03118

Evans, J.D., 1996. Straightforward Statistics for the Behavioural Sciences. Brooks/Cole Publishing Company.

Faupel, J.H., 1956. Yielding and bursting characteristics of heavy walled cylinders. Trans. American Society Mechanical Engineers. 78: 1031-1064.

Fields, R.J., Foecke, T.J., deWit, R., 1994. Effect of Dents and Gouges on the Integrity of pipelines. NISTIR 5479. U.S. Department of Energy, Washington, D.C. 20858.

Fletcher, L., 2003. Private communication.

Gadamchetty, G., Pandey, A., Gawture, M., 2016. On Practical Implementation of the Ramberg-Osgood Model for FE Simulation. SAE International Journal of Materials and Manufacturing, 9(1), 200-205. Retrieved April 9, 2020, from www.jstor.org/stable/26268819

Gerdeen, J.C., 1979. A critical evaluation of plastic behavior data and a united definition of plastic loads for pressure components. WRC Bulletin. 254.

Goodfellow, G.D., Lyons, C.J., Haswell, J.V., 2019. UKOPA Pipeline Product Loss Incidents and Faults Report (1962-2017). United Kingdom Onshore Pipeline Operators' Association, Derbyshire, U.K. UKOPA/RP/18/002.

Green, K.P., Jackson, T., 2015. Safety in the Transportation of Oil and Gas: Pipelines or Rail? Fraser Research Bulletin by the Fraser Institute, Canada.

He, K., Zhang, X., Ren, S., Sun, J., 2015. Delving deep into rectifiers: surpassing human-level performance on imagenet classification. arXiv: 1502.01852v.

Hopkins, P., Jones, D.G., Clyne, A.C., 1983. Recent studies of the significance of mechanical damage in pipelines. The American Gas Association and European Pipeline Research Group Research Seminar V, San Francisco, USA.

Hopkins, P., Jones, D.G., Clyne, A.C., 1989. The significance of dents and defects in transmission pipelines. Proceedings of International Conference on Pipework, Engineering and Operation, London: Institution of Mechanical Engineers.

Hopkins, P., Corder, I., and Corbin, P., 1992. The resistance of gas transmission pipelines to mechanical damage. Canada: N. p., 1992. Web.

Jin, X., Xu, C., Feng, J., Wei, Y., Xiong, J., Yan, S., Deep Learning with S-shaped Rectified Linear Activation Units. arXiv. [Online]. Available: https:// https://arxiv.org/abs/1512.07030.

Jones, D.G., 1982. The significance of mechanical damage in pipelines. 3R International, 21, Jahrgang, Heft.

Kiefner, J. F., Alexander, C.R., 1997. Effects of smooth and rock dents on liquid petroleum pipelines. American Petroleum Institute Publication 1156

Kiefner, J.F., Alexander, C.R., Fowler, J.R., 1996. Repair of dents containing minor scratches. 9th Symposium on Line Pipe Research, Houston, Texas: Pipeline Research Committee of the American Gas Association.

Kim, G.Y., Ban, I.J., Park, B.C., Oh, S.J., Lim, C.O., Shin, S.C., 2019. Estimation of Lightweight in the Initial Design of Ships Using Deep Neural Networks. Journal of Korean Institute of Intelligent Systems. 29(6): 416-423.

Kingma, D.P., Ba, J., 2015, Adam: A Method for Stochastic Optimization. 3rd International Conference for Learning Representations, San Diego. arXiv. [Online]. Available: https://arxiv.org/abs/1412.6980.

Kirkwood, M.G., 1986. Finite element stress analysis of an equal diameter branch pipe intersection subjected to out-of-plane and twisting moments. Strain Anal. 21(1): 171-183.

Kirkwood, M.G., 1989. Techniques for measuring plastic loads in branch pipe connections loads by pressure and in-plane moments. Pipework Engineering and Operation. London. UK: 197-208.

Klambauer, G., Unterthiner, T., Mayr, A., Hochreiter, S., 2017. Self-Normalizing Neural Networks. Advances in Neural Information Processing Systems 30. arXiv. [Online]. Available: https://arxiv.org/abs/1706.02515

Kulkarni, A.M., Wankhade, R.L., 2015, Design by analysis of liquid petroleum gas cylinder using twice elastic slope criteria to calculate the burst pressure of cylinder. International journal of engineering research & technology.

Law, M., Bowie, G., 2007. Prediction of failure strain and burst pressure in high yield-to-tensile strength ratio line pipe. International Journal of Pressure Vessels and Piping. 84: 487-492.

Lewis, C.D., 1982. Industrial and business forecasting methods: A practical guide to exponential smoothing and curve fitting. London; Boston: Butterworth Scientific.

Li, C., Dang, S., 2017. Plastic damage analysis of oil and gas pipelines with unconstrained and constrained dents. Engineering Failure Analysis. 77. 39-49.

Liessem, A., Graef, M.K., Knauf, G., Marewski, U., 2004. Influence of thermal treatment on mechanical properties on UOE linepipe. Proceedings of the 4th International Conference of Pipeline Technology. Ostend. Belgium, 1263-1281.

Liu, X., Zhang, H., Wang, B., Xia, M., 2017. Nonlinear finite element analysis of the limit state and pressure of dented X60 steel pipeline. 23(6): 814-819.

Liu, X., Xia, M., Bolati, D., Liu, J., Zheng, Q., Zhang, H., 2020. An ANN-based failure pressure prediction method for buried high-strength pipes with stray current corrosion effect. Energy Science & Engineering. 8. 248-259

Lower, M.D., 2014. Strain-based design methodology of large diameter grade X80 linepipe. Oak Ridge National Laboratory. Oak Ridge, Tennessee, USA

Lynch, M.A., Moffat, D.G., 2000. Limit load for cracked piping branch junctions under pressure and branch out-of-plane bending. International Journal of Pressure Vessels and Piping. 77(5). 185-194.

MacDonald, B.J., 2007. Practical Stress Analysis with Finite Elements. Ireland: Glasnevin Publishing.

Marin, J., Rimrott, FPJ., 1958. Design of thick walled pressure vessels based upon the plastic range.Wel Res Coun Bullet. 41.

Marin, J., Sharma, M., 1958. Design of a thin walled cylindrical vessel based upon plastic range and considering anisotropy. Wel Res Coun Bullet. 40.

Maas, A.L., Hannun, A.Y., Ng, A.Y., 2013. Rectifier nonlinearities improve neural network acoustic models. Proceedings of the 30th International Conference on Machine Learning. Atlanta, Georgia.

McLamb, M., Hopkins, P., Marley, M., Nessim, M., 2002. A justification for designing and operating pipelines up to stresses of 80% of SMYS. Proceedings of IPC 2002. Calgary, Canada

Miklus, S., Kosel, F., 1991. Plastic collapse of pipe bi-furcation, International Journal of Pressure Vessels and Piping: 79-92.

Muscat, M., Mackenzie, D., Hamilton, R., 2003. A work criterion plastic collapse, International Journal of Pressure Vessels and Piping. 80(1): 49-58.

Nadai, A., 1931. Plasticity: a mechanics of the plastic state of matter. New York: McGraw-Hill Book Co.

Nadai, A., 1963. Theory of flow and fracture of solids. Vol. 2. New York: McGraw-Hill Book Co.

Nair, V., Hinton, G.E., 2010. Rectified Linear Units Improve Restricted Boltzmann Machines. Proceedings of the 27th international conference on machine learning (ICML-10), 807–814.

Nielsen, M.A., 2015. Neural Networks and Deep Learning. Determination Press.

Norman, E., 2013. Mechanical Behavior of Materials, England: Pearson Education Limited

Noronha, D.B., 2010. Procedures for the strain based assessment of pipeline dents. International Journal of Pressure Vessels and Piping. 87: 254-265

Nwankpa, C.E., Ijomah, W., Gachagan, A., Marshall, S., 2018. Activation Functions: Comparison of trends in Practice and Research for Deep Learning. arXiv. [Online]. Available: http://arxiv.org/abs/1811.03378

Orynyak, I.V., Rozgonyuk, V.V., Shlapak, L.S., 1999. Residual strength of pipelines with dents. Material Science. Vol. 35(5), 689-694.

Orynyak, I.V., Bogdan, A.V., Rozgonyuk, V.V., 2004. Ductile fracture model for a pipe with a dent. Proceedings of the 4th International conference on pipeline Technology. Ostend, Belgium. vol. II. 949–60.

Oshana, J.J., 2014. Dent behaviour of steel pipes under pressure load. Electronic Theses and Dissertations. 5025. https://scholar.uwindsor.ca/etd/5025.

Oyane, M., Sato, T., Okimoto, K., Shima, S., 1980. Criteria for ductile fracture and their applications. Journal of Mechanical Working Technology. 4:65-81.

Panchal, F.S., Panchal, M., 2014. Review on Methods of Selecting Number of Hidden Nodes in Artificial Neural Network. International Journal of Computer Science and Mobile Computing. 3(11):455-464

Patel, D.M., Kumar, B., 2014. Pressure vessel limit load estimation by FEM and experimental method. International Journal of Innovative Research in Advanced Engineering. 9:109-114.

Pedamonti, D., 2018. Comparison of non-linear activation functions for deep neural networks on MNIST classification task. arXiv. [Online]. Available: http://arxiv.org/abs/1804.02763

PHMSA, 2020. Significant Incident Consequences Summary Statistics, US Department of Transportation (DOT) Pipelines and Hazardous Material Safety Administration. https://portal.phmsa.dot.gov/PDMPublicReport/?url=https://portal.phmsa.dot.gov/analytics/saw.dll?Portalpages&PortalPath=%2Fshared%2FPDM%20Public%20Website%2F_portal%2FSC%20Incident%20Trend&Page=Significant%20Incidents%20Consequences

PHMSA, 2012. Failure Report - Chevron Pipe Line Compay 1/26/11. https://www.phmsa.dot.gov/safety-reports/failure-report-chevron-pipe-line-company-12611

Race, J.M., 2008. Integrity assessment of plain dents subject to fatigue loading. Report Prepared for UKOPA. Newcastle University.

Ramberg, W., Osgood, W.R., 1943. Description of Stress-Strain Curves by Three Parameters. Technical Note-902, National Advisory Committee for Aeronautics. Washington, DC, USA.

Roovers, P., Bood, R., Galli, M., Marewski, U., Steiner, M., Zaréa, M., 2000. EPRG methods for assessing the tolerance and resistance of pipelines to external damage. In: Denys R, editor. Proceedings of the Third International Pipeline Technology Conference, vol. II, Brugge, Belgium, Amsterdam. 405–25.

Save, M., 1972. Experimental verification of plastic limit analysis of tori-spherical and tori-conical heads. Pressure Vessel and Piping: Design and Analysis. 1(1), 382-416

Schroeder, J., 1980. A plastic modulus approach to experimental limit loads. ASME Paper No. 80-C2/PVP-1.

Schroeder, J., 1985. Experimental limit couples for branch moment loads on 4 in. ANSI B16.9 Tees. WRC Bulletin 304.

Shen, S., Li, G., Song, H., 2009. Effect of Seasonality Treatment on the Forecasting Performance of Tourism Demand Models. Tourism Economics. 15(4), 693-708.

Shuai, Y., Shuai, J., Zhang, X., 2018. Experimental and numerical investigation of the strain response of a dented API 5L X52 pipeline subjected to continuously increasing internal pressure. Journal of Natural Gas Science and Engineering. 56: 81-92

Soderberg, C.R., 1941. Interpretation of creep tests on tubes. Trans. American Society Mechanical Engineers. 63: 737-748.

Stewart, G., Klever, F.J., Ritchie, D., 1994. An analytical model to predict the burst capacity of pipelines. International conference. Paper presented at: 13th International conference on Offshore Mechanics and Arctic engineering; February 27-March 3; Houston, TX, USA.

Su, W.X., Zheng, J.Y., Kai, F.M., 2005. A 5% maximum principal strain criterion to prevent gross plastic deformation. Vessel Technol. 22(12): 17-21.

Svensson, N.L., 1958. Bursting pressure of cylindrical and spherical pressure vessels. Trans. American Society Mechanical Engineers. 80: 89-96.

Townley, CHA., Findlay, G.E., Goodman, A.M., Stanley, P., 1971. Elastic-plastic computations a basic for design charts for tori-spherical pressure vessel ends. Proceedings of the Institution of Mechanical Engineers. Part E: Journal of Process Mechanical Engineering. 185(63), 869-877.

Trottier, L., Giguere, P., Chaib-draa, B.C., 2017. Parametric Exponential Linear Unit for Deep Convolutional Neural Networks. 16th IEEE International Conference On Machine Learning And Applications. arXiv. [Online]. Available: https://arxiv.org/abs/1605.09332

Turner, L.B., 1910. The stresses in a thick hollow cylinder subjected to internal pressure. Trans Camb Philos Soc. 21: 377-396.

Wang, K.C., Smith, E.D., 1982. The effect of mechanical damage on fracture initiation in linepipe: part I—dents. Report ERP/PMRL 82-11 (TR), Canada: Canadian Centre for Mineral and Energy Technology (CANMET).

Wong, E.W.C., Kim, D.K., 2018. A simplified method to predict fatigue damage of TTR subjected to short-term VIV using artificial neural network. Advances in Engineering Software. 126. 100-109.

Wu, Y., Tang, N., Zhang, P., 2015. The comparison of dented pipeline displacement calculation methods. Engineering Failure Analysis. 57. 562-573

Wu, Y., Xiao, J., Zhang, P., 2016. The analysis of damage degree of oil and gas pipeline with type II plain dent. Engineering Failure Analysis. 66. 212-222

Wu, Y., Zhang, P., Liu, W., 2012. FE calculation and analysis of plain dent size influence on pipeline displacement. Applied Mechanics and Material. Vols. 155-156, 176-180.

Xu, B., Wang, N., Chen, T., Li, M. 2015. Empirical Evaluation of Rectified Activations in Convolutional Network. arXiv. [Online]. Available: https://arxiv.org/abs/1505.00853

Xu, W., Li, C.B., Choung, J., & Lee, J. 2017. Corroded pipeline failure analysis using artificial neural network scheme. Advances in Engineering Software. 112. 255-266.

Zhang, S.H., Zhao, D.W., Wang, X.N., 2014. Influence of yield to tensile strength ratio (Y/T) on failure assessment of defect free and corroded X70 steel pipeline. Journal of Central South University. 21, 460–465

Zhang, W.M., Lu, M.W., Zhang, R.Y., 1989. A zero-curvature criterion to determine the practical collapse load, Proceedings of the 6th International conference on Pressure Vessel Technology. Beijing, China. 1, 551-558.

Zhou, W., Huang, G.T., 2012. Model error assessment of burst capacity models for defect free pipes. International Pipeline Conference. Paper presented at: 9th International Pipeline Conference; September 24-28; Calgary, Alberta, Canada.

Zhu, X.K., Leis, B.N., 2005. Influence of yield to tensile strength ratio on failure assessment of corroded pipelines. ASME transactions. American Society Mechanical Engineers. 127: 436-442.

Zhu, X.K., Leis, B.N., 2006. Average shear stress yield criterion and its application to plastic collapse analysis of pipelines. International Journal of Pressure Vessel and Piping. 83: 663-671.

Zhu, X.K., Leis, B.N., 2007. Theoretical and numerical predictions of burst pressure of pipelines. Journal of Pressure Vessel Technology. 129: 644-652.

Zhu, X.K., Leis, B.N., 2010. Prediction and comparison of burst pressure for line pipes. International Pipeline Conference. Paper presented at: 8th International Pipeline Conference; September 27-October 1; Calgary, Alberta, Canada.

Zhu, X.K., Leis, B.N., 2012. Evaluation of burst pressure prediction models for line pipes. International Journal of Pressure Vessels and Piping. 89: 85-97.

APPENDIX A

Table A.1 Geometric information for the parametric analysis.

No.	X52, X56, X60, X65 and X70			X80		
	Outer dia. (*D*, *mm*)	thickness (*t*, *mm*)	*D/t*	Outer dia. (*D*, *mm*)	thickness (*t*, *mm*)	*D/t*
1	60.3	3.9	15.42	323.9	4.775	67.82
2	60.3	5.5	10.88	323.9	5.156	62.81
3	73.0	5.2	14.15	323.9	5.563	58.22
4	73.0	7.0	10.41	323.9	6.350	51.00
5	88.9	5.5	16.19	323.9	7.137	45.37
6	88.9	7.6	11.67	323.9	7.925	40.87
7	114.3	6.0	18.99	323.9	8.382	38.64
8	114.3	8.6	13.35	323.9	8.738	37.06
9	114.3	11.1	10.30	323.9	9.525	34.00
10	141.3	6.6	21.57	323.9	10.312	31.40
11	141.3	9.5	14.84	323.9	11.125	29.11
12	168.3	7.1	23.67	323.9	12.700	25.50
13	168.3	11.0	15.34	355.6	4.775	74.47
14	168.3	12.7	13.25	355.6	5.156	68.97
15	168.3	14.3	11.79	355.6	5.563	63.93
16	219.1	6.4	34.50	355.6	6.350	56.00
17	219.1	8.2	26.78	355.6	7.137	49.82
18	219.1	10.3	21.25	355.6	7.925	44.87
19	219.1	12.7	17.25	355.6	8.382	42.42
20	219.1	15.9	13.80	355.6	8.738	40.70
21	219.1	19.1	11.50	355.6	9.525	37.33
22	273.0	6.4	42.99	355.6	10.312	34.48
23	273.0	9.3	29.45	355.6	11.125	31.96
24	273.0	12.7	21.50	355.6	12.700	28.00
25	273.0	15.9	17.19	406.4	6.350	64.00
26	273.0	19.1	14.33	406.4	7.137	56.94
27	273.0	21.4	12.73	406.4	7.925	51.28
28	273.0	25.4	10.75	406.4	8.738	46.51
29	323.8	9.5	33.98	406.4	9.525	42.67
30	323.8	10.3	31.41	406.4	10.312	39.41

Table A.1 (*cont.*) Geometric information for the parametric analysis.

No.	X52, X56, X60, X65 and X70			X80		
	Outer dia. (*D*, *mm*)	thickness (*t*, *mm*)	*D/t*	Outer dia. (*D*, *mm*)	thickness (*t*, *mm*)	*D/t*
31	323.8	12.7	25.50	406.4	11.125	36.53
32	323.8	14.3	22.69	406.4	11.913	34.12
33	323.8	15.9	20.39	406.4	12.700	32.00
34	323.8	17.5	18.52	406.4	14.275	28.47
35	323.8	19.1	17.00	406.4	15.875	25.60
36	323.8	21.4	15.10	457.2	6.350	72.00
37	323.8	25.4	12.75	457.2	7.137	64.06
38	323.8	31.8	10.20	457.2	7.925	57.69
39	355.6	9.5	37.31	457.2	8.738	52.33
40	355.6	11.1	31.95	457.2	9.525	48.00
41	355.6	12.7	28.00	457.2	10.312	44.33
42	355.6	15.9	22.39	457.2	11.125	41.10
43	355.6	19.1	18.67	457.2	11.913	38.38
44	355.6	25.4	14.00	457.2	12.700	36.00
45	355.6	31.8	11.20	457.2	14.275	32.03
46	406.4	9.5	42.64	457.2	15.875	28.80
47	406.4	12.7	32.00	508.0	6.350	80.00
48	406.4	14.3	28.48	508.0	7.137	71.17
49	406.4	15.9	25.59	508.0	7.925	64.10
50	406.4	16.7	24.39	508.0	8.738	58.14
51	406.4	17.5	23.25	508.0	9.525	53.33
52	406.4	19.1	21.33	508.0	10.312	49.26
53	406.4	21.4	18.96	508.0	11.125	45.66
54	406.4	25.4	16.00	508.0	11.913	42.64
55	406.4	31.0	13.11	508.0	12.700	40.00
56	406.4	31.8	12.80	508.0	14.275	35.59
57	406.4	38.1	10.67	508.0	15.875	32.00
58	457.2	12.7	36.00	558.8	6.350	88.00
59	457.2	15.9	28.79	558.8	7.137	78.29
60	457.2	19.1	24.00	558.8	7.925	70.51

Table A.1 (*cont.*) Geometric information for the parametric analysis.

No.	X52, X56, X60, X65 and X70			X80		
	Outer dia. (*D*, *mm*)	thickness (*t*, *mm*)	*D/t*	Outer dia. (*D*, *mm*)	thickness (*t*, *mm*)	*D/t*
61	457.2	23.8	19.19	558.8	8.738	63.95
62	457.2	25.4	18.00	558.8	9.525	58.67
63	457.2	31.8	14.40	558.8	10.312	54.19
64	457.2	38.1	12.00	558.8	11.125	50.23
65	457.2	45.2	10.11	558.8	11.913	46.91
66	508.0	12.7	40.00	558.8	12.700	44.00
67	508.0	15.9	31.99	558.8	14.275	39.15
68	508.0	17.5	29.06	558.8	15.875	35.20
69	508.0	19.1	26.67	609.6	6.350	96.00
70	508.0	25.4	20.00	609.6	7.137	85.41
71	508.0	26.2	19.39	609.6	7.925	76.92
72	508.0	31.8	16.00	609.6	8.738	69.77
73	508.0	32.5	15.63	609.6	9.525	64.00
74	508.0	38.1	13.33	609.6	10.312	59.11
75	508.0	50.8	10.00	609.6	11.125	54.79
76	559.0	12.7	44.02	609.6	11.913	51.17
77	559.0	19.1	29.34	609.6	12.700	48.00
78	559.0	25.4	22.01	609.6	14.275	42.70
79	559.0	31.8	17.61	609.6	15.875	38.40
80	559.0	38.1	14.67	-	-	-
81	610.0	9.5	64.08	-	-	-
82	610.0	12.7	48.03	-	-	-
83	610.0	14.3	42.75	-	-	-
84	610.0	15.9	38.41	-	-	-
85	610.0	17.5	34.90	-	-	-
86	610.0	19.1	32.02	-	-	-
87	610.0	25.4	24.02	-	-	-
88	610.0	31.8	19.21	-	-	-
89	610.0	38.1	16.01	-	-	-
90	610.0	50.8	12.01	-	-	-

Table A.2 Burst pressure for the flawless pipelines by Finite Element Analysis (X52, X56, X60, X65, and X70).

			Burst Pressure (MPa)				
No.	Outer Dia. (*mm*)	Thickness (*mm*)	X52	X56	X60	X65	X70
1	60.3	3.91	62.82	69.12	71.68	74.80	80.18
2	60.3	5.54	90.94	98.04	103.79	108.36	116.32
3	73.0	5.16	69.55	74.91	79.52	82.92	88.82
4	73.0	7.01	96.07	104.85	109.84	114.82	122.35
5	88.9	5.49	59.86	65.59	68.32	71.52	76.38
6	88.9	7.62	84.77	91.19	96.81	101.00	108.29
7	114.3	6.02	50.26	54.12	57.42	59.76	64.16
8	114.3	8.56	73.74	79.46	84.37	88.03	94.27
9	114.3	11.1	97.55	104.83	111.22	116.61	124.78
10	141.3	6.55	44.59	48.96	50.80	52.77	56.82
11	141.3	9.52	65.36	70.41	74.70	77.80	83.25
12	168.3	7.11	39.96	43.03	45.64	47.78	50.63
13	168.3	10.97	63.53	69.54	72.40	75.86	81.00
14	168.3	12.7	73.99	81.49	84.59	88.37	94.60
15	168.3	14.27	84.29	90.53	96.10	100.26	107.58
16	219.1	6.35	27.42	29.52	31.20	32.63	34.85
17	219.1	8.18	35.31	38.01	40.29	42.16	45.03
18	219.1	10.31	44.84	49.15	51.19	53.12	56.69
19	219.1	12.7	55.88	61.38	63.80	66.59	71.35
20	219.1	15.88	71.10	77.98	80.96	84.82	90.66
21	219.1	19.05	86.51	95.20	98.88	103.03	110.15
22	273.0	6.35	21.83	23.57	24.90	26.04	27.81
23	273.0	9.27	32.13	35.52	36.65	38.00	40.54
24	273.0	12.7	44.44	48.85	50.56	52.92	56.54
25	273.0	15.88	56.14	61.55	64.08	67.04	71.63
26	273.0	19.05	68.24	73.38	77.88	81.21	86.66
27	273.0	21.44	77.09	83.01	88.12	92.17	98.54
28	273.0	25.4	93.02	100.09	106.28	110.94	118.20
29	323.8	9.53	27.57	30.43	31.36	32.79	35.00
30	323.8	10.31	29.86	33.06	34.14	35.32	38.12
31	323.8	12.7	37.18	39.86	42.30	44.25	47.28
32	323.8	14.27	41.97	46.10	47.94	50.05	53.24
33	323.8	15.88	46.96	50.43	53.49	55.99	59.83
34	323.8	17.48	51.98	57.09	59.28	61.65	65.83
35	323.8	19.05	56.87	61.17	64.91	67.96	72.62
36	323.8	21.44	64.19	69.07	73.25	76.47	81.41
37	323.8	25.4	77.15	83.08	88.20	92.28	98.61
38	323.8	31.75	98.71	106.26	112.60	117.59	126.19
39	355.6	9.53	24.95	26.85	28.47	29.80	31.64
40	355.6	11.13	29.35	31.54	33.39	34.95	37.33
41	355.6	12.7	33.65	36.23	38.41	40.18	42.93
42	355.6	15.88	42.48	45.73	48.52	50.78	53.83
43	355.6	19.05	51.63	56.89	58.94	61.18	65.33

Table A.2 (*cont.*) Burst pressure for the flawless pipelines by Finite Element Analysis (X52, X56, X60, X65, and X70).

			Burst Pressure (MPa)				
No.	Outer Dia. (*mm*)	Thickness (*mm*)	X52	X56	X60	X65	X70
44	355.6	25.4	69.75	75.16	79.79	83.22	89.19
45	355.6	31.75	89.16	95.73	101.68	106.41	113.24
46	406.4	9.53	21.78	23.48	24.81	25.96	27.74
47	406.4	12.7	29.39	31.59	33.44	34.99	37.37
48	406.4	14.27	33.11	35.64	37.82	39.61	42.24
49	406.4	15.88	37.10	40.75	42.19	44.08	47.07
50	406.4	16.66	38.98	42.91	44.55	46.26	49.39
51	406.4	17.48	40.92	44.06	46.70	48.52	52.13
52	406.4	19.05	44.83	49.14	51.17	53.11	56.67
53	406.4	21.44	50.43	54.32	57.62	59.96	64.39
54	406.4	25.4	60.45	65.06	69.04	72.27	77.26
55	406.4	31	74.94	82.02	85.47	89.54	95.11
56	406.4	31.75	76.95	82.84	87.93	91.92	98.37
57	406.4	38.1	93.71	103.45	107.20	111.62	119.34
58	457.2	12.7	25.98	28.62	29.73	30.66	33.16
59	457.2	15.88	32.72	35.94	37.41	38.97	41.73
60	457.2	19.05	39.69	42.58	45.20	47.27	50.56
61	457.2	23.83	49.80	53.62	56.89	59.55	63.61
62	457.2	25.4	53.36	57.46	60.90	63.78	68.13
63	457.2	31.75	67.85	74.07	77.38	80.80	86.02
64	457.2	38.1	82.38	88.80	94.06	98.57	104.85
65	457.2	45.24	99.38	109.54	113.48	118.49	126.55
66	508.0	12.7	23.35	25.10	26.58	27.83	29.73
67	508.0	15.88	29.45	31.65	33.49	35.04	37.43
68	508.0	17.48	32.43	35.75	37.12	38.52	41.32
69	508.0	19.05	35.48	38.19	40.51	42.38	45.26
70	508.0	25.4	47.84	51.51	54.60	56.75	60.63
71	508.0	26.2	49.39	54.02	56.35	59.01	62.90
72	508.0	31.75	60.55	65.17	69.16	72.40	77.40
73	508.0	32.5	62.01	66.82	70.94	73.79	78.87
74	508.0	38.1	73.48	79.16	84.14	87.67	93.91
75	508.0	50.8	100.81	110.28	115.08	120.17	128.16
76	559.0	12.7	21.13	22.71	24.08	25.04	26.63
77	559.0	19.05	32.21	35.58	36.78	38.14	40.71
78	559.0	25.4	43.22	46.54	49.37	51.56	55.09
79	559.0	31.75	54.81	60.39	62.57	65.06	69.52
80	559.0	38.1	66.39	73.19	75.89	79.13	84.71
81	610.0	9.52	14.39	15.44	16.42	16.94	18.36
82	610.0	12.7	19.37	20.75	22.01	22.81	24.63
83	610.0	14.27	21.83	23.57	24.90	26.04	27.81
84	610.0	15.88	24.30	26.72	27.82	28.89	30.78

Table A.2 (*cont.*) Burst pressure for the flawless pipelines by Finite Element Analysis (X52, X56, X60, X65, and X70).

			Burst Pressure (MPa)				
No.	Outer Dia. (*mm*)	Thickness (*mm*)	X52	X56	X60	X65	X70
85	610.0	17.48	26.85	28.91	30.57	32.08	34.03
86	610.0	19.05	29.46	31.66	33.51	35.06	37.44
87	610.0	25.4	39.59	43.23	45.06	47.05	50.36
88	610.0	31.75	49.88	53.70	56.98	59.64	63.70
89	610.0	38.1	60.41	65.01	68.99	72.22	77.19
90	610.0	50.8	82.32	88.73	93.99	98.51	104.76

Table A.3 Burst pressure of the flawless pipelines by Finite Element Analysis (X80).

			Burst Pressure (MPa)
No.	Outer Dia. (*mm*)	Thickness (*mm*)	X80
1	323.9	4.775	19.28
2	323.9	5.156	20.80
3	323.9	5.563	22.49
4	323.9	6.350	25.71
5	323.9	7.137	28.81
6	323.9	7.925	32.34
7	323.9	8.382	34.22
8	323.9	8.738	35.69
9	323.9	9.525	39.04
10	323.9	10.312	42.39
11	323.9	11.125	45.80
12	323.9	12.700	52.55
13	355.6	4.775	17.54
14	355.6	5.156	18.98
15	355.6	5.563	20.48
16	355.6	6.350	23.45
17	355.6	7.137	26.36
18	355.6	7.925	28.95
19	355.6	8.382	31.09
20	355.6	8.738	32.26
21	355.6	9.525	35.48
22	355.6	10.312	38.46
23	355.6	11.125	41.56
24	355.6	12.700	47.70
25	406.4	6.350	20.44
26	406.4	7.137	23.02
27	406.4	7.925	25.61
28	406.4	8.738	28.24
29	406.4	9.525	30.74
30	406.4	10.312	32.93
31	406.4	11.125	36.25
32	406.4	11.913	38.98
33	406.4	12.700	41.47
34	406.4	14.275	46.96
35	406.4	15.875	52.35
36	457.2	6.350	18.20
37	457.2	7.137	20.42
38	457.2	7.925	22.74

Table A.3 (*cont.*) Burst pressure for the flawless pipelines by Finite Element Analysis (X80).

			Burst Pressure (MPa)
No.	Outer Dia. (*mm*)	Thickness (*mm*)	X80
39	457.2	8.738	25.13
40	457.2	9.525	27.39
41	457.2	10.312	29.69
42	457.2	11.125	32.20
43	457.2	11.913	34.32
44	457.2	12.700	36.80
45	457.2	14.275	41.56
46	457.2	15.875	46.33
47	508.0	6.350	16.33
48	508.0	7.137	18.25
49	508.0	7.925	20.40
50	508.0	8.738	22.56
51	508.0	9.525	24.64
52	508.0	10.312	26.61
53	508.0	11.125	28.85
54	508.0	11.913	30.80
55	508.0	12.700	33.01
56	508.0	14.275	37.24
57	508.0	15.875	41.47
58	558.8	6.350	14.71
59	558.8	7.137	16.67
60	558.8	7.925	18.55
61	558.8	8.738	20.47
62	558.8	9.525	22.30
63	558.8	10.312	24.24
64	558.8	11.125	26.20
65	558.8	11.913	28.08
66	558.8	12.700	29.96
67	558.8	14.275	33.72
68	558.8	15.875	37.62
69	609.6	6.350	13.56
70	609.6	7.137	15.23
71	609.6	7.925	16.97
72	609.6	8.738	18.70
73	609.6	9.525	20.44
74	609.6	10.312	21.71
75	609.6	11.125	23.98
76	609.6	11.913	25.68

Table A.3 (*cont.*) Burst pressure for the flawless pipelines by Finite Element Analysis (X80).

			Burst Pressure (MPa)
No.	Outer Dia. (*mm*)	Thickness (*mm*)	X80
77	609.6	12.700	27.39
78	609.6	14.275	30.87
79	609.6	15.875	34.26

APPENDIX B

Table B.1 *La, La/D, Da, Da/D* and Burst pressure for the FEA based Parametric Study (I).

No.	L_a (*mm*)	L_a/D (%)	D_a (*mm*)	D_a/D (%)	Burst pressure (MPa)	
					PD formula	FEA
1	150.03	46.33	2.185	0.67	15.823	15.881
2	83.01	25.63	2.961	0.91	15.759	15.881
3	59.59	18.40	3.604	1.11	15.712	15.881
4	49.41	15.26	3.908	1.21	15.692	15.785
5	44.24	13.66	4.102	1.27	15.679	15.785
6	34.89	10.77	4.420	1.36	15.631	15.294
7	31.02	9.58	4.496	1.39	14.413	13.802
8	28.77	8.88	4.533	1.40	14.403	13.911
9	26.40	8.15	4.577	1.41	14.391	14.043
10	25.24	7.79	4.603	1.42	14.383	14.090
11	163.00	50.33	8.927	2.76	15.476	15.597
12	94.07	29.05	10.244	3.16	15.447	15.597
13	72.68	22.44	10.625	3.28	15.439	15.548
14	62.38	19.26	10.801	3.34	15.419	15.280
15	56.57	17.47	10.904	3.37	15.091	14.901
16	47.40	14.64	11.063	3.42	13.186	12.395
17	44.66	13.79	11.093	3.43	13.143	12.364
18	44.42	13.72	11.112	3.43	13.139	12.367
19	43.58	13.46	11.112	3.43	13.136	12.356
20	43.26	13.36	11.112	3.43	13.136	12.342
21	187.16	57.79	23.146	7.15	15.359	15.436
22	124.61	38.48	23.913	7.38	15.354	15.436
23	106.46	32.87	24.077	7.43	15.251	15.275
24	98.82	30.52	24.167	7.46	14.570	14.291
25	94.65	29.23	24.211	7.48	13.709	13.507
26	88.07	27.19	24.279	7.50	12.833	12.273
27	86.52	26.72	24.296	7.50	12.763	12.241
28	86.14	26.60	24.300	7.50	12.750	12.325
29	85.75	26.48	24.303	7.50	12.739	12.317

Table B.1 (*cont.*) *La, La/D, Da, Da/D* and Burst pressure for the FEA based Parametric Study (I).

No.	L_a (*mm*)	L_a/D (%)	D_a (*mm*)	D_a/D (%)	Burst pressure (MPa)	
					PD formula	FEA
30	85.62	26.44	24.304	7.50	12.735	12.320
31	224.29	69.26	36.610	11.30	15.292	15.413
32	167.57	51.74	37.458	11.57	15.266	15.413
33	152.54	47.10	37.700	11.64	14.876	15.010
34	145.98	45.08	37.781	11.67	14.170	14.273
35	142.62	44.04	37.821	11.68	13.697	13.223
36	137.33	42.41	37.881	11.70	13.100	12.341
37	136.16	42.04	37.895	11.70	13.011	12.334
38	135.74	41.92	37.899	11.70	12.984	12.477
39	135.36	41.80	37.910	11.71	12.958	12.594
40	135.26	41.77	37.911	11.71	12.953	12.606
41	286.60	88.50	51.000	15.75	15.302	15.339
42	220.55	68.10	51.264	15.83	15.188	15.339
43	206.33	63.71	51.451	15.89	14.552	14.491
44	200.12	61.79	51.544	15.92	13.873	13.877
45	196.89	60.80	51.590	15.93	13.467	13.024
46	192.10	59.32	51.655	15.95	12.925	12.438
47	191.13	59.02	51.666	15.95	12.834	12.404
48	190.80	58.92	51.670	15.95	12.805	12.393
49	190.56	58.84	51.674	15.96	12.784	12.383
50	190.47	58.81	51.675	15.96	12.776	12.380

Table B.2 The 150 data generated by linear interpolation from the 50 FEA based Parametric Study (I) results.

No.	D_a/D (%)	L_a (mm)	L_a/D (%)	Burst pressure (MPa)
1	1	152.06	46.95	15.84
2	1	83.44	25.76	15.87
3	1	58.91	18.19	15.90
4	1	48.15	14.87	15.83
5	1	42.68	13.18	15.90
6	1	32.67	10.09	15.81
7	1	28.42	8.78	14.08
8	1	25.69	7.93	14.21
9	1	22.88	7.07	14.39
10	1	21.47	6.63	14.46
11	2	158.29	48.88	15.70
12	2	88.35	27.28	15.74
13	2	64.95	20.06	15.74
14	2	54.25	16.75	15.60
15	2	48.55	14.99	15.48
16	2	38.77	11.97	14.40
17	2	35.12	10.84	13.37
18	2	33.39	10.31	13.45
19	2	31.40	9.69	13.55
20	2	30.43	9.40	13.59
21	3	164.34	50.75	15.59
22	3	93.27	28.80	15.62
23	3	70.98	21.92	15.59
24	3	60.34	18.63	15.36
25	3	54.42	16.80	15.06
26	3	44.86	13.85	12.98
27	3	41.82	12.91	12.66
28	3	41.10	12.69	12.69
29	3	39.91	12.32	12.72
30	3	39.39	12.16	12.72
31	4	169.84	52.44	15.55
32	4	100.13	30.92	15.57
33	4	78.53	24.25	15.50
34	4	68.25	21.08	15.12
35	4	62.44	19.28	14.69
36	4	53.22	16.43	12.38
37	4	50.56	15.61	12.35

Table B.2 (*cont.*) The 150 data generated by linear interpolation from the 50 FEA based Parametric Study (I) results.

No.	Da/D (%)	La (mm)	La/D (%)	Burst pressure (MPa)
38	4	50.25	15.52	12.36
39	4	49.47	15.28	12.35
40	4	49.17	15.18	12.34
41	5	175.35	54.14	15.51
42	5	107.36	33.15	15.53
43	5	86.66	26.76	15.44
44	5	77.08	23.80	14.88
45	5	71.70	22.14	14.35
46	5	63.19	19.51	12.35
47	5	60.83	18.78	12.32
48	5	60.49	18.68	12.35
49	5	59.83	18.47	12.34
50	5	59.57	18.39	12.33
51	6	180.85	55.84	15.48
52	6	114.59	35.39	15.49
53	6	94.79	29.27	15.37
54	6	85.91	26.53	14.64
55	6	80.97	25.00	14.01
56	6	73.15	22.59	12.32
57	6	71.10	21.95	12.29
58	6	70.74	21.84	12.34
59	6	70.18	21.67	12.33
60	6	69.97	21.61	12.33
61	7	186.35	57.54	15.44
62	7	121.83	37.62	15.45
63	7	102.92	31.78	15.30
64	7	94.74	29.25	14.40
65	7	90.24	27.86	13.67
66	7	83.12	25.67	12.29
67	7	81.37	25.12	12.26
68	7	80.98	25.01	12.33
69	7	80.53	24.87	12.32
70	7	80.37	24.82	12.32
71	8	194.78	60.14	15.43
72	8	130.93	40.43	15.43
73	8	112.65	34.78	15.24
74	8	104.85	32.38	14.29

Table B.2 (*cont.*) The 150 data generated by linear interpolation from the 50 FEA based Parametric Study (I) results.

No.	Da/D (%)	La (mm)	La/D (%)	Burst pressure (MPa)
75	8	100.63	31.07	13.47
76	8	93.97	29.02	12.28
77	8	92.41	28.53	12.25
78	8	92.01	28.41	12.34
79	8	91.60	28.29	12.35
80	8	91.47	28.24	12.35
81	9	203.71	62.90	15.43
82	9	141.21	43.60	15.43
83	9	123.61	38.17	15.18
84	9	116.07	35.84	14.28
85	9	112.05	34.60	13.40
86	9	105.70	32.64	12.30
87	9	104.23	32.18	12.27
88	9	103.82	32.06	12.38
89	9	103.41	31.93	12.42
90	9	103.28	31.89	12.42
91	10	212.64	65.66	15.42
92	10	151.48	46.78	15.42
93	10	134.56	41.55	15.11
94	10	127.29	39.31	14.28
95	10	123.46	38.12	13.34
96	10	117.43	36.26	12.31
97	10	116.05	35.83	12.30
98	10	115.63	35.71	12.42
99	10	115.22	35.58	12.48
100	10	115.10	35.54	12.49
101	11	221.57	68.42	15.41
102	11	161.75	49.95	15.42
103	11	145.52	44.93	15.05
104	11	138.51	42.77	14.28
105	11	134.88	41.65	13.27
106	11	129.15	39.88	12.33
107	11	127.86	39.48	12.32
108	11	127.44	39.35	12.45
109	11	127.02	39.22	12.55
110	11	126.91	39.19	12.56
111	12	234.04	72.27	15.40

Table B.2 (*cont.*) The 150 data generated by linear interpolation from the 50 FEA based Parametric Study (I) results.

No.	Da/D (%)	La (mm)	La/D (%)	Burst pressure (MPa)
112	12	172.96	53.41	15.41
113	12	157.09	48.51	14.97
114	12	150.23	46.39	14.24
115	12	146.72	45.31	13.21
116	12	141.23	43.61	12.35
117	12	140.02	43.23	12.34
118	12	139.59	43.10	12.47
119	12	139.17	42.97	12.58
120	12	139.07	42.94	12.59
121	13	248.06	76.60	15.38
122	13	185.39	57.24	15.39
123	13	169.75	52.42	14.84
124	13	162.97	50.32	14.15
125	13	159.49	49.25	13.16
126	13	154.11	47.59	12.37
127	13	152.95	47.23	12.36
128	13	152.54	47.10	12.45
129	13	152.16	46.99	12.53
130	13	152.07	46.96	12.54
131	14	262.09	80.93	15.37
132	14	197.81	61.08	15.37
133	14	182.42	56.33	14.72
134	14	175.71	54.26	14.06
135	14	172.26	53.19	13.11
136	14	166.99	51.56	12.39
137	14	165.87	51.22	12.37
138	14	165.49	51.10	12.43
139	14	165.15	51.00	12.48
140	14	165.06	50.97	12.48
141	15	276.11	85.26	15.35
142	15	210.24	64.92	15.35
143	15	195.09	60.24	14.60
144	15	188.45	58.19	13.96
145	15	185.02	57.13	13.07
146	15	179.87	55.54	12.42
147	15	178.80	55.21	12.39
148	15	178.44	55.10	12.41

Table B.2 (*cont.*) The 150 data generated by linear interpolation from the 50 FEA based Parametric Study (I) results.

No.	Da/D (%)	La (mm)	La/D (%)	Burst pressure (MPa)
149	15	178.14	55.01	12.43
150	15	178.05	54.98	12.43

Table B.3 *La, La/D, Da, Da/D* and Burst pressure for the FEA based Parametric Study (II) for X52 material pipelines with a hemispherical dent.

Case	L_a (*mm*)	L_a/D (%)	D_a (*mm*)	D_a/D (%)	Burst pressure (MPa)	
					PD formula	FEA
1	166.984	51.56	2.248	0.69	13.538	14.172
2	84.334	26.04	3.076	0.95	13.460	14.071
3	59.644	18.42	3.654	1.13	13.410	14.067
4	49.274	15.22	3.946	1.22	13.386	14.025
5	43.692	13.49	4.133	1.28	13.372	14.022
6	32.306	9.98	4.447	1.37	12.399	12.769
7	160.556	49.58	9.159	2.83	13.069	14.113
8	93.538	28.88	10.352	3.20	13.018	14.036
9	72.252	22.31	10.678	3.30	13.005	14.02
10	61.582	19.02	10.792	3.33	12.982	12.584
11	55.898	17.26	10.894	3.36	12.659	11.722
12	45.600	14.08	11.016	3.40	11.308	11.148
13	188.400	58.18	23.611	7.29	12.616	13.952
14	124.728	38.51	23.883	7.37	12.608	13.902
15	105.548	32.59	24.150	7.46	12.510	12.935
16	97.068	29.97	24.236	7.48	11.859	11.509
17	94.224	29.09	24.179	7.47	11.508	10.794
18	87.176	26.92	24.235	7.48	10.966	10.963
19	226.618	69.98	37.061	11.44	12.229	13.643

Table B.3 (*cont.*) *La, La/D, Da, Da/D* and Burst pressure for the FEA based Parametric Study (II) for X52 material pipelines with a hemispherical dent.

Case	L_a (*mm*)	L_a/D (%)	D_a (*mm*)	D_a/D (%)	Burst pressure (MPa)	
					PD formula	FEA
20	167.120	51.60	37.575	11.60	12.201	13.271
21	151.080	46.65	37.780	11.67	11.932	11.388
22	142.542	44.01	37.777	11.66	11.412	11.016
23	138.960	42.91	37.836	11.68	11.185	10.982
24	133.504	41.22	37.915	11.71	10.986	10.994
25	271.870	83.95	50.396	15.56	11.911	13.635
26	220.318	68.03	51.352	15.86	11.830	10.645
27	202.902	62.65	51.520	15.91	11.376	10.442
28	193.310	59.69	51.592	15.93	10.858	10.461
29	190.790	58.91	51.616	15.94	10.745	10.444
30	181.872	56.16	51.740	15.98	10.510	10.439

Table B.4 *La, La/D, Da, Da/D* and Burst pressure for the FEA based Parametric Study (II) for X65 material pipelines with a hemispherical dent.

Case	L_a (*mm*)	L_a/D (%)	D_a (*mm*)	D_a/D (%)	Burst pressure (MPa)	
					PD formula	FEA
1	82.094	25.35	2.497	0.77	15.720	16.177
2	57.694	17.82	3.014	0.93	15.654	16.175
3	47.812	14.76	3.321	1.03	15.616	16.164
4	42.462	13.11	3.525	1.09	15.592	16.159
5	30.982	9.57	3.835	1.18	14.647	15.688
6	90.044	27.80	9.220	2.85	15.072	16.175
7	69.532	21.47	9.723	3.00	15.036	16.161
8	59.322	18.32	9.924	3.06	15.010	15.866
9	53.734	16.59	10.070	3.11	14.735	15.214
10	43.190	13.34	10.267	3.17	13.282	13.954
11	120.920	37.34	22.533	6.96	14.332	15.067
12	102.568	31.67	22.708	7.01	14.279	14.819
13	94.104	29.06	22.814	7.04	13.840	13.435
14	90.004	27.79	22.877	7.06	13.292	13.147
15	82.112	25.35	22.980	7.10	12.739	13.196
16	162.912	50.30	35.670	11.01	13.638	13.684
17	147.470	45.54	35.943	11.10	13.527	12.841
18	139.186	42.98	35.958	11.10	13.248	12.367
19	135.394	41.81	36.027	11.12	13.052	12.510
20	127.718	39.44	36.105	11.15	12.804	12.620
21	215.576	66.57	49.110	15.16	12.999	11.824
22	198.768	61.38	49.322	15.23	12.858	11.804
23	189.740	58.59	49.390	15.25	12.626	11.643
24	184.762	57.05	49.430	15.26	12.483	11.707
25	182.062	56.22	49.536	15.30	12.409	11.814

Table B.5 *La, La/D, Da, Da/D* and Burst pressure for the FEA based Parametric Study (II) for X80 material pipelines with a hemispherical dent.

Case	L_a (*mm*)	L_a/D (%)	D_a (*mm*)	D_a/D (%)	Burst pressure (MPa)	
					PD formula	FEA
1	80.120	24.74	2.024	0.62	18.412	19.251
2	56.824	17.55	2.463	0.76	18.336	19.251
3	46.910	14.49	2.738	0.85	18.289	19.186
4	41.728	12.88	2.936	0.91	18.257	19.184
5	32.042	9.89	3.305	1.02	18.196	19.261
6	86.732	26.78	7.901	2.44	17.594	19.261
7	66.800	20.63	8.605	2.66	17.519	18.925
8	57.222	17.67	8.902	2.75	17.487	18.472
9	51.904	16.03	9.100	2.81	17.368	17.048
10	41.518	12.82	9.373	2.89	15.674	13.954
11	117.008	36.13	20.949	6.47	16.481	17.479
12	99.282	30.66	21.153	6.53	16.445	16.914
13	90.790	28.03	21.280	6.57	16.166	15.489
14	86.702	26.77	21.372	6.60	15.655	15.434
15	78.958	24.38	21.499	6.64	14.908	15.705
16	158.490	48.94	33.651	10.39	15.480	15.697
17	142.794	44.09	33.948	10.48	15.424	14.734
18	135.372	41.80	34.001	10.50	15.314	14.885
19	131.820	40.70	34.091	10.53	15.202	14.767
20	126.242	38.98	34.201	10.56	15.026	14.861
21	209.458	64.68	46.638	14.40	14.527	13.543
22	193.632	59.79	46.953	14.50	14.502	13.575
23	189.740	58.59	49.390	15.25	14.336	13.560
24	184.762	57.05	49.430	15.26	14.335	13.546
25	182.062	56.22	49.536	15.30	14.330	11.133

Table B.6 *Da, Da/D, La, La/D, Wa, Wa/D,* and Burst pressure of the FEA based Parametric Study for X52 material pipelines with a spheroidal dent.

No.	D_b/D (%)	L_I (*mm*)	W_I (*mm*)	D_a (*mm*)	D_a/D (%)	L_a (*mm*)	L_a/D (%)	W_a (*mm*)	W_a/D (%)	Burst Pressure (MPa)		
										FEA	*PD formula*	
											L_a based	W_a based
1	2.5	50	50	4.41	1.36	33.74	10.42	29.05	8.97	13.2	12.43	12.41
2	2.5	75	50	4.25	1.31	41.36	12.77	31.64	9.77	13.57	13.36	12.45
3	2.5	100	50	3.99	1.23	49.72	15.35	34.16	10.55	13.58	13.38	13.38
4	2.5	150	50	3.58	1.11	67.4	20.81	37.9	11.7	13.6	13.42	13.42
5	2.5	50	75	4.3	1.33	36.82	11.37	32.95	10.18	13.52	13.36	12.44
6	2.5	75	75	4.33	1.34	36.63	11.31	31.12	9.61	13.56	13.36	12.43
7	2.5	100	75	4.35	1.34	34.35	10.61	30.06	9.28	13.27	13.17	12.42
8	2.5	150	75	4.08	1.26	43.43	13.41	32.27	9.96	13.57	13.38	12.49
9	2.5	50	100	4.09	1.26	39.49	12.19	36.86	11.38	13.47	13.38	13.38
10	2.5	75	100	4.27	1.32	38.8	11.98	34.07	10.52	13.54	13.36	13.11
11	2.5	100	100	4.32	1.34	38.22	11.8	32.31	9.98	13.55	13.36	12.43
12	2.5	150	100	3.97	1.23	51.66	15.95	35.72	11.03	13.59	13.39	13.39
13	2.5	50	150	3.83	1.18	43.18	13.33	42.74	13.2	13.47	13.4	13.4
14	2.5	75	150	3.99	1.23	42.21	13.03	39.89	12.32	13.52	13.38	13.38
15	2.5	100	150	4.11	1.27	42.09	13	37.69	11.64	13.55	13.37	13.37
16	2.5	150	150	4.33	1.34	39.74	12.27	33.41	10.32	13.56	13.36	12.44
17	5.0	50	50	11.08	3.42	49.5	15.28	40.75	12.58	11.45	11.41	11.29
18	5.0	75	50	10.98	3.39	59.41	18.34	43.88	13.55	12.32	12.92	11.3
19	5.0	100	50	10.71	3.31	71.65	22.12	46.77	14.44	13.6	13	11.37
20	5.0	150	50	10.09	3.12	99.11	30.6	50.68	15.65	13.62	13.03	12.15
21	5.0	50	75	10.89	3.36	54.03	16.68	47.08	14.54	13.31	12.31	11.35

Table B.6 (*cont.*) *Da, Da/D, La, La/D, Wa, Wa/D,* and Burst pressure of the FEA based Parametric Study for X52 material pipelines with a spheroidal dent.

No.	D_b/D (%)	L_I (*mm*)	W_I (*mm*)	D_a (*mm*)	D_a/D (%)	L_a (*mm*)	L_a/D (%)	W_a (*mm*)	W_a/D (%)	Burst Pressure (MPa)		
										FEA	*PD formula*	
											L_a based	W_a based
22	5.0	75	75	11	3.4	54.32	16.77	44.03	13.6	12.49	12.29	11.3
23	5.0	100	75	10.92	3.37	57.86	17.87	44.62	13.78	12.41	12.85	11.31
24	5.0	150	75	10.51	3.25	78.93	24.37	47.52	14.68	13.52	13.01	11.44
25	5.0	50	100	10.61	3.28	58.11	17.94	53.36	16.48	13.43	12.93	12.37
26	5.0	75	100	10.89	3.36	57.43	17.73	49.09	15.16	13.39	12.83	11.44
27	5.0	100	100	10.98	3.39	58.89	18.18	46.85	14.47	13.1	12.9	11.33
28	5.0	150	100	10.67	3.3	75.36	23.27	49.67	15.34	13.6	13.01	11.57
29	5.0	50	150	10.16	3.14	63.15	19.5	62.97	19.45	13.44	13.02	13.02
30	5.0	75	150	10.44	3.23	62.23	19.22	58.06	17.93	13.49	13.01	12.96
31	5.0	100	150	10.7	3.3	62.57	19.32	54.61	16.86	13.51	12.99	12.56
32	5.0	150	150	10.81	3.34	65.52	20.23	50.61	15.63	13.56	13	11.64
33	10.0	50	50	24.35	7.52	89.72	27.7	63.63	19.65	10.72	11.05	10.88
34	10.0	75	50	24.29	7.5	99.01	30.57	66.41	20.51	11.03	12.07	10.88
35	10.0	100	50	24.18	7.47	110.64	34.16	68.67	21.2	11.29	12.58	10.88
36	10.0	150	50	23.76	7.34	139.54	43.09	70.66	21.82	13.64	12.61	10.88
37	10.0	50	75	24.16	7.46	97.25	30.03	70.16	21.66	12.64	11.92	10.88
38	10.0	75	75	24.26	7.49	95.28	29.42	66.9	20.66	11.08	11.61	10.88
39	10.0	100	75	24.24	7.49	100.64	31.08	67.95	20.98	11.75	12.25	10.88
40	10.0	150	75	24.08	7.44	126.73	39.13	70.27	21.7	12.37	12.6	10.88
41	10.0	50	100	23.92	7.39	104.05	32.13	77.41	23.9	13.12	12.5	10.88
42	10.0	75	100	24.12	7.45	100.89	31.15	72.39	22.35	13.15	12.3	10.88

Table B.6 (*cont.*) *Da, Da/D, La, La/D, Wa, Wa/D,* and Burst pressure of the FEA based Parametric Study for X52 material pipelines with a spheroidal dent.

No.	D_b/D (%)	L_I (*mm*)	W_I (*mm*)	D_a (*mm*)	D_a/D (%)	L_a (*mm*)	L_a/D (%)	W_a (*mm*)	W_a/D (%)	Burst Pressure (MPa)		
										FEA	*PD formula*	
											L_a based	W_a based
43	10.0	100	100	24.19	7.47	101.01	31.19	69.88	21.58	12.39	12.29	10.88
44	10.0	150	100	24.06	7.43	117.46	36.27	72.32	22.33	13.2	12.6	10.88
45	10.0	50	150	23.36	7.21	111.97	34.58	91.47	28.24	13.32	12.62	11.51
46	10.0	75	150	23.65	7.3	108.92	33.63	84.08	25.96	13.46	12.59	10.93
47	10.0	100	150	23.95	7.39	109.11	33.69	79.55	24.56	13.59	12.58	10.89
48	10.0	150	150	24.09	7.44	110.07	33.99	74.54	23.02	13.36	12.58	10.88

APPENDIX C

INTERNATIONAL JOURNALS

1. **Oh, D.H.**, Race, J.M., Oterkus, S., Chang, E., 2020. *A New Methodology for the Prediction of Burst Pressure for API 5L X grade flawless Pipelines.* Ocean Engineering. (Accepted)

ADDITIONAL JOURNALS DONE DURING Ph.D. PERIOD

1. **Oh, D.H.**, Koo, B.G., 2018. *Empirical Initial Scantling Equations on Optimal Structural Design of Submarine Pressure Hull.* Journal of Advanced Research in Ocean Engineering. 4(1), 7-15, https://dx.doi.org/10.5574/JAROE.2018.4.1.007
2. Cho, Y.S., **Oh, D.H.**, Paik, J.K., 2019. *An empirical formula for predicting the collapse strength of composite cylindrical-shell structures under external pressure loads.* Ocean Engineering. 172, 191-198, https://doi.org/10.1016/j.oceaneng.2018.11.028
3. **Oh, D.H.**, Ahn, N.H., 2019. *Review of the Structural Shape for Aft Transition Ring of Submarine.* Journal of the Korean Society of Marine Environment & Safety. 25(7), 936-944, https://doi.org/10.7837/kosomes.2019.25.7.936

INTERNATIONAL CONFERENCES

1. **Oh, D.H.**, Race, J.M., Oterkus, S., Chang, E., 2019. *Burst pressure prediction method for thin-walled API 5L X grades pipelines with dent*, The 12th Europe Korea Conference on Science and Technology, Vienna, Austria. From 15th to 18th July, 2019.
2. **Oh, D.H.**, Race, J.M., Oterkus, S., Chang, E., 2019. *Burst pressure prediction method for API 5L X grade dented pipeline*. 2019 Korean Association of Ocean Science and Technology Societies spring joint conference, Jeju island, Republic of Korea. From 15th to 17th May, 2019.
3. **Oh, D.H.,** Koo, B.G., 2018. *Empirical Initial Scantling Equations on Optimal Structural Design of Submarine Pressure Hull.* The 11th Europe Korea Conference on Science and Technology, Glasgow, UK. From 20th to 24th August, 2018.
4. **Oh, D.H.**, Race, J.M., Oterkus, S., 2018. *Burst pressure prediction method for flawless pipeline*. The 3rd Workshop on Ships and Offshore Structure 2018, Glasgow, UK. From 7th to 10th February, 2018.